INFORMATION TO USERS

This manuscript has been reproduced from the microfilm master. UMI films the text directly from the original or copy submitted. Thus, some thesis and dissertation copies are in typewriter face, while others may be from any type of computer printer.

The quality of this reproduction is dependent upon the quality of the copy submitted. Broken or indistinct print, colored or poor quality illustrations and photographs, print bleedthrough, substandard margins, and improper alignment can adversely affect reproduction.

In the unlikely event that the author did not send UMI a complete manuscript and there are missing pages, these will be noted. Also, if unauthorized copyright material had to be removed, a note will indicate the deletion.

Oversize materials (e.g., maps, drawings, charts) are reproduced by sectioning the original, beginning at the upper left-hand corner and continuing from left to right in equal sections with small overlaps. Each original is also photographed in one exposure and is included in reduced form at the back of the book.

Photographs included in the original manuscript have been reproduced xerographically in this copy. Higher quality 6" x 9" black and white photographic prints are available for any photographs or illustrations appearing in this copy for an additional charge. Contact UMI directly to order.

UMI

A Bell & Howell Information Company
300 North Zeeb Road, Ann Arbor MI 48106-1346 USA
313/761-4700 800/521-0600

TIME RESOLVED SURFACE ENHANCED RAMAN SCATTERING STUDIES OF IRON-BLEOMYCIN AND 3-HYDROXYFLAVONE ON A Ag ELECTRODE

by

MINFA WANG

A dissertation submitted to the Graduate Faculty in Chemistry in partial fulfillment of the requirements for the degree of Doctor of Philosophy, The City University of New York.

1997

This manuscript has been read and accepted for the Graduate Faculty in Chemistry in satisfaction of the dissertation requirement for the degree of Doctor of Philosophy.

1/23/97
Date

Ronald D. Burke
Chair of Examining Committee

1/24/97
Date

Executive Officer

Supervisory Committee

THE CITY UNIVERSITY OF NEW YORK

ABSTRACT

Time Resolved Surface Enhanced Raman Scattering Studies of Iron-Bleomycin and 3-Hydroxyflavone on a Ag Electrode

by

Minfa Wang

Advisers: Professors Ronald L. Birke and John R. Lombardi

Drug mechanism and kinetics of oxygen activation of Fe-Bleomycin (BLM) and O_2-Fe-BLM systems were studied by time resolved surface enhanced Raman spectroscopy (TRSERS) combined with electrochemical methods. By applying an electrode potential step from 0.02 V to -0.65 V, reduction reactions of O_2-Fe-BLM system can be initiated which are similar to that of in the drug system. Three intermediates were observed during the potential initiated reduction of O_2-Fe-BLM system by monitoring the changes of SERS band at 1574 cm^{-1}, which is sensitive to the redox state of central iron and assigned to the carbonyl stretching vibration of the β-hydroxyhistidinyl amide. One of the intermediates may correspond to the so called "activated BLM". Our experiments also confirmed two of ligands in the iron-drug complex which were controversial assigned by previous researches. The TRSERS, SERS and cyclic voltammetry experimental results revealed more information of the oxygenate activated mechanism.

Normal Raman and surface enhanced Raman scattering of 3-hydroxyflavone (3-HF) have been obtained and used to interpret the low frequency of the carbonyl stretching in 3-HF. Photo initiated intramolecular ground state reverse proton transfer of 3-HF was also studied by TRSERS. By

measuring vibrational spectra of the ground state tautomer of 3-HF, two dynamic processes were observed during the ground state tautomer decay. One process may simply correspond to the reverse proton transfer with life time about 1.4 μs. The second may correspond to a peroxide intermediate formed in the proton transfer cycle. In spite of the ultrafast rate of the proton transfer in the excited state, the measurements by TRSERS technique demonstrate that a long-lived ground-state tautomer at room temperature is involved in the ground state proton transfer. The mechanism of the photooxygenation of 3-HF in the tautomer ground state has been proposed.

TABLE OF CONTENTS

Chapter I

Introduction and Organization

of

This Thesis

1.1 Introduction

The actual time-dependent behavior of real systems can often be very effectively described using time-resolved methods. Kinetic information, such as order and timing of events in a physical, chemical or biochemical process, can be obtained by various time-resolved approaches. Such information, especially the information for short-lived transient species, is very useful in our understanding of mechanisms that show how reactants become products. Which time-dependent approach is best may differ depending on the nature and complexity of the problem. In surface science, time-resolved surface enhanced Raman scattering (TRSERS) spectroscopy is an idea tool for short time resolved surface chemistry of adsorbed molecules at the metal-solution interface.[1-5] So called TRSERS is a real-time *in-situ* methodology which combines surface enhanced Raman scattering (SERS) spectroscopy with time-resolved techniques where multichannel detection techniques are generally used. SERS is a special case of Raman scattering spectroscopy, which provides a molecular structure method capable of investigating events which occur directly at the metal-solution interface after a reaction takes place.[6-7] When used in time-resolved approaches, it shows the following advantages:

1. Most other optical spectroscopes are frequently limited to studying systems with broad optical absorption spectra. The rates of formation and decay of many transients have been carefully determined with these techniques. However, due to the lack of vibration structure, structural information concerning these transients are rarely obtainable. In order to accurately understand natural changes, it is imperative that we determine the corresponding structural changes occurring during the course of time over the period during which these changes are taking place. For this reason, time-resolved vibrational spectroscopy

becomes one of the most useful tools presently available for investigating the mechanisms of rapid physical and chemical changes.[3-4, 8]

2. Although both Raman and infrared reflection/absorption spectroscopy can provide detailed vibrational information, their realms of applicability are noticeably different. In the case of metal-solution interface, such as in electrochemistry, the infrared method requires a thin-layer geometry for *in-situ* applications. While this arrangement enables molecular structural changes both in the solution and interfacial region to be examined, it also restricts the electrochemical methods that can be used. Despite being limited primarily to roughened silver, gold, and copper surfaces, the intrinsic selectivity of SERS for interfacial species enables surface spectra to be obtained readily without bulk solution-phase interferences even when conventional electrochemical cells are used. This in principle makes the SERS technique generally suitable for examining irreversible as well as reversible electrode processes under either steady-state or transient conditions, in conjunction with the gamut of conventional electrochemical methods.[3-4, 9]

3. The overall enhancement of 10^5 to 10^6 over the normal Raman scattering for an isolated molecule was found in the case of SERS. This makes it possible to observe the detailed vibrational signature of the adsorbate on the metal surfaces and obtain the satisfactory signal to noise ration (S/N) in spectra even when the integration time is very short, as higher time resolution requires.[1,5]

4. While the SERS technique is commonly restricted to silver, gold, and copper surfaces, a broad range of adsorbates can readily be examined, including important organic molecules and biomolecules.[10,11] The information on adsorption, orientation, electron transfer between adsorbate and the surface, and surface chemical reaction processes obtained by TRSERS are not only useful for

elucidation of metal (Ag, Au and Cu)-molecule interactions, but also might simulate other conductive surface-molecule interactions, such as a biomembrane case.

5. Theoretically, a picosecond to femtoseconds time scale Raman process could enable SERS experiments to follow the fastest reaction processes. Thus, TRSERS would allow one to detect the rapid changes in the surface Raman spectra caused by the generation of short-lived transient species on a metal surface during various reactions, such as potential induced electrochemical reactions and photoinduced surface photochemical reactions.

Given the excellent resolution and wide frequency range of SERS, as well as its surface sensitivity, TRSERS has attracted much attention for the study of surface molecular structural changes attending electrochemical and photochemical processes through detailed analysis on the molecular level.[1,9,11,12] However, such applications of TRSERS have so far been surprisingly sparse. The reasons for the limited reports may be threefold. First, the silver surfaces, on which most SERS is undertaken, provide a potential window that is unsuitable for some electrode reactions, and the Raman signals often exhibit instability following large potential excursions.[9] Second, existing controversies about SERS mechanisms and uncertainties in the enhancement factor for several of the less controversial mechanisms may have delayed the merging of SERS and time-resolved approach.[2] Third, the adaptation of SERS techniques have mainly been limited to simpler molecules with smaller molecular weight; there is a need to find more applications to larger biological molecules. Recent developments[13-15] in TRSERS have been made in the hope that experimentalists engaged in time-resolved vibrational spectroscopy will find it easier to adapt to their research. It is hoped that the knowledge of the time-dependence of vibrational bands from various system will not only aid the

identification of surface species, but also ultimately the nature of the SERS effect itself.

In the past five years, our laboratory have reported time dependent SERS spectra from the study of radical ions formed by photochemical and electrochemical reactions at the surface of SERS active metals. These adsorbed reaction systems encompass electroreduction processes of adsorbed *p*-Nitrobenzoic acid,[13] 4-Cyanopyridine,[14] 4-Pyridine carboxaldehyde[14] and direct photoinduced radical cation formation from flavin mononucleotide, FMN.[15] The latter application[15] has demonstrated *ns* time scale TRSERS spectroscopy as a useful technique to study surface photochemistry, which includes monitoring surface photochemistry dynamics and determining the chemical structure of surface photochemical intermediates. These applications have also demonstrated μs and *m*s time scale TRSERS spectroscopy as a useful technique to study electrochemical kinetics with identification of the chemical structure of intermediates. These applications not only enrich the fundamental knowledge of primary photochemical and electrochemical processes which can occur at metal surfaces but also stimulate new application of TRSERS. As Pimentel[16] pointed out, in general, our knowledge of the chemical dynamics of molecules is not commensurate with our knowledge of the analysis, synthesis, and structure elucidation of molecules. This lack of knowledge is unfortunately even more true for the dynamics of molecular reactions at surfaces. Thus, the future should bring increased application of TRSERS, particularly under conditions where there is no competing technique: in electrochemistry, catalysis, and in such areas as those involving surface photochemical effects and surface nonlinear optical phenomena.

The objective of this dissertation is continually to exam the problems and the possibilities of time-resolved surface enhanced Raman spectroscopy in

studies of photoinduced surface photochemistry and potential induced electrochemistry for important organic and biochemical compounds on a Ag electrode. Two TRSERS procedures have been used in the research of this dissertation. The single shot TRSERS experimental method is illustrated in the study of oxygen activation of Fe-Bleomycin for *ms* time resolution. Pump-probe TRSERS experimental method is illustrated in the study of photochemistry of 3-Hydroxyflavone for *ns* time resolution.

In the future, we envision frequent application of TRSERS to study more and more interesting systems involving large biological molecules.

1.2 Organization of this Thesis

For the consideration of the context, the organization of this thesis naturally divides into two parts. The first deals with the Raman spectroscopic aspects, while the second demonstrates my research in studies of time-resolved surface enhanced Raman scattering spectroscopy of Fe-Bleomycin and 3-Hydroxyflavone on a Ag Electrode.

The first part is composed of Chapters 1, 2 and 3 and deals with the theoretical and experimental aspects of Raman, SERS and TRSERS. The first chapter discusses the significance of TRSERS and the objective of the thesis. The second chapter contains a brief explanation of Raman, SERS and TRSERS spectroscopes, a discussion of the advantages and disadvantages of the techniques (Section 2.1-2.4), and a brief overview of the applications of time resolved surface enhanced Raman spectroscopy (Section 2.5). The experimental aspects of TRSERS spectroscopy are taken up in Chapter 3, which ranges from a description of the basic optics of a routine SERS experiment to a

discussion of some very sophisticated instrumental and data acquisition modes used in TRSERS experiment in our laboratory. The design of a microelectrochemical SERS cell and pretreatments to activate SERS surfaces in the experiments are also discussed in this chapter.

The second part of this thesis, which consists of Chapters 4-6, contains the results and discussions of the applications of the TRSERS spectroscopy from my research. The study of oxygen activation of Fe-Bleomycin by TRSERS through a controlled potential induced electrochemical reduction on a Ag electrode is taken up in Chapter 4. In order to elucidate the drug mechanism of oxygen activation, cyclic voltammetry experiments are also discussed in this Chapter. Chapter 5 contains normal Raman and SERS spectra of 3-hydroxyflavone. Raman characteristics of 3-hydroxyflavone are discussed by comparing with its FTIR spectra. TRSERS spectra of photo initiated intramolecular ground state proton transfer of 3-hydroxyflavone are taken up in Chapter 6. Chapter 4, 5 and 6 begin with an introduction to their own special topics. The introductions are not extensive, but they should be enough to show what the problems are and how significant they are.

Chapter II

Principles and Overview

2.1 Raman Effect

Raman spectroscopy provides detailed information on the vibrational motions of atoms in molecules. This method causes molecules to undergo changes in vibrational energy state by subjecting them to an excitation radiation in selected spectral regions. The theory and selection rules of Raman transitions have been discussed by Herzberg[1] and Steinfeld[2] in detail. Only qualitative descriptions of the principles of Raman effect are given in this thesis.

The origin of Raman spectroscopy is an inelastic scattering effect, involving an inelastic collisions between the molecules composing the sample and photons composing the excitation radiation. In the classical mechanical model, the Raman effect is depicted as a molecular light-scattering phenomenon in which a change in frequency of the light occurs. When electromagnetic radiation (excitation source for Raman scattering) interacts with matter, the oscillating electric field causes the matter to oscillate at the same frequency as the radiation. This response is expressed in terms of the induced dipole moment μ, which may be written as:

$$\mu = \alpha E \qquad (1)$$

Where $E = E_0 \cos \omega t$ is the electric field due to light of frequency ω, and α is the polarizability of a sample molecule, a second-rank tensor. The oscillations induced through the polarizability cause the sample molecule to radiate light in all directions at the same frequency as the incident light. This process is known as Rayleigh scattering. In addition, if the sample molecule itself has natural oscillation frequencies ω_{if} (such as the normal modes of a molecule), some light also will be radiated by molecule at the sum and difference frequencies, $\omega \pm \omega_{if}$.

This process is known as Raman scattering. In order to conserve the total energy in Raman process, the sample molecule is left either in a state of lower energy (for the sum, called the anti-Stokes spectrum), or higher energy (for the difference, called the Stokes spectrum).

In the quantum mechanical model, light scattering is depicted as a two-photon process. In Rayleigh scattering, the sample molecule is excited to a higher virtual state by combination with a photon, and then relaxes "immediately" to the original vibrational state by re-emitting a photon at the same frequency as the incident light. The molecule "absorbs" no energy from the incident radiation in this case. Only a very small fraction of molecules undergo Raman scattering (inelastic scattering). When Raman scattering occurs, the excited molecule relaxes "immediately" to a different vibrational level, rather than to the original state. The energy carried by an inelastically scattered photon is different from that of the incident light. The various kinds of Raman processes may now be outlined again. In the Stokes process, the second photon has a frequency $\omega - \omega_{if}$, and in the anti-Stokes process, the second photon has a frequency $\omega + \omega_{if}$, giving the same results as the classical model.

Now we see that in a Raman spectrum, the energy difference between the incident and scattered lights appears as a frequency shift between the excitation frequency ω and the scattered light $\omega' = \omega \pm \omega_{if}$. These two frequencies, ω' and ω, are related to the vibrational energy of sample molecule by the following equation:

$$h\omega = h\omega' + \Delta E_{vibration} \qquad (2)$$

where h is Plank constant. It follows that by monitoring the inelastically scattered photons we can probe molecular vibrations, and thus the Raman spectrum is a

vibrational spectrum of a molecule.

The utility of the Raman spectrum lies in the fact that the vibrational spectrum of a molecule is a sensitive indicator of chemical properties. The vibrational spectrum reflects the disposition of atomic nuclei and chemical bonds within a molecule as well as the interactions between the molecule and its immediate environment. Because of these sensitivities, the Raman spectra can be used as a monitor of molecular chemistry. Essentially, the same kind of vibrational motion that produces the peaks in Raman spectra also produces the "peaks" (actually, absorption maxima) in infrared spectra. However, it is often impossible to obtain the infrared spectrum of an organic or a biological material in water; under these conditions, the Raman data are the sole source of information. Also when using a time-dependent approach, Raman spectroscopy has some advantages over infrared spectroscopy:[3]

1. The entire vibrational spectrum from 10 to 4000 cm^{-1} can be covered in a single scan of a conventional Raman spectrometer. In infrared spectroscopy special instrumentation is normally required to cover the region below approximately 600 cm^{-1}.

2. The time scale of the Raman effect are essentially instantaneous. Therefore, the Raman spectrum represents an instantaneous "snapshot" of all molecules. Hence, in a system where rapid chemical exchange is occurring, each species contributes a Raman signature in direct proportion to its concentration.

3. Complete Raman spectra may be recorded in much less than 1 sec.

However, the Raman effect is extremely weak and only a minute proportion of the incident photons become Raman photons. The inherent weakness of the effect not only makes sophisticated optical and electronic equipment required to detect the scattered photons, but also limits applications of

Raman spectroscopy in time-dependent studies.

Fortunately, the discoveries of resonance Raman (RR) and surface-enhanced Raman scattering (SERS) effects have provided ways to increase the Raman scattering efficiency. Therefore, the detection limit and applications of the Raman technique have been greatly improved.

2.2 Resonance Raman and Raman Intensities

When the excitation frequency is not in the absorbing band of the molecule, the spectrum detected is called the normal Raman (NR) spectrum. Resonance Raman occurs when the laser wavelength, used to excite the Raman spectrum, lies under an intense electronic absorption band of a molecule. Absorption of a photon can now occur, and by the prompt reemission of a second photon can give rise to the resonance Raman process. Under these conditions considerable intensity enhancement of certain Raman bands may occur with the result that the absolute intensities are increased by a factor of 10^3 to 10^5. For understanding the intensity enhancement in the resonance Raman, it might be helpful to exam the relationship for Raman intensities.

In the quantum mechanical treatment, the total intensity of the scattered light I_s in terms of the intensity of the exciting light I_L is:[4,5]

$$I_s = K_E 8\pi[(\omega \pm \omega_{if})^4 / 9c^4] I_L \sum_{\sigma,\rho} |\alpha_{\sigma\rho}|^2 \qquad (3)$$

Where K_E is a parameter which gathers the instrumental factors and $\alpha_{\sigma\rho}$ is the $\rho\sigma$ component of the transition polarizability tensor (ρ and σ refer to *x*, *y*, or *z*), which has been derived based on second-order perturbation theory and the zero-

order Born-Oppenheimer approximation:[4]

$$\alpha_{\sigma\rho} = \sum_{K\neq G}\sum_{\upsilon}\left[\frac{M^{\sigma}_{KG}(Q_0)M^{\rho}_{KG}(Q_0)}{\hbar(\omega_{K\upsilon,Gi}-\omega)}+\frac{M^{\rho}_{KG}(Q_0)M^{\sigma}_{KG}(Q_0)}{\hbar(\omega_{K\upsilon,Gf}+\omega)}\right]\langle i|\upsilon\rangle\langle\upsilon|f\rangle$$
$$+\sum_{K\neq G}\sum_{\upsilon}M^{\rho}_{KG}(Q_0)\left[\frac{\partial M^{\sigma}_{KG}}{\partial Q}\right]_0\left[\frac{\langle f|Q|\upsilon\rangle\langle\upsilon|i\rangle+\langle f|\upsilon\rangle\langle\upsilon|Q|i\rangle}{\hbar(\omega_{K\upsilon,Gi}-\omega)}\right.$$
$$\left.+\frac{\langle f|Q|\upsilon\rangle\langle\upsilon|i\rangle+\langle f|\upsilon\rangle\langle\upsilon|Q|i\rangle}{\hbar(\omega_{K\upsilon,Gf}+\omega)}\right] \qquad (4)$$

where i and f represent initial and final vibrational levels of the ground electronic state G, υ represents vibrational levels of excited electronic states K, and $\omega_{K\upsilon,Gi}$, etc., represents characteristic frequency between the two states K_υ and G_i. Matrix elements of the type $\langle i|\upsilon\rangle$, etc., correspond to Franck-condon overlap integrals. Q is a normal coordinate, and M_{KG} is the pure electronic transition moment from the ground to the Kth excited electronic state:

$$M_{KG}(Q) = \langle G_e|\mu|K_e\rangle \qquad (5)$$

The two terms in Eq. (4) each contribute to the overall scattering. However, in certain limits, one or the other is dominant.

In normal Raman Scattering, where the frequency of the incident light is considerably less than that needed to induce an optically allowed transition, This means $\omega_{K\upsilon,Gi} >> \omega$, and thus, the denominator in both terms of Eq. (4) essentially may be considered constant as $(\omega_{K\upsilon,Gi}-\omega)\cong(\omega_{KG}-\omega)$ and $(\omega_{K\upsilon,Gf}+\omega)\cong(\omega_{KG}+\omega)$. This permits the sum over υ for a given K in Eq. (4) to apply to the integrals over nuclear space.[5] Note that $\sum|\upsilon\rangle\langle\upsilon| = 1$, where the sum extends over all states. Equation (4) then becomes:[4]

$$\alpha_{\sigma\rho} = \sum_{K \neq G} [M^{\rho}_{KG}(Q_0) M^{\sigma}_{KG}(Q_0) \frac{2\omega_{KG}}{\hbar(\omega_{KG}^2 - \omega^2)}] \langle i | f \rangle$$
$$+ \sum_{K \neq G} M^{\rho}_{KG}(Q_0) [\frac{\partial M^{\sigma}_{KG}}{\partial Q}]_0 [\frac{2\omega_{KG}}{\hbar(\omega_{KG}^2 - \omega^2)}] \langle f | Q | i \rangle \qquad (6)$$

The first term in Eq. (6) gives rise to Rayleigh scattering, since for the vibrational wave functions in the same electronic state $\langle i | f \rangle = 0$, unless i=f. The second term in Eq. (6) gives rise to Raman scattering only when $f = i \pm 1$. So normal Raman spectra are largely confined to fundamental frequencies. Usually, the first term is considerably more intense than the second term since for allowed transitions M_{KG}, the electronic transition moment, is much larger than $\partial M_{KG} / \partial Q$, the derivative of an electronic dipole moment. That is why generally the normal Raman effect is extremely weak. Indeed, experimentally it is found that Raman intensities are often three orders of magnitude less intense than Rayleigh intensities.

Immediately, we see from Eq. (4) when ω approaches the energy of an allowed molecular transition $\omega_{Kv,Gi}$, the denominator $(\omega_{Kv,Gi} - \omega)$ becomes smaller and smaller. It is not possible to perform the sum over vibrations because the frequency denominator is now sensitive to this sum. But we still can understand that one term in the sum must become very large. This is the resonance condition. Under the resonance condition Franck-Condon overlap factors are not zero, because the vibrational levels involved belong to different electronic states and are therefore not orthogonal. Thus, it is reasonable to expect a considerable increase in intensity for resonance Raman spectrum since it arises from the first term in the Eq. (4). Due to the same reason, resonance Raman spectra tend to be rich in overtones (f=i+2, i+3,...) in contrast with the normal Raman spectra which are largely confined to fundamental frequencies.

However, two other processes compete with the resonance Raman effect, and both of these occur with higher probability than resonance Raman scattering. One process is the nonradiative pathway and in this case the molecule returns to the lower electronic state by dissipating the energy of the photon as heat. The second process is fluorescence. Since the resonance Raman spectrum often coincides with the fluorescence spectrum, especially in the case of biochemistry, it may be obscured by the latter, so that the advantage afforded by the increased intensity must often be forgone by moving the exciting light off resonance to obtain a weaker, but observable normal Raman spectrum. Thus, techniques to avoid interference from fluorescence in resonance Raman are very important.

In SERS, the intensity is much stronger than in normal Raman, or even in resonance Raman, and fluorescence can be quenched effectively by metal surface.

2.3 SERS Effect

Molecules adsorbed onto some specially pretreated metal surfaces under certain conditions exhibit an anomalously large interaction cross-section for the Raman effect. Thus, a 'giant' enhancement can be provided by the metal surface. The overall enhancement of 10^5 to 10^6 over the normal Raman scattering of an isolated molecule was found in this case, and the effect was termed as surface enhanced Raman scattering. This makes it possible to observe the detailed vibrational signature of the adsorbate on the metal surfaces. The SERS active metals includes Ag, Cu and Au, which show larger enhancement.[6-15] It should be noted that the use of SERS active metals of Ag and Au for electrochemical studies is of particular significance because these

metals are general-purpose working electrodes, since Ag has a high overpotential for hydrogen ion reduction and Au is a noble metal. In addition to electrochemical systems, that is, electrode-electrolyte interface (solid/solution), which has been most widely investigated, the SERS effect also has been observed for may different interfaces and environments. In fact, SERS effect has been observed at metal/gas (vacuum) interface[16-20], the colloid/liquid interface[21-25], and the solid/solid interface[26-29], and it is possibly the most sensitive surface high-resolution vibrational spectroscopic technique available as an analytical probe.

The first report of surface Raman spectroscopy of a molecule adsorbed at the Ag electrode/solution interface under potentiostatic electrochemical control was the paper of Fleischmann et al. in 1974.[30] Soon after this initial report a great interest was aroused in the physics, chemistry, surface and material science research communities to study SERS both as a fundamental phenomenon and as a new technique.[31-32] More than 12% of the publications reported at the XVth. international conference on Raman Spectroscopy in Pittsburgh (1996) were based on SERS.[33-37] SERS intensities, linewidths, and line shapes[38], as well as shifts in peak positions dependent on the applied potential[39-40], the wavelength dependence of the enhancement[41-42], and parameters influencing the usually employed oxidation-reduction cycle in an electrochemical environment[43-44] have all been studied. The origin of SERS has been ascribed to (1) resonance Raman scattering process[45-50], (2) a reflection modulation effect[51-53], (3) electron-hole pair excitation[54-55], and many theoretical models have been proposed.[55-56] The SERS effect from the metal/solution interface in an electrochemical cell has been discussed by Birke and Lombardi in detail.[57-58] Only qualitative descriptions of the principles of the SERS effect are given in the following.

Mainly there are two theories for surface enhancement mechanisms. One is called the electromagnetic (EM) field enhancement theory which deals with the enhancement of the electromagnetic field of the exciting light; and the other is the charge transfer (CT) theory which deals with the enhancement of the Raman scattering cross-section (polarizibility) by a metal/adsorbate resonance Raman processes. The equation for the enhanced scattering intensity in SERS has been written as:[57]

$$I_{SERS} = K_E 8\pi[(\omega \pm \omega_{if})^4 / 9c^4] I_L L^2(\omega) L^2(\omega_{if}) \sum_{\sigma,\rho} |\alpha_{\sigma\rho}|^2 \qquad (7)$$

The source of enhanced scattering is contained in the factors:

$$L^2(\omega) L^2(\omega_{if}) \sum_{\sigma,\rho} |\alpha_{\sigma\rho}|^2$$

Two factors, $L^2(\omega)L^2(\omega_{if})$ reflect the electromagnetic field enhancement effect which is the larger of the two mechanisms. $L^2(\omega)$ is considered to come from the interaction of the uniform EM field of the exciting light with the metallic particle. The metallic particle has a high conductivity which is expressed by its dielectric function ε_m, and it is assumed to be surrounded by a homogeneous medium of dielectric function ε_0. In the small-sphere particle approximation, the exciting EM field induces an electric dipole located at the center of metallic particle, polarizes the metal particle so that there develop surface charges of opposite sign on either side of the particle which alternate with frequency ω as the electric field of the incident light changes sign. Thus the local electric potential in the proximity of the metallic particle is not just equal to the applied incident EM field, but the sum of that generated by the applied incident field and

a reflected field produced by the metal particle. This EM enhancements can be expressed in terms of the dielectric constants of the metal and the surrounding medium:[57]

$$L^2(\omega) \propto (1+2g)^2 \tag{8}$$

with

$$g = [\varepsilon_m(\omega) - \varepsilon_0]/[\varepsilon_m(\omega) + 2\varepsilon_0] \tag{9}$$

This mode is called a localized surface plasmon mode. When the incident light satisfies a resonance condition for a localized surface plasmon, for example, when $\varepsilon_m(\omega) = -2\varepsilon_0$ a large field is generated at the metal interface.

There is also a further EM enhancement effect which is caused by the oscillating dipole of the adsorbed molecule in the proximity of the metallic particle inducing a dipole in the metal particle. The metal sphere acts as an antenna for the near field of the oscillating molecular dipole, and the emitted Raman radiation from the molecule at frequency ω_{if} is then enhanced by the presence of the metal particle. The dipole moment of the entire system, the so-called emission dipole of the molecule plus metal particle system, includes the effect of both the enhanced laser electric field and the antenna effect. The antenna effect, to a good approximation, has the same form as $L^2(\omega)$; however, the frequency of light is now the Raman frequency, ω_{if}, giving a factor $L^2(\omega_{if})$. This frequency is manifested in the dielectric function which becomes:[57]

$$L^2(\omega_{if}) \propto (1+2g_0)^2 \tag{10}$$

with

$$g_0 = [\varepsilon_m(\omega_{if}) - \varepsilon_0]/[\varepsilon_m(\omega_{if}) + 2\varepsilon_0] \tag{11}$$

Thus, for a molecule adsorbed on the surface of a metal sphere the average EM enhancement is:[57]

$$L^2(\omega)L^2(\omega_{if}) = (1/9)(1+2g)^2(1+2g_0)^2 \qquad (12)$$

The EM enhancements relies on the dielectric constants of the metal and the surrounding medium, and the geometry and the size of the metal particles. Experimental values for ε_m are available for Ag, Au and other metals at optical frequencies. For water at optical frequencies, ε_0 equals 1.77, and thus the resonance condition for small spherical metallic particle is $\varepsilon_m(\omega) = -2\varepsilon_0$ = -3.54, which occurs for Ag at 382 nm. If the geometry of metal particle is considered to be a prolate spheroid with an aspect ratio of a/b=2, the resonance condition for Ag occurs at 480 nm, and with a/b=3, the resonance frequency is 590 nm. So, as aspect ratio a/b increases, the resonance frequency moves to longer wavelengths.[57, 59-62] In addition to the shape, the localized plasmon resonance is observed for small metal structures on the size order of 10 to 100 nm. Thus, a method for producing these surface roughness features is required in order to obtain the EM enhancement.

The enhancement in factor $\sum_{\sigma,\rho}|\alpha_{\sigma\rho}|^2$ deals with the charge transfer theory, which is based on the interaction between the adsorbed molecule and surface adatoms of metal.[57-58, 63-64] Generally, polyatomic molecules have sets of rather discrete energy levels. Metals, on the other hand, tend to have large numbers of states bunched together in bands. The most important band is the conduction band which formed by valence electrons in the metal. Often this band is not completely filled with electrons, and the highest filled level of this band is called the Fermi level. When a molecule is weakly bound to the metal surface at some equilibrium distance we can not consider the energy levels of the molecule

to be distinct from those of the metal. We must speak of the levels of the molecule-metal system. Thus, the molecular states are broadened and mixed with those of the metal by this interaction, and the exciting light, if it is in resonance with the energy difference between metallic and molecular states, can cause **resonant charge transfer transitions** between the molecular states and metal states. There are two situations. In a metal-to-molecule charge transfer process, a metallic electron in the conduction band absorbs a photon and is promoted to the vacant bands above the Fermi level; it either tunnels to a temporary negative molecular complexes or crosses over to an excited state of the molecule-metal system. Then the electron returns to the original level in the metal and in the process reradiates a Raman-shifted photon. The charge transfer energy in this case would be close to the difference between the Fermi level and excited state of the molecule-metal system. In a molecule-to-metal charge transfer process, a similar set of steps happen. A ground state electron of the molecule absorbs a photon and is vertically excited; it either tunnels to a vacant level above the Fermi level of the metal, or crosses over to the lowest unoccupied level of the molecule-metal system. Then the electron returns to the molecular ground state and in the process reradiates a Raman-shifted photon. The charge transfer energy in this case would be the difference between the molecular ground state and Fermi level in molecule-metal system. It might be better to reexamine the Eq. (6) for $\alpha_{\sigma\rho}$ again:

$$\alpha_{\sigma\rho} = \sum_{K\neq G}[M^{\rho}_{KG}(Q_0)M^{\sigma}_{KG}(Q_0)\frac{2\omega_{KG}}{\hbar(\omega_{KG}{}^2-\omega^2)}]\langle i|f\rangle$$
$$+\sum_{K\neq G}M^{\rho}_{KG}(Q_0)[\frac{\partial M^{\sigma}_{KG}}{\partial Q}]_0[\frac{2\omega_{KG}}{\hbar(\omega_{KG}{}^2-\omega^2)}]\langle f|Q|i\rangle \qquad (6)$$

We again consider the situation in which the frequency of the exciting light

is far from any molecular resonance $\omega << \omega_{KG}$. Thus, the first term in Eq. (6) contributes only the Rayleigh line, and the second term contributes a weak normal Raman line. If, alternately, we consider those states in which either K or G is actually a Fermi level (M) of the metal state, we might still expect resonant contributions to the intensity. For example, when the frequency of the exciting light is close to the difference between the molecular ground state and Fermi level, i.e., $\omega \cong \omega_{MG}$ for $|K\rangle = |M\rangle$, or when the frequency of the exciting light is close to the difference between the Fermi level and excited state of the molecule-metal system, i.e., $\omega \cong \omega_{KM}$ for $|G\rangle = |M\rangle$, then a resonant process might occur if there is some mixing of the metal and molecular wave functions, so the momentum selection rule has no meaning. Generally an adatom or other point defect site is necessary to relax the momentum selection rule. Thus a method for producing a roughen surface is also required in the CT enhancement. In such a case, the charge transfer process takes place between the surface adatom and the chemisorbed molecule, i.e., within the adatom-molecule complex. This is the case for SERS. In fact, the resonant condition can easily be met in SERS since there is a mixing of metal and molecular quantum states in a pretreated metal surface; and the resonant condition can also be realized in SERS by applying the potential to the metal to add or remove electrons from the conduction band, thus changing the Fermi level of molecule-metal system. We see that the case $|K\rangle = |M\rangle$ represents resonant molecule-to-metal charge transfer from the molecular ground state to one of the unfilled metal levels M. The case $|G\rangle = |M\rangle$ represents resonant metal-to-molecule charge transfer from a filled metal state M to an excited state K of the molecule.

Although the enhancement in the factor $\alpha_{\sigma\rho}$ is from resonant charge transfer transitions, SERS is different from RR. As we discussed before, intense overtones will be allowed by the first term in Eq. (6) but not the second term.

This is the case for RR. In SERS, very few observations of overtones have been reported, and even those that have been reported are quite weak, but non-totally symmetric vibrations are often as intense as totally symmetric ones. It is likely that the resonant contributions from the second term in Eq. (6) are also available, and as important as the first term in SERS. Complete analysis for the charge transfer cases has been given by Lombardi et al.[57] They derive a Raman polarizability for SERS which is the sum of three terms:

$$\alpha_{\sigma\rho}=A+B+C \qquad (13)$$

The A term comes from Franck-Condon coupling and the B and C terms from Herzberg-Teller coupling. The B term represents the transition from the ground state of the adsorbed molecule to the metal Fermi level and the C term represents the transition from the metal Fermi level to an excited state of the molecule. They concluded that the latter two terms give a charge transfer resonance Raman effect in which intensity is borrowed from an allowed molecular transition, and in which the selection rules are like those of normal Raman. Thus all terms in Eq. (13) will strongly contribute to the line intensity and more fundamental frequencies can appear in SERS than in RR.

Both the EM and CT resonance processes are necessary to achieve the 10^5 to 10^6 surface enhancement observed in SERS.

2.4 Time-Resolved SERS

A time-resolved method is one where the observation of the process is made over a time interval which is short with respect to the time interval over which the process occurs. Time-resolved Raman spectroscopy, then refers to the recording of **complete Raman spectra** in a **short time span** such as

milliseconds, microseconds, nanoseconds, or even picoseconds.[3] Here, short time span is a key point.

As an example, we can examine a compound A undergoing a series of changes after or during the perturbation shown as following:

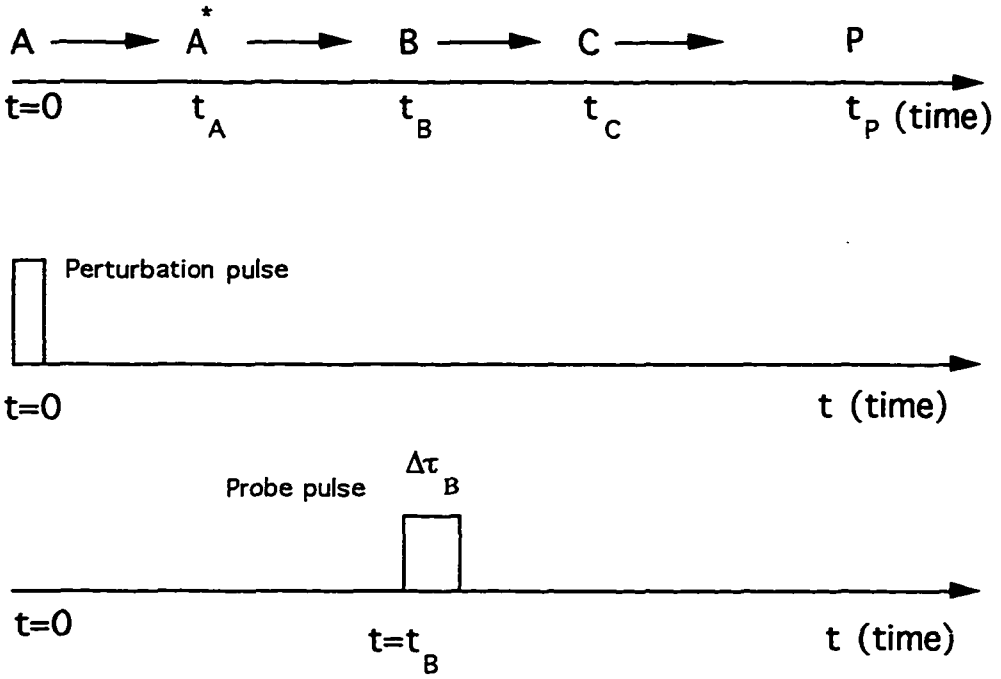

In order to obtain information from intermediate B, a probe beam (Raman excitation source) should be sent to the sample after the perturbation to generate a detectable Raman signal from intermediate B, and a detection process should be performed by setting a proper delay time t_B, which is equal to the time interval between the initial perturbation pulse and the probe pulse, and then integrating the Raman signal only within a time interval $\nabla\tau_B$, which must be a very short time span since it has to be shorter than the life time of the intermediate B. In order to realize such a method, a nonscanning grating spectrometer with a multichannel detection system can be used.

The principal pioneers in the development of time-resolved Raman spectroscopy are Bridoux, Delhaye, and co-workers at Lille, France. They

obtained a complete spectra of acetone from a single 25-picosecond pulse by using an image intensifier. They have summarized their work and outlined the advantages of multichannel detection system in a review.[66]

Considering time-resolved Raman spectroscopy in general, the limiting factors in pushing the method to shorter times are the sensitivity of the detection system and the intensity of the signal, which is generated from an intermediate in a Raman process to get a reasonable signal-to-noise (S/N) ratio. Generally, the Raman signal at the intermediate is always very weak when compared with the parent molecule Raman signal. This is due to the fact that only a small amount of parent molecules can be converted to intermediate after a perturbation but also, more seriously, to the short detection time which is limited by the intermediate life time. Thus, a Raman process with great enhancement in signal intensity is really preferred in time-resolved method. In fact, any increase in scattering cross section results in improved S/N ratio or faster time resolution, and a time-resolved Raman spectroscopy technique only works well when a high sensitive detection system is coupled with an enormous enhancement in signal intensity provided in some kinds of Raman processes. Partly for this reason, time-resolved resonance Raman spectroscopy (TRR) was developed faster than normal Raman and was applied in more investigations.[67-70]

As we mentioned before, signal intensity in SERS spectroscopy is much more intense and although resonance Raman scattering can be used at smooth surfaces of any metal, it is not as sensitive as SERS for the case of SERS active surfaces. With advancements in the development in multichannel detection such as the photodiode array (PDA), the charge coupled detector (CCD) and the charge injection detector (CID),[71] complete SERS spectra measurements (probe) following either pulsed laser perturbation or pulsed electrochemical perturbation (pump) of adsorbed molecules on the surface could respond

possibly within picoseconds of the pulse. Thus, time-resolved SERS method could, in principal, be a powerful tool to investigate extremely rapid surface phenomena to provide kinetic and structural information on intermediates. Two TRSERS methods based on optical multichannel analyzer (OMA) detection system have been developed in our laboratory and discussed by Birke and Lombardi in detail:[72] (1) a single shot method where a series of complete Raman spectra are recorded during the time course of a radical ion producing perturbation, and (2) a pump-probe ensemble averaging method which affords the fastest time resolution for obtaining a full surface Raman intensity vs. wavelength spectrum at some fixed time delay from an initiating pulse. These two methods take advantages of the multiplexing and signal averaging afforded by OMA detection, coupled with the enormous enhancement in signal intensity provided by SERS process. The single shot method is developed for time-resolved SERS in μs time domain to study electrochemical events and also can routinely be used in the *m*s and s time domains. The pump-probe method is developed for time-resolved SERS in the *n*s time domain to study photochemical events such as photoionization, photoisomerization, and photodecomposition etc.. The experimental details for these two methods will be discussed in detail in the chapter 3.

Once time dependent spectra are obtained by these two TRSERS methods, additional procedures may be needed to determine the nature of any observed transients. In many cases it is useful to take difference spectra. This is because the predominant species on the surface is usually not the transient of interest, and spectral lines of the reactants or products tend to obscure the transient spectra. The resulting difference spectra are often much clearer and easier to interpret. Another important aspect from the applications of these two TRSERS methods is that repetitive pump-probe detection operation mode may

be necessary for most time-resolved experiments in order to obtain a reasonable signal to noise ratio (S/N), especially for a time domain shorter than a few *ms*. With an OMA detection system, it is not hard to achieve good S/N ratio within a few *ms* by a single scan detection with laser power of 30 to 40 mw for the probe beam at an electrode. With this power, the energy delivered to a sample on an electrode during a 1 *ms* detection time will be $3X10^{-5}$ to $4X10^{-5}$ J. Using the same laser power, however, only $3X10^{-9}$ to $4X10^{-9}$ J energy can be delivered to sample on an electrode during a 100 ns detection time. So, at least 10,000 repetitive pump-probe cycles are needed to deliver the same energy to the sample in order to generate the same S/N ratio as in the case of 1 *ms*. Here, the increased repetitive detection cycles compensate for the short exposure time. One thing we have to note is that the repetitive pump-probe TRSERS can only be applied to study "reversible" reactions in order to ensure that each pump-probe detection is started from the parent or **initial** reactant.

When the detection time is as short as the *ns* time domain such as in the pump-probe method, there is still a question whether it is possible to generate enough intermediate population from a photo perturbation to give a detectable Raman signal. Sometimes this question can be solved by properly choosing the experiment conditions, such as the wavelength of pump pulse and the applied potential in SERS.[95] For example, in the case of the photoinduced surface photochemistry of an adsorbate, the population of a relatively stable intermediate strongly depends on: the surface density of adsorbate N_0 (number of reactants), the pump laser pulse intensity I_0 (number of photons), the absorptivity of the adsorbate molecule at given excitation wavelength ε_λ, the quantum efficiency between ground state and excited state ϕ_1, and the charge transfer efficiency between adsorbate and substrate ρ_E. The total efficiency ρ therefore is represented by:

$$\rho = \varepsilon_\lambda \phi_1 \rho_E \qquad (16)$$

and the population of intermediates n_{int} is given by:

$$n_{int.} = N_0 I_0 \varepsilon_\lambda \phi_1 \rho_E \qquad (17)$$

Thus, in order to convert larger amount of adsorbate to the intermediate, it is necessary to select the wavelength of the pump laser pulse to give the highest absorption coefficient ε_λ. It is also necessary to have a proper molecule-electrode system which facilitates charge transfer, i.e., to have a high ρ_E, which can be obtained by applying a proper electrode potential to adjust the Fermi level of the electrode to facilitate electron transfer between electrode and adsorbed molecules to obtain a higher ρ_E. The intermediate population also depends on the intensity of the pump laser pulse I_0 and the surface density of the adsorbed molecules N_0. Therefore, a higher pump laser intensity is preferred, and proper pretreatment of the electrode is always preferred. One must also be concerned with the fact that if I_0 is too high, the adsorbate can be thermally desorbed from the surface.

2.5 A Brief Overview of the Applications of Time-Resolved Surface Enhanced Raman Spectroscopy

In spite of extensive research, SERS has been studied almost exclusively under steady state conditions. TRSERS of molecular adsorbates on metallic surfaces has been reported by only a few research groups. With limited

applications, TRSERS spectroscopy has been mainly applied to study slow or the slow part of dynamic processes involved in electrochemical events such as adsorption/desorption dynamics, growth or aggregation of Ag particles, development of SERS bands during the oxidation reduction cycle (ORC), and formation of intermediates or radical ions during linear sweep or cyclic voltammetry processes (LSV or CV). TRSERS also has been applied to study surface photochemical reactions.

Jeanmaire and Van Duyne reported the first application of SERS in time dependent approach for the investigation of an adsorption/desorption process in an electrochemical systems to obtain information about rates of adsorption/desorption.[40] In their work, the SERS intensity of pyridine at a silver electrode surface was monitored as a function of time after the silver electrode potential was stepped from a value where pyridine was presumably not adsorbed to a value where pyridine was adsorbed. The 'intensity-time' profiles reversibly tracked the potential as it was stepped back and forth between the two values, with only a small amount of time lag which is attributed to double layer charging time. This experimental results led to a conclusion that the pyridine Raman signal was indeed of surface origin, rather than a diffusion or bulk solution effect. Although no attempt was made to analyze the 'intensity-time' data, their work did suggest that such information was available from surface Raman spectroelectrochemical experiments. In order to explore the extent to which quantitative analysis of surface Raman spectroelectrochemical intensity-time data could be performed, Pemberton and Buck[74] have analyzed the time dependence of a surface enhanced resonance Raman scattering signal to obtain quantitative adsorption parameters and adsorption rates for dithizone anion adsorption on silver. Again, the Raman 'intensity-time' data were obtained by monitoring the intensity of one surface band with time after the electrode potential

was stepped between potentials at which adsorption did and did not occur. They measured and obtained diffusion-controlled adsorption rate for dithizone adsorption at a silver foil electrode in pH 12 aqueous alkaline medium. Their work demonstrated the potential of surface Raman spectroelectrochemistry as a method capable of providing quantitative information on rates of adsorption in electrochemical systems. The studies of electrochemical adsorption of other systems, such as thiocyanate at silver electrode during potential cycles and potential step also have been reported by other research groups.[75-76]

Following Jeanmaire and Van Duyne, M. Takahashi et al.[77-78] have used the similar method of step potential change to further verify the origin of the SERS intensity enhancement. As we discussed before, SERS is highly sensitive to adsorbed species on roughened silver surfaces. It is well-known that two kinds of roughness are necessary for SERS: i.e. large scale roughness of an order of 100 nm, and small scale roughness of an order of atoms. M. Takahashi et al. focused on the contribution of the latter roughness, small scale roughness, formed by the electrochemical treatment and concluded that the latter is originated from atomic scale metal clusters.[77] In order to further reveal the role of the clusters, they stepped the electrode potential to different values and measured the time response of SERS intensity due to the ring breathing mode 984 cm^{-1} of benzene in benzene, pyridine, and 4-cyanopyridine. From their result, they found the resonance state for the Raman scattering of adsorbed species is located much higher than 514.5 nm excitation and therefore, suggested that there is no CT level at around 500 nm.[78]

All of the above research was obtained by monitoring 'intensity-time' on one SERS band at constant frequency. This is the conventional time dependent SERS but not exactly TRSERS we mentioned in this theses, because a complete spectra is not recorded by that method. Using that conventional time dependent

method, the study of Ag particle growth and their surface potential change with time in Ag halide solutions and in photographic emulsions was carried out by Kneipp et al.[79-81]. In these experiments, SERS spectra of pseudoisocyanine dye (PIC) in silver bromide sols show a strong time dependence. The enhancement factor, in general, following the formation (and destruction) of SERS active colloidal silver in the silver halide sols has been examined by laser illumination during the Raman measurement. Further time dependent SERS studies of kinetics of colloid aggregation and the fractional structure of colloidal aggregations were carried out by Zhang et al.[82-83] Good relationships between time dependent SERS intensity and the fractional dimension of colloidal fraction aggregates were established.

Although the conventional time dependent SERS method might offer kinetic information such as a "rate constant", the problem is the paucity of structural information available from such a method. For example, intense SERS is generated from ions and molecules adsorbed on Ag, Cu or Au electrodes immersed in aqueous electrolytes after the electrode has been subject to an oxidation-reduction cycle (ORC). The processes occurring during the ORC are amenable to study in great detail. Dornhaus and Chang et al.[84] reported an experimental determination of the time development of SERS during the oxidation-reduction cycle as early as 1980. Using a SIT vidicon, They have studied the TRSERS from various compounds adsorbed on Ag electrodes during an oxidation reduction cycle. Data obtained provided some insight into several predictions of the theoretical models for SERS, including the role of dipole moments present in the purely infrared active vibrations and absent in the purely Raman active vibrations of liquid pyrazine. From their results, it has been determined that SERS appears after reduction of only a small part of the AgCl formed during the oxidation phase in amine/KCl solutions. The time development

of SERS from silver electrodes immersed in chloride and thiocyanate electrolytes has been measured during and after oxidation-reduction cycles of the linear scan and double step type by Philpott and Weaver et al.[85] Raman spectra were recorded in times as short as 0.1 s. Correlations were found between Raman spectra and the current-potential-time curves. In mixed electrolytes the displacement of one anion by a more strongly adsorbing anion was observed. In addition, unexpectedly large effects of laser irradiation and hydrogen evolution prior to the oxidation-reduction cycle have been observed in the intensity of SERS bands. These last two effects were attributed to the formation of peculiar surface morphologies. Their work described representative results demonstrating for Ag electrodes that intensity, band shape and peak frequency are all affected by adjusting the parameters specifying the ORC.

A topic of prevailing importance in electrochemistry concerns the elucidation of complex reaction mechanisms at electrode surfaces. While the judicious application of conventional electrochemical perturbation methods can provide a surprisingly detailed picture, it has long been recognized that it is desirable to supplement this with the more molecule-specific information as furnished by *in-situ* optical spectroscopes such as TRSERS. Perhaps one good approach for obtaining coupled SERS and electrochemical information for electrode processes involves linear sweep voltammetry (LSV) and cyclic voltammetry (CV), because current/potential responses arising primarily from adsorbed as well as from diffusing species can be brought about by suitable choices of potential sweep rate, bulk reactant concentration, and so on. Coupling LSV or CV with SERS requires acquiring a series of Raman spectra on a time scale commensurate with the potential scan. By using multichannel detection, individual spectra can be obtained sufficiently rapidly to enable conventional LSV or CV conditions to be used. Gao and Michael et al.[86] have illustrated

applications of LSV/SERS, by using a conventional spectrograph/diode-array detector arrangement, to the elucidation of irreversible redox transformation involving aromatic adsorbates at the gold/aqueous interface. The examples involve the electro-oxidation of surface-attached benzidine and the electro-reduction of azoxybenzene. The most significant limitation of the arrangement in their work was that the relatively long (1-5s) integration time was required to obtain satisfactory signal-to-noise (S/N) ratio, coupled with the desirability of recording a large number of spectra to provide sufficient resolution with respect to electrode potential. This restricts the sweep rates that can be used to below ca. 50 mV/s. Nevertheless, for such "single-shot" spectral acquisitions, involving measurements made during a single linear-sweep voltammogram, the array detector provides a crucial, as well as substantial, time-scale advantage over the alternative scanning monochromator method of spectral acquisition. This approach also has been used to examine potential-dependent adsorption and redox processes by other research groups.[87-88]

In order to get more insight into the redox reaction process, it is of crucial importance to know what kinds of species (or radicals) are present or formed in the processes and to determine the interaction mode of the species with the electrode surface. Some representative radical ion systems which have been studied by our laboratory and other research groups include viologen homologs, *p*-nitrobenzoic acids (PNBA), and *p*-substituted pyridine compounds.

1,1'-diphenyl-4,4'-bipyridinium compounds have been extensively studied at electrode surfaces because of their use as electron mediators,[89] electrochromic display materials,[90-92] surface adsorbates for modified electrodes,[93] and redox reagents in photoelectrolysis systems.[94] The resonance and surface Raman spectroscopy of the dications methylviologen (MV^{2+}) and heptylviologen (HV^{2+}) have been broadly studied by many research

groups.[95-101] T. Lu et al. in our laboratory have shown[97] that the SERS spectrum of three redox forms of methyl viologen, $MV^{2+\cdot}$, $MV^{+\cdot}$, and MV^{0}, can be observed on a roughened Ag electrode as the potential is moved from -0.1 V to -1.1 V. Osawa et al.[102-103] have applied time-resolved resonance Raman scattering to study the initial stage of the monocation radical formation from 1,1'-diphenyl-4,4'-bipyridinium dication (HV^{2+}) at a platinum electrode surface. The time-resolution of their measurement system is about 5 ms. Recently, Y. Misono and K. Itoh et al.[104] constructed a time-resolved Raman scattering electrospectroscopy apparatus, which allowed them to observe spectra of electrochemically generated species near and /or at electrode surfaces with a time-resolution of submilliseconds. In their report, time-resolved SERRS spectra were measured for the monocation radical of heptylviologen ($HV^{+\cdot}$) formed on a silver (Ag) electrode surface as a function of time after switching the electrode potential from -0.2 V (vs Ag/AgCl) to -0.65 V (the monocation radical formation potential). The time-resolved SERRS studies reveal new kinetic and structural aspects of the monocation radical film formation processes of HV^{2+} at electrode surfaces. They conclude that the radical formation at the smooth silver electrode surface proceeds following three steps; the first step consists of an instantaneous formation of nuclei and subsequent three-dimensional growth of the nuclei; after the nuclei cover the electrode surface by 1 monolayer of the radical film, the process is switched to one-dimensional diffusion-controlled film growth (the second step). When the radicals are accumulated forming 2 or 3 monolayers the process is converted to another one-dimensional diffusion-controlled process (the third step), the rate of which is smaller than that of the second step.

P-nitrobenzoic acid, PNBA, in an alkaline medium is photo-electrochemically reduced on roughened Ag electrodes.[105] In the presence of the laser excitation, a time dependency in the spectra is observed even at

potentials positive to the electrochemical reduction wave.[105] This behavior was attributed to a photoinduced reduction process. The electroreduction of this kind compounds is a complicated process which has received much attention.[106-108] Investigations of the electroreduction of nitrocompounds have been carried out by time-resolved SERS on slower time scales in order to identify products or intermediates,[86,109] however, only the long-lived or stable intermediates were detected since the time scale was in seconds. Shi et al. in our laboratory have applied a single shot TRSERS method to elucidate the mechanism of electrochemical and photoelectrochemical reduction of *p*-nitrobenzoic acid on a Ag electrode in basic solution.[110-111] The single shot TRSERS method employed a triggered shutter and sequential triggering of the OMA on a triangular potential sweep or a potential step. Rapid scan TRSERS spectra (10 ms to 100 ms dwell time) were obtained at various times on CV sweeps or on a potential step. These *in-situ* TRSERS spectra during the CV experiment show that *p*-nitrosobenzoate, hydroxylamine, and azoxy compounds appear in the reduction process and are stable in certain regions of potential. Furthermore, by using a step potential waveform, they were able to observe TRSERS spectra of a transient intermediate species which they attribute to the *p*-nitrosobenzoate radical anion. The life time of this transient species on the Ag electrode surface is about 70 ms. On the basis of the TRSERS results which show spectral lines which can be assigned to the nitro, nitroso, nitroso radical anion, hydroxylamine, and azoxy compounds, an overall electrode process for the electrochemical mechanism of reduction of *p*-nitrosobenzoate on Ag have been proposed.

Many *para*-X substituted pyridine (C_6H_5X) compounds are electrochemically active in the negative potential range (-0.9 V to -1.2 V vs. SCE) on Ag. Shi et al. in our laboratory have found,[112] using TRSERS studies, that when -X is a cyano group (-CN), aldehyde group (-CHO), or hydroxymethyl (-

CH_2OH) group that a radical can form which then dimerizes to form products. These mechanisms are complicated because further reduction usually takes at the electrode surface. TRSERS in a pump-probe mode has been used to study these reactions, with a voltage step from relative positive potential to relative negative potential as the pump and a 488 nm Ar^+ CW laser as the probe with a gated detection on a linear diode array detector. For 4-cyanopyridine (4-CNPy), a dimerization reaction occurs when the parent compound is both adsorbed on the surface and in the bulk solution at relatively high concentrations. At low bulk concentrations, however. the molecule is directly reduced at Ag to pyridine and cyanide. For 4-pyridine carboxyaldehyde (4-CHO-Py), an intermediate radical species (Py-CHOH·) is formed, then further reduction of this radical species gives the product, 1, 2-bis (4-pyridyl) ethane (BPE), Py-CH_2-CH_2-Py. An overall reduction process has been suggested. Similar study also have been reported on 4-hydroxymethylpridine (Py-CH_2OH) compound.

Another important class of multiple-step electrode processes involving complex (and often unknown) pathways is provided by aromatic reactants in protic media. The suitability of such processes to examination by TRSERS has been evidenced by the rich and structurally revealing spectra provided by aromatic adsorbates on gold electrodes.[113-114] In particular, the sensitivity of the Raman spectra even to subtle structural changes in substituent groups makes this approach a potential powerful means of examining redox-induced structural transformation for such adsorbates.

An understanding of the photochemical process is challenging not only because of its fundamental biological importance, but also because such knowledge could provide insights regarding the development of efficient artificial photoelectrochemical devices. An interesting research is to model photosynthetic charge transfer reactions at electrode surfaces[115]. TRSERS has

proven to be an useful technique to investigate photoinduced electron transfer or charge transfer processes. For example, in the study of the time evolution of the SERS spectrum of *p*-nitrobenzoate adsorbed on Ag island films and roughened Ag electrodes, Sun et al. in our laboratory found that a red-shifted photoinduced charge transfer process occurs at the Ag-adsorbate surface as a result of illumination with 488 nm Raman excitation light.[105] This process involved electrochemical and chemical reactions coupled to the photoprocess, causing spectral changes to takes place in the millisecond to second time range.[105,110-111] The rate of photolysis was determined as a function of photon flux, excitation energy, electrode potential, and the nature of the solvent. Franzke and Wokaun[116] have used TRSERS to study the mechanism of photochemical decomposition reactions of azosulfonate (Azo) compounds, and of the model compound 4-nitrobenzoic acid. The reactants are deposited onto silver island films by spin coating. Subsequent to pulsed excimer laser irradiation at 308 nm, Raman spectra are excited using a cw visible laser. In the case of 4-nitrobenzoic acid, the formation of an azodibenzoate radical recombination product is confirmed. For azosulfonate, the photolysis yield has been determined by monitoring the decrease in Raman intensities of the -N=N- stretching mode at 1486 cm^{-1} and of the 1064 cm^{-1} skeletal vibration. Their experiments show that SERS on silver island films is a suitable technique for monitoring the course of selected photochemical reactions.

Another example of photochemical reactions that have studied by TRSERS is the biologicol cofactor flavin mononucleotide (FMN). Flavin mononucleotice is a coenzyme which plays an important role in redox enzymes and is well known to have interesting excited state chemistry.[117] It has also been used as a reagent to produce a highly oxidizing excited state redox species in a photogalvanic cell which utilizes solar energy to oxidizes organic material at

the illuminated electrode and reduces H^+ to hydrogen gas at the dark electroder.[118] The photochemical decomposition of FMN on a Ag colloidal surface has been observed by Lee et al..[119] The direct photoinduced charge transfer from adsorbed FMN to a Ag electrode has been observed by Zhang et al. in our laboratory, using a *n*s pulse laser pump-cw laser probe TRSERS system.[120-121] Two short-lived photoproduct radical ion intermediates were observed, as the enol and keto forms of a photo-oxidized falvin monocation radical in aqueous and deuterated solution. After 337 nm excitation the first product, an enol configuration of the FMN cation which formed by electron injection to the metal and an intramolecular proton transfer, is obtained within the laser pulse duration plus an instrumental delay of 75 ns. It then decays to the second photoproduct, a keto configuration of the FMN cation by 775 ns. New mechanisms of photoinduced charge transfer between FMN and a Ag electrode and the photogalvanic effect on a dye-modified metal electrode are proposed based on these TRSERS results.[117]

The development of TRSERS methods for the ns time scale should lead to the study of many other surface processes of adsorbed molecules on SERS active metals. This development will depend mainly on finding systems which have a high SERS scattering cross section and which undergo a reversible surface process.

Chapter III

Experimental Techniques

3.1 Steady State SERS Experimental Setup

The basic elements of the SERS experimental setup used in this thesis are identical to those used in a normal Raman or resonance Raman instrument, except for the Raman cell, or in our code a SERS cell. The SERS measurements in this thesis are made at a Ag electrode surface and the SERS cell is an electrochemical cell which contains an activated Ag electrode surface with adsorbed molecules, or ions which are the scattering centers for the incident laser light. The potential of the Ag SERS electrode is controlled by a potentiostat coupled with a waveform generator. A block diagram of a computer-interfaced scanning monochromator SERS instrument with photon counting detection is shown in Figure 3.1. Detailed explanation is as following:

The excitation radiation source we used for SERS is a continuous wave (cw) argon-ion laser (Spectra Physics Model 164). The band at 488 nm is used as Raman excitation source for all experiments in this thesis.

An interference filter is used and placed in the optical path before the focusing lens to eliminate unwanted lasing lines and plasma emission lines from the gaseous ion laser sources.

A collection lens with low f number is used to collect as much scattered light as possible, and the f number of the second lens should match that of the monochromator in order to optimize the optical system.

The electrochemical cell is a three-electrode cell consisting of SERS-active Ag electrode, a platinum wire counter electrode, and a reference electrode. Many different three-electrode cell designs have been used in SERS experiments. The cell which we designed and used will be discussed in the next section 3.2. Pretreatment methods for obtaining a SERS-active Ag electrode also will be discussed in that same section.

A scanning double monochromator (Spex Model 1401) is used to disperse the SER scattered light, and a photomultiplier tube (PMT, model FW-130/72, Products For Research. Inc.) serves as the detector. The operation mode of PMT is photon counting. The output anode pulses of the PMT are fed to a low-noise amplifier whose output then goes to a pulse-height discriminator. The pulse-height discriminator level is set to pick up the largest number of signal pulses while rejecting background (dark-current) pulses. The pulses from the discriminator then are counted by a digital counter which is interfaced to a digital computer (PC compatible model 386). The spectrum then is stored on magnetic medium and displayed through a monitor or in hardcopy form on a printer.

The advantages of this system are its high spectral resolution, good spectral range (about 100-4000 cm^{-1}), and very sensitive detection with a high-quality cooled photomultiplier tube and photon counting detection. Properly selecting entrance and exit slit widths (60 μ m), scan rate (20 cm^{-1}/min), and data acquisition time (1.2 s), we can successfully resolved two peaks with a difference of 1.6 cm^{-1} at around 19,436 cm^{-1}. All steady state SERS spectra in this thesis are recorded by this scanning spectrometer system.

3.2 SERS Cell And Pretreatment Of A Ag Electrode

A SERS cell which we have designed for use with a 90° scattering geometry is illustrated in Figure 3.2. This cell has two compartments connected by salt bridge. The working compartment is very small so that, if necessary, 0.5 ml sample solution is enough for taking SERS spectra. The optically flat window of the working compartment of this cell has been made at an 45° angle to facilitate the 90° scattering angle with the laser beam. The Ag electrode is also

cut at a 45° angle to make the electrode working surface parallel to the optical window. Thus, the electrode can be positioned as close to the window as possible. The small thickness of the solution pathlength (a few millimeters) between the electrode surface and the window greatly reduces the amount of Raman scattering from solution and absorption of the scattered light in the solution. The design of this cell also allows us to bubble inert gas (N_2 or He) for deoxygenation and to purge inert gas during the experiment to prevent oxygen from redissolving.

As we discussed in chapter 2, there are two main enhancement mechanisms operating. One is an electromagnetic (EM) enhancement that can be observed for small metal structures on the size order of 10-100 nm (large-scale metal surface structures), and another is a charge transfer (CT) resonance Raman type enhancement related to adatoms or adatom clusters (atomic-scale metal surface structures). Both of these types of surface roughness can be created by various pretreatment methods, such as electrochemical oxidation reduction cycle (ORC), electrodeposition, chemical deposition, chemical etching, and coldly evaporating metal films in an ultrahigh-vacuum system, etc.. In this thesis, we have used two pretreatment methods, which are electrochemical oxidation-reduction cycle (ORC) and constant potential deposition, to create a SERS-active Ag electrode surface.

The electrochemical instrumentation necessary for the ORC and electrochemical deposition includes a potentiostat (EG&G PARC Model 173) and a waveform generator (EG&G PARC Model 175). The latter should be capable of generating a potential pulse and a triangular waveform on top of an initial potential. In the double potential step ORC procedure, the Ag electrode is first polished with a finely divided alumina slurry (0.3 and 0.05 μm), cleaned with deionized distilled water, and ultrasonicated in distilled water to remove any

adhering alumina. The initial potential is set negative to the onset of Ag oxidation, and then the electrode potential is stepped to a potential where Ag oxidation occurs. The dwell time at the potential of oxidation is typically 1-5 s, or determined empirically. When the sample molecule is a weakly adsorbed neutral molecule or a cation, an electrolyte containing an anion can form a precipitate with the Ag ion produced by the oxidation of the electrode, is generally used, e.g. KCl. In this case the sample molecule is coadsorbed with the anion and a precipitate film is formed on the Ag electrode surface by oxidation of electrode, which can then be reduced back to a roughened surface with metallic nodules by potential reversal. When the sample molecule is a strongly adsorbed species, it is best to use an electrolyte solution such as K_2SO_4, which does not precipitate Ag ion, so that the anion of the electrolyte does not displace the sample species from the Ag surface after the ORC pretreatment. In this case, a concentration gradient of Ag ion is formed in the diffusion layer and on potential reversal the diffusing Ag ion is reduced to form the roughened SERS-active surface. K_2SO_4 was chosen to use in the experiments reported in this thesis. In fact, the electrochemical oxidation reduction cycle method is the most common way to create SERS activity at silver electrode surfaces. Especially, when the sample molecule is present during an ORC, the SERS intensities are much stronger than when the sample molecules are added after the ORC. To avoid oxidation of the test molecules by ORC, another technique is to make roughened SERS-active surfaces by direct reduction of silver ions, such as by electrochemical deposition.

In constant potential deposition procedure, the polished Ag electrode was dipped in the 0.05 M $AgNO_{3\,aq}$ solution with the presence of sample molecules ($2X10^{-5}$ M). Then a reduction potential of -0.4 V was applied on the working electrode (Ag) for 10-12 seconds. Ag^+ ions in the solution were reduced and deposited on the Ag electrode together with sample molecules. Nonadsorbed

sample molecules were then washed out from the electrode surface by deionized-distilled water. After the *ex-situ* pretreatment, the activated Ag electrode was placed in 0.1 M K_2SO_4 aqueous solution for carrying out SERS and TRSERS experiments at certain potentials. The SERS spectra obtained from the two procedures are exactly the same in the region of 100-2000 cm^{-1}, but the intensity of Raman signals in the second procedure is stronger. Thus, in the TRSERS experiment the second procedure has been used for activating electrode.

3.3 Time-Resolved SERS Experimental Setup

Although the scanning spectrometer with a PMT detection which we discussed in section 3.1 is very sensitive, the simplex mode of recording a spectrum consumes a rather large amount of time. With a scan rate of 50 cm^{-1}/min, it takes 20 min to record a 1000 cm^{-1} region of a SERS spectrum. This disadvantage eliminates recording an entire band in a dynamic study. Thus a nonscanning spectrometer with a multichannel detector has to be used for time-resolved purpose.

In this thesis a triplemate monochromator (model 1877, SPEX industries, Inc.) coupled with an intensified photodiode array (IPDA, model 1455, EG&G PARC) which is controlled by an optical multichannel analyzer (OMA) is used for the time resolved experiments.

In order to suppress the grating scatter from the Rayleigh light, the triple monochromator is mounted where the front end is a double monochromator in a subtractive dispersion mode. This stage produces a nondispersed spectrum while rejecting nearly all of the Rayleigh scattered light. The final stage is a

single grating monochromator which disperses the spectrum on a flat focal plane which is coupled to the multichannel detector IPDA.

The IPDA we used is a linear array of discrete diodes with an intensifier. Sensitivities in the range of a good PMT can be attained. When dispersed photons from the triplemate strike the IPDA, a charge pattern in the diodes is produced, which can be periodically read out into an laboratory computer. Such a linear diode array device with 1024 discrete diodes spaced over 25.4 mm allows a SERS spectrum covering about 1000 cm^{-1} to be recorded by the laboratory computer in a short time span. The limit of recording speed is 30 milliseconds in the nongated mode. With gateable intensifiers, the limiting recording speed is 100 nanoseconds. The complete detection instrument is usually referred to as an optical multichannel analyzer (OMA). The use of an OMA device for recording SERS spectra not only has the advantage of fast recording of a single spectrum but also allows successive spectra to be recorded as a function of time for kinetic studies or as a function of electrode potential for three-dimensional recordings of SERS intensity-wavenumber-potential plots.

In more detail, the OMA (EG&G PARC) system that was used for this thesis includes a model 1461 main controller, a model 1303 gate pulse interface, a model 1304 gate pulse amplifier, a model 1302 high voltage fast pulser, and a model 1455 IPDA detector. The entire system was controlled by a Macintosh computer through the model 1461 main controller. The program MacOMA version 1.02 was used to take spectrum and to process data. The model 1455 IPDA detector can operate either in a gated detection mode or normal detection mode. When operating in the normal detection mode, the detector is activated by the "scan" command of the program with the shortest data acquisition time, 30 ms. When operating in the gated detection mode, the detector only integrates signal while it is supplied with a -200 V high voltage gate pulse from the model

1304. The model 1304 only amplifies TTL gate pulse signals from the model 1303, and outputs -200 V high voltage gate pulses to activate the detector with the same gate pulse profile as that received from the model 1303. The model 1303, which was controlled by the model 1461, outputs a TTL gate pulse to the model 1304 after receiving an input trigger signal which can be either an optical pulse or an electrical pulse. The delay time between input trigger signal and output TTL gate pulse was determined by the program, MacOMA version 1.02 with a 1 ns time interval increment. The TTL gate pulse width also can be programmed from 100 ns to 13 ms. With system model 1303 and 1304, the instrument has an intrinsic delay time of 75 ns which includes trigger pulse input at the model 1303 and high voltage gate pulse output (-200 v) at the model 1304 detector. Therefore, the minimum delay time of this system is 75 ns and the minimum gate width is 100 ns.

As in the scanning spectrometer, a small f number (f/d=1.2) lens, is placed near the electrode cell to collect as much Raman signal as possible. A second lens should match the f number of the triplemate monochromator. Using this OMA and optical system, two TRSERS experiment methods have been designed as follows, with a spectral range of 850 cm^{-1} and a resolution of about 1.2 cm^{-1}/channel.

3.3.1 Single-Shot Time-Resolved SERS Method

Figure 3.3 shows the diagram of the experimental set-up that we have used for a single shot method.

The single-shot TRSERS instrumentation has proven to be a powerful tool for studying electrochemical reactions. An Ar^+ laser was used as SERS probe source with output laser power of 140 mw and about 30 mw at electrode surface.

An excitation wavelength of 488 nm or 514.5 nm was used in most of our experiments. An electronic shutter was used to eliminate possible photoinduced chemical reactions by the probe beam. The full open time of the electronic shutter is shorter than 7 ms. A potentiostat and a waveform generator was used to initiate an electrochemical reaction by applying a potential on the working electrode. The delay time from the trigger-in signal at the waveform generator to the potential applied on the electrode is a few μ s which is fast enough to carry out the single-shot TRSERS which is normally in the ms time scale. An OMA system operating in the normal detection mode, as discussed as above, was used for detection of the TRSERS spectrum. The trigger generator is used to synchronize the electronic shutter, the pump potential (the potential for initiating an electrochemical reaction), and the OMA detection system. In our laboratory, we can obtain very reasonable signal to noise ratio for SERS spectra with exposure times of about 30 ms for most of organic compounds with this OMA system. With data acquisition mode 7 of the OMA system, 12 single-short spectra with the same exposure time can be recorded one by one continuously. This method can be applied to ms or longer time domain TRSERS. Since some electrochemical reactions, many chemical reactions following electrochemical reactions, as well as adsorption/desorption processes takes place in the ms time domain, this system proved very successful for the study of electrochemical dynamics. The advantage of this system is that it can be applied for studying both reversible and irreversible reaction since no repetitive pump-probe detection is required. Figure 3.4 shows the time sequence of single-shot detection which was applied to monitor a cyclic voltammetry process.

3.3.2 Optical Pump-Probe Time-Resolved SERS Method

Figure 3.5 shows the diagram of the experimental set-up that we have used for a optical pump-probe method

Due to instrumental limitations, we applied a nitrogen pulse laser (Model NRG-0.5-150/B, National Research Group, Inc.) as a pump source and a cw Ar^+ laser (Model 164, Spectra Physics) as a probe source. The system shown in Figure 3.5 proved successful for time resolved SERS from 200 ns to the ms time domain. The pump pulse of 337 nm from the nitrogen laser and the probe beam of 488 nm from the Ar^+ laser were focused on Ag electrode on which the test molecules were adsorbed. A dichroic mirror which totally reflects the 337 nm laser light was placed at 45^0 to the normal of the incident nitrogen laser beam and transmits the 488 nm probe beam, allowing the two laser beams to overlap at the electrode. In order to ensure the overlap of the pump pulse with the probe beam and to avoid surface damage, we defocused the 337 nm laser pulse at the electrode to about a 0.1 cm^2 size, and focused the 488 nm beam to about a 60 μ m diameter size.

A very small portion of the pump pulse ("leaked" from the dichroic mirror) was collected by an optical adapter and transmitted through a fiber optics to trigger the model 1303 gate detection system, OMA (EG&G PARC). In this method the OMA was set in the gated detection mode. After receiving the optical pulse trigger signal, the model 1303 outputs a TTL gate pulse which has a delay time t_1 which is related to the trigger-in optical pulse signal, and has a pulse duration t_2 (so called gate pulse width) to trigger model 1304. The t_1 and t_2 of the TTL gate pulse can be preset by program through the Macintosh computer and are determined by the intensity of SERS signal from intermediate and the life time of the intermediate. The model 1304 amplifies the TTL gate pulse which is

from the model 1303 and outputs a high voltage gate pulse, -200V potential to activate the gate detector. The gate detector, model 1455 operating in the gate mode, only records SERS signal while it is gated by the gate pulse, the -200 V potential. Therefore, the SERS signal detected by the gate detector is that delayed by time t_1 from the nitrogen laser pump pulse and the signal integrated within the gate pulse time t_2. If an intermediate is formed on the electrode by the pump pulse with a life time longer than t_1+t_2, the SERS spectrum obtained will represent the intermediate information. The timing sequence for pump-probe instrumental set up is shown in Figure 3.6.

Since the delay time t_1 was limited by the instrumental intrinsic delay time (75 ns) and the gate width t_2 was limited by SERS signal intensity from intermediate, the shortest time resolution of the TRSERS spectra which we obtained by this method is 75 ns time delay after pump pulse with a 200 ns gate width. At this time data acquisition mode 5 from MacOMA program version 1.02 (EG&G, PARC) was used for gated repetitive detection. With 25,000 pump-probe repetitive scanning, good TRSERS spectrum can be obtained.

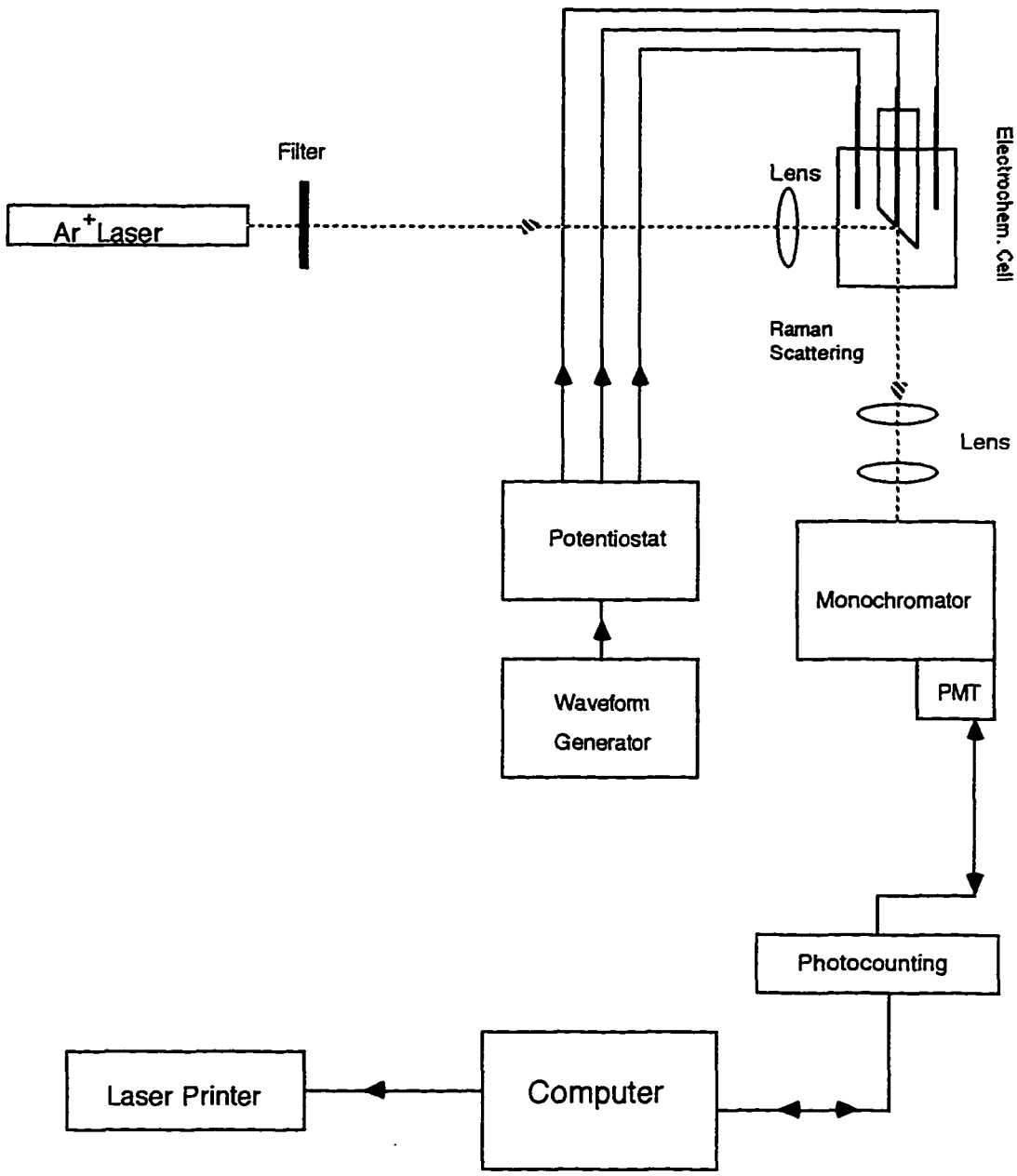

Figure 3-1. Surface enhanced Raman scattering instrumental system

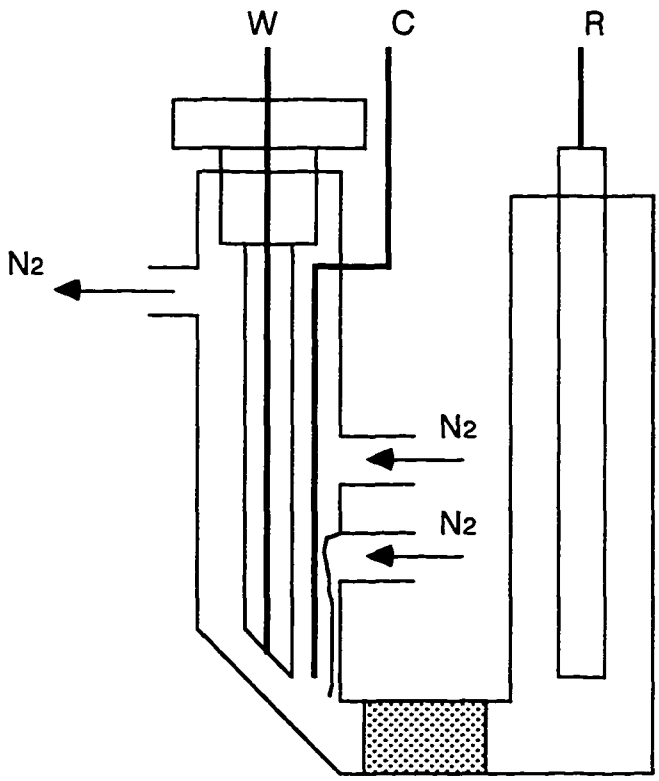

W: Working electrode,
C: Counter electrode,
R: Reference electrode.

Figure 3-2: Micro SERS Cell with 90° Collection Geometry.

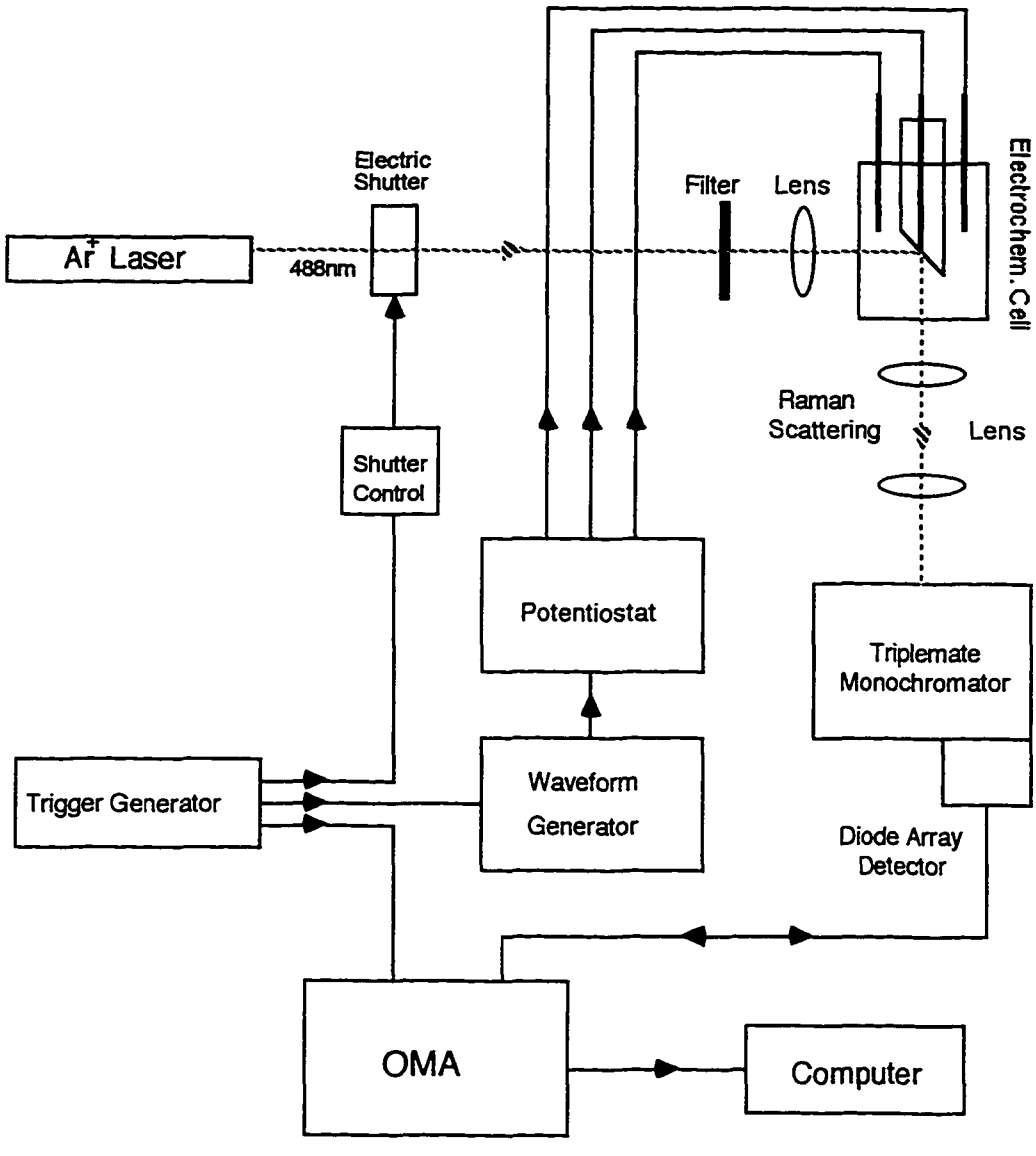

Figure 3-3: Single-Shot TRSERS Instrument for ms to second in-situ real-time detection of potential induced reaction

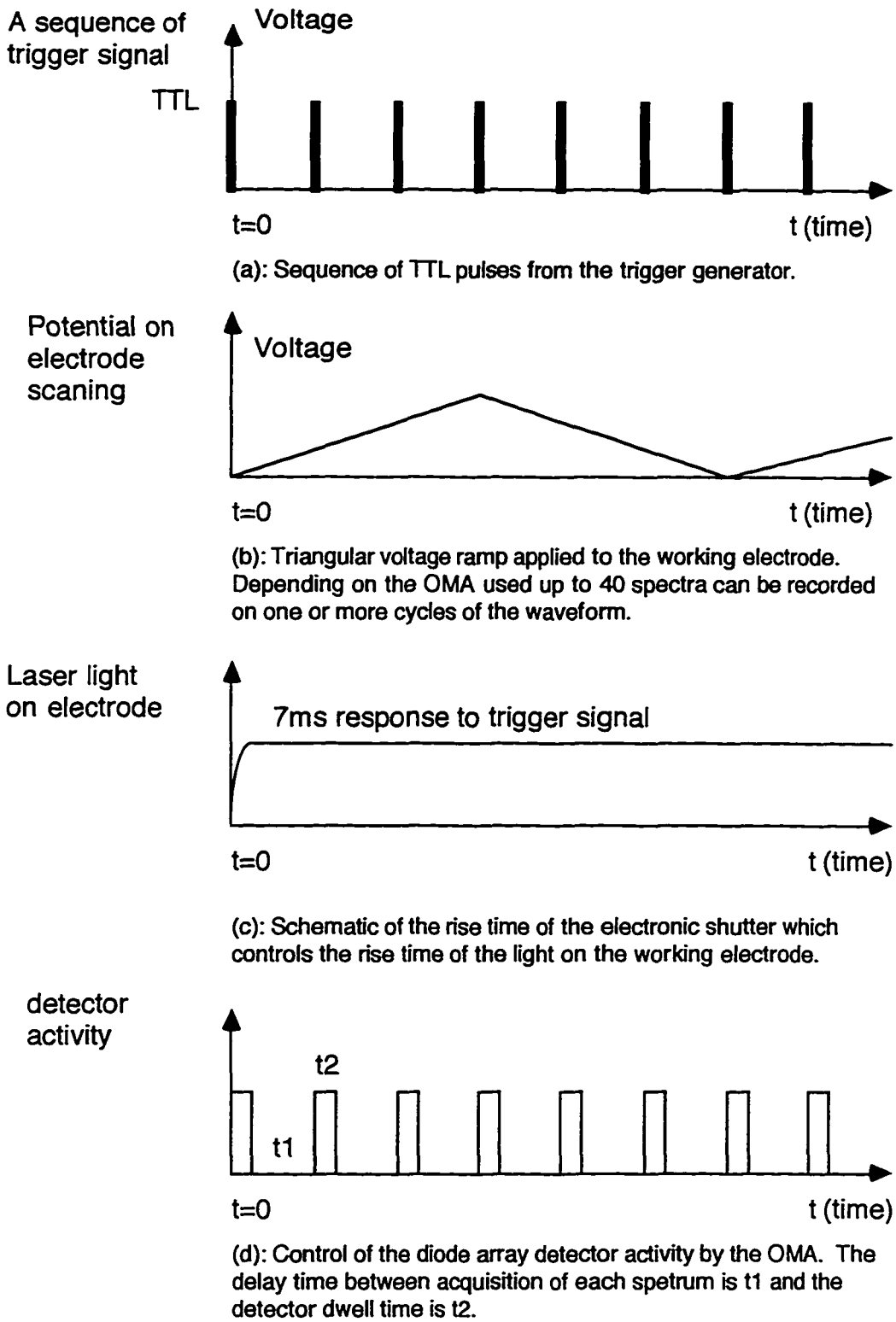

(a): Sequence of TTL pulses from the trigger generator.

(b): Triangular voltage ramp applied to the working electrode. Depending on the OMA used up to 40 spectra can be recorded on one or more cycles of the waveform.

(c): Schematic of the rise time of the electronic shutter which controls the rise time of the light on the working electrode.

(d): Control of the diode array detector activity by the OMA. The delay time between acquisition of each spetrum is t1 and the detector dwell time is t2.

Figure 3-4: Timing sequence for TRSERS measurements with a voltage ramp waveform in the instrumental set-up of Figure 3-3.

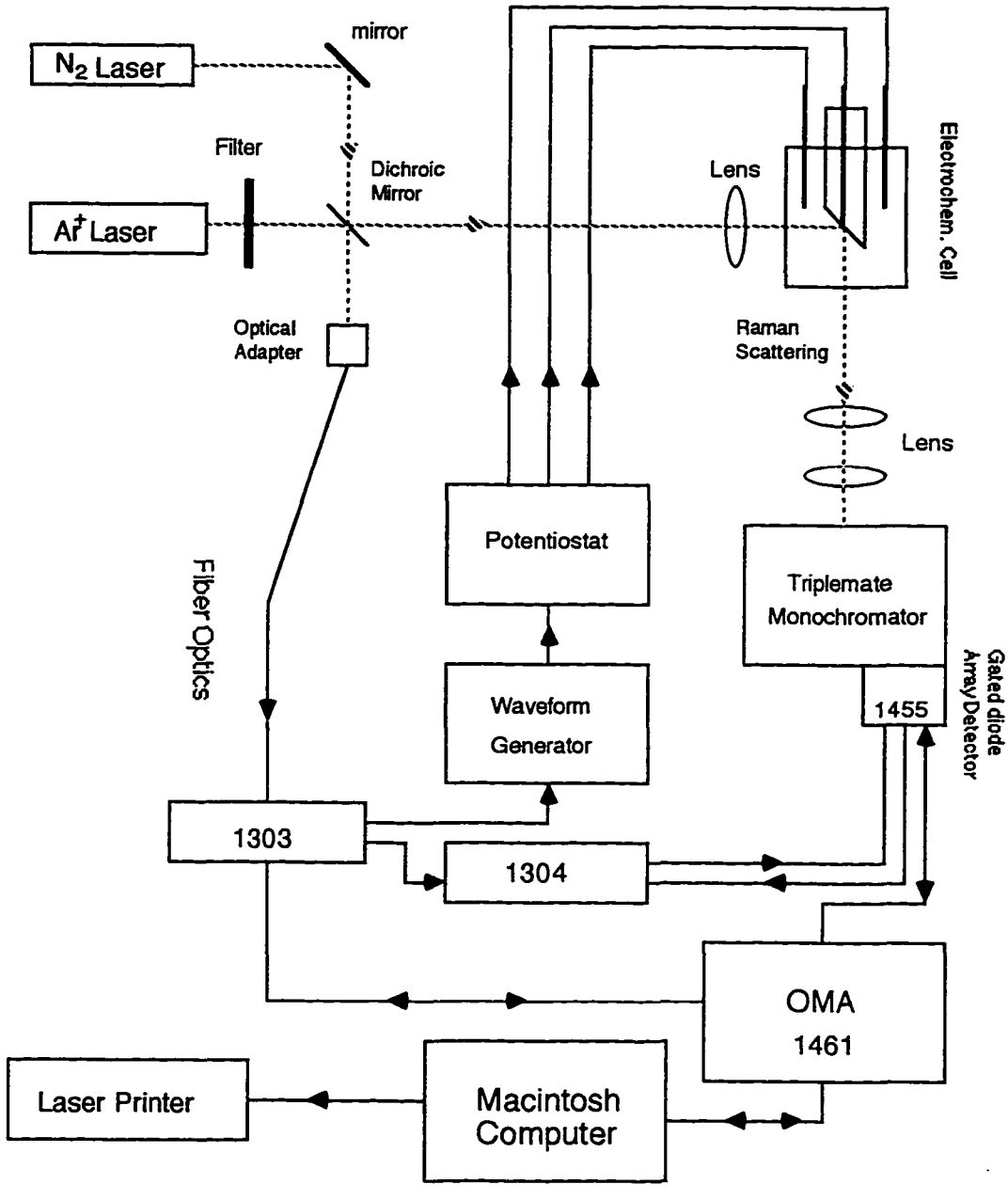

Figure 3-5: Optical pump-probe TRSERS instrument for ns time scale photoinduced surface photochemistry studies

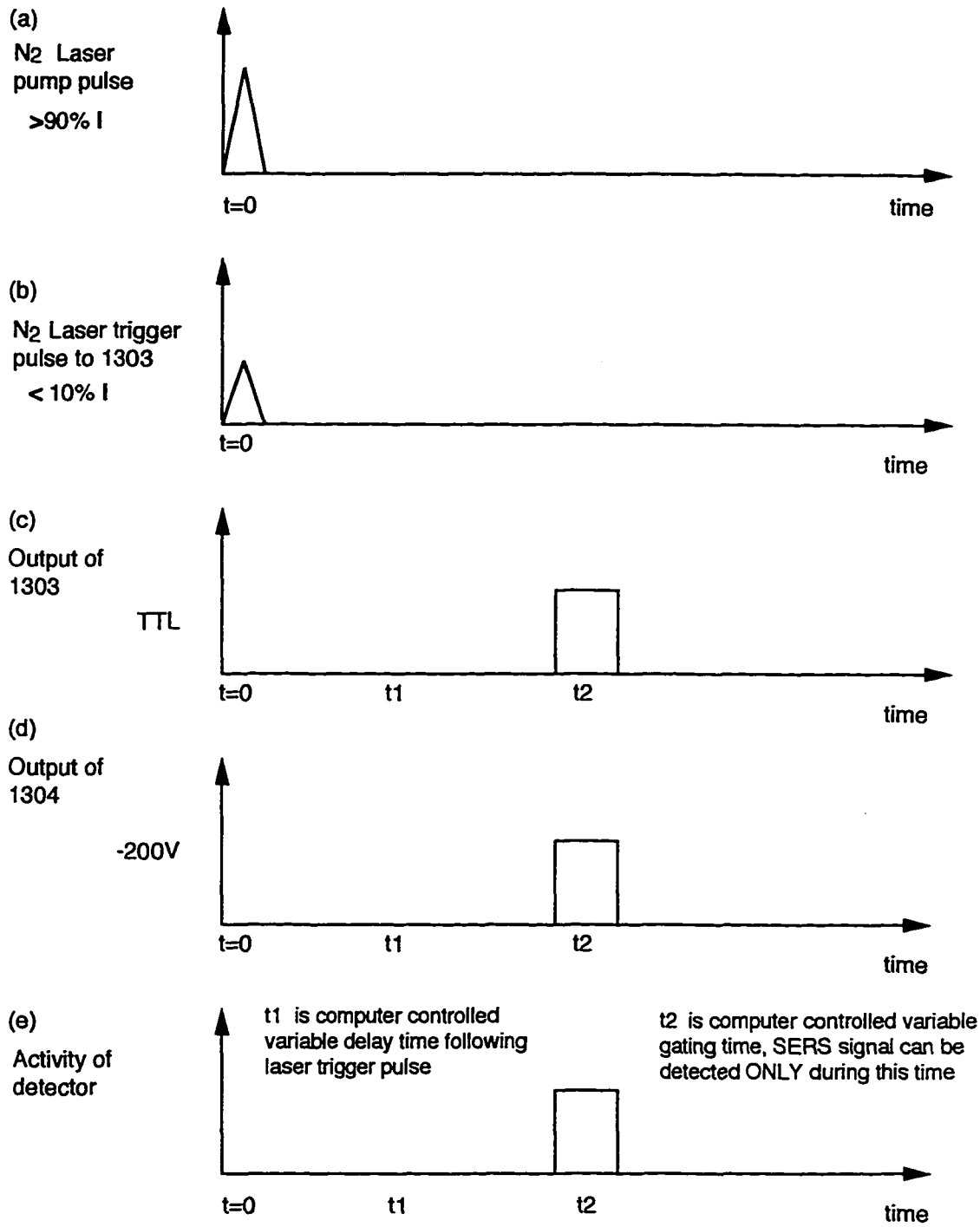

Figure 3-6: Timing sequence for the pump-probe instrumental set-up of Figure 3-5.

Chapter IV

SERS Study of the Mechanism of Oxygen Activation of Fe-Bleomycin

4.1. Introduction

Bleomycin (BLM) is a DNA-cleaving glycopeptide antibiotic which is clinically used for the treatment of various types of cancer.[1] It has been shown that bleomycin is capable of forming 1:1 complexes with Fe(II), Zn(II), Cu(II), and other transition metal ions. Of these metal complexes, only the Fe(II) complex, when binding with oxygen, is active in the cleavage of DNA.[1,2] The complex of Fe-BLM, despite its lack of a heme prosthetic group, resembles several hemoproteins in its ability to activate oxygen.[3] For example, an oxygenated intermediate of ferrous bleomycin has been investigated by stopped-flow spectrophotometry, and it has been shown to give rise to ferric bleomycin.[4] How bleomycin uses oxygen to degrade DNA has been the object of several investigations for many years using a variety of physical and chemical probes such as NMR, EPR, optical absorption, cyclic voltammetry, NR and RR. Mainly there are two questions which attracted researchers: (1) the elucidation of the structure of various metal-drug complexes and (2) the oxygen activation mechanism of the drug, since they are crucial points for designing new medicines.

Knowledge of the local environment of the metal site in Fe-BLM complex is critical to understanding the mechanism of oxygen activation of the drug. Unfortunately, there is a lack of direct evidence concerning the ligands which coordinate to the metal in iron-bleomycin complex (Fe-BLM), and in oxygenated iron-bleomycin complex (O_2-Fe-BLM). Previous EPR and NMR spectroscopic investigations have identified six nitrogen atoms on the bleomycin molecule as potential ligands to iron in the ferric and CO-bound ferrous complexes.[1,5,6] Figure 4-1 shows the positions of these ligands and one proposed Fe-BLM complex structure. These potential nitrogen ligand atoms are (1^*) the primary

and (2^*) secondary amines of the β-aminoalanine residue, (3^*) nitrogen of the pyrimidine ring, (4^*) nitrogen of the imidazole and (5^*) amide nitrogen of β-hydroxyhistidine, and (6^*) the mannose carbamyl nitrogen. Takita et al.[7] proposed a structure for CO-bound ferrous complexes in which both amine functions (1^* and 2^*), the pyrimidine and imidazole groups (3^* and 4^*), the histidine amide (5^*), and the carbon monoxide molecule are chelated to the iron ion. Furthermore, Sugiura[8] has proposed that Fe(III)-BLM has an octahedral geometry with the β-aminoalanyl secondary amine (2^*), pyrimidine (3^*), imidazole nitrogen atoms (4^*), and β-hydroxyhistidinyl amide (5^*) bound equatorially, and the β-aminoalanyl primary amine (1^*) and hydroxide as axial ligands. At least two other structures, however, have been proposed. The group of Oppenheimer et al.[9,10] suggest that for the carbon monoxy-ferrous form of the drug (CO-Fe(II)-BLM), both β-aminoalanyl amine nitrogen atoms (1^* and 2*), the pyrimidine (3^*), and imidazole (4*) are equatorial ligands and the mannosyl carbamyl group (6^*) is bound axially. Thus, instead of the histidine amide, the mannose carbamyl group is coordinated to the iron ion. Akkerman et al.[6] contended that the CO-Fe(II)-BLM has the secondary amine (2^*), pyrimidine (3^*), imidazole nitrogen atoms (4^*), and β-hydroxyhistidinyl amide (5^*) as equatorial ligands and the sugar carbamyl group (6^*) was bound axially. Thus, there is a general agreement that the secondary amine, pyrimidine, and imidazole are equatorial ligands to the iron, but there is still argument about the histidine amide, primary amine and mannosyl carbamyl groups.

Takahashi et al.[9] have studied the structural characterization of Fe-BLM by resonance Raman spectroscopy. They concluded that the β-hydroxyhistidinyl amide (5^*) is conjugated to the pyrimidine ring (3^*) in Fe-BLM and these two ligands together comprise a delocalized π-electron buffer similar in function to the electron-buffering capabilities of the porphyrin macrocycle. This delocalized

system may partially explain the similar spectroscopic characteristics and reactivity of Fe-BLM and heme proteins.

Horwitz and co-workers[2,11,12] were the first to show that Fe(II)-BLM is an air sensitive compound and that it readily oxidizes to Fe(III)-BLM in the atmosphere. They postulated that this oxidation process occurs in the tumor cell while the iron-bleomycin is bound to DNA, and that DNA damage is the result of radical production by iron-bleomycin in the vicinity of the biopolymer. Chemically defining the attacking species has been the important goal. Burger and co-workers[4,13,14] found there is an oxygen-ligated ferric drug species formed during the drug reaction which generates the attacking species, and they named that species "activated bleomycin" in which the bound oxygen is at the level of peroxide. The structure of the activated bleomycin and whether it is the attacking drug species need further confirmation.

An interesting research approach is to model the oxygen activation process of the drug complex at electrode surfaces, then study the drug complex structure and monitor the drug activation mechanism by surface enhanced Raman scattering (SERS) spectroscopy and time-resolved SERS (TRSERS) spectroscopy. SERS is able to provide intense vibrational spectra which give molecular structure information of the species adsorbed on the electrode. Also, SERS has been used for probing heme iron systems.[15,16] The quenching of fluorescence makes SERS reasonable for monitoring biological molecules which normally have relatively intense fluorescence when exciting by uv or visible light. More importantly, SERS can be combined with electrochemistry which can provide a controlled process of oxidation or reduction of the iron system. As we mentioned before, these oxidation or reduction processes occur when the iron-bleomycin is bound to oxygen. There are several ways that have been reported to form activated bleomycin. According to these chemical pathway, we have

designed an electrode potential induced electrochemical reaction to simulated the drug activation process as following: we used BLM and Fe (III) ions as initial reactants, after purging oxygen, supply electrons to them by applying a negative potential on the electrode. A superoxide species is supposed to form in the first reduction step. When second electron is added to the superoxide species, we may get 'activated bleomycin'. These electrochemical reductions should be similar to that chemical reductions proceeding in the drug system.[26]

In the present thesis, we report the first demonstration of surface enhanced Raman scattering spectra of the Fe-BLM complex in the ferric, ferrous, and O_2-ligated forms. We present evidence for pyrimidine and the β-hydroxyhistidinyl amide as ligands in Fe-BLM. Furthermore, evidence of the bound oxygen at the level of peroxide in one form of O_2-Fe-BLM has been obtained by TRSERS.

4.2. Experimental Section

Bleomycin (BLM) was a gift from Dr. Richerd Burger of Public Health Research Institute and Bristol-Meyer Co. and was used as received. Analytical grade $Fe_2(SO_4)_3$ was purchased from Fisher Scientific Company and Fe_2SO_4 was purchased from J. T. Baker Chemical Corp. Reagent grade K_2SO_4 served as electrolyte with concentration of 0.05M. BLM-Fe(II) and BLM-Fe(III) solution were prepared in a nitrogen bag with concentrations of $2x10^{-4}$ for SERS, $5x10^{-4}$ for cyclic voltammetry, and were bubbled with nitrogen gas for 20 min before starting each experiments. O_2-Fe-BLM was prepared from Fe(III)-BLM solution by bubbling with oxygen gas for half an hour. The pH of solutions were about pH 4.3, as measured by an Orion Research digital ionalyzer Model 720 pH meter.

The sample cell for SERS and electrochemistry is specially designed to have a nitrogen or oxygen purge on the top of sample solution during the experiment and only requires 0.5-1 ml sample solution for each experiment. The sample cell consists of an Ag working electrode, a Pt counter electrode, and an Ag/AgCl electrode as the reference. The potential applied on the Ag electrode is controlled by a waveform generator and a potentiostat (EG&G PAR Model 179 and 173). All potentials in this report are quoted vs. the Ag/AgCl reference electrode. The *ex-situ* oxidation-reduction pretreatment was carried in 0.1 M K_2SO_4 solution in the absence of BLM by applying a potential step from -0.3 V to +0.5 V for two seconds. The pretreated Ag working electrode then was transferred to the sample cell for SERS or electrochemistry experiments.

Cyclic voltammetry experiments were carried out with the same waveform generator, potentiostat and x-y recorder. Cyclic voltammograms were recorded at different scan rates on a smooth Ag electrode.

The SERS experimental setup was similar to that described else where.[16] A Spectra Physics Model 164 argon ion laser at 488 nm was used as an excitation source. The laser power at the electrode was approximately 30 mW. Steady state SERS spectra were record with a Spex Model 1401 double monochromator with a wave number resolution of 2 cm^{-1}. A photomultiplier tube was used as detector, operating in the photon counting mode.

Potential dependent SERS and TRSERS experiments were carried out by a SPEX triple monochromator coupled with gated diode array detector (EG&G PAR Mode 1455) and OMA system (EG&G PAR Mode 1461) which was controlled by a Macintosh computer. The instrumental set up was similar to that described in our previous work.[17] Laser and electrochemical systems used in the TRSERS experiments are the same as used in SERS experiments described above. Electronic trigging was used to synchronize the applied potential at the

electrode where reactions take place with the detection system. The detector gate width and delay time were controlled by computer software through the OMA system. In the potential dependent SERS experiments, SERS spectra were taken at a steady state electrode potential. While TRSERS spectra were taken by electronic synchronizing the detection with the applied reduction potential step from 0.02 V to -0.65 V at which the Fe(III)-BLM system must be reduced.

4.3. Results and Discussion

High-frequency region. The high-frequency region (800 cm^{-1}-1700 cm^{-1}) of the SERS spectrum of metal-free BLM at applied potential +0.02 V is shown in Figure 4-2. Only two broad bands around at 1520 cm^{-1} and 1320 cm^{-1} were observed in this region. The stronger band in the spectrum around at 1520 cm^{-1} is attributed mainly to Raman scattering of the bithiazole moiety in BLM.[9,18] Comparing with the normal Raman spectrum and resonance Raman spectrum of metal-free BLM, the band around at 1520 cm^{-1} in SERS is much broadened. The rather large line width of this band may be attributed to the following facts: (1) on an Ag surface many different sites for binding are available to the molecule causing a broadening in the vibrational mode which is most sensitive to surface interactions,[19] (2) the band can also attribute in some degree to the other vibrational modes in SERS because of the surface enhanced effect.[16,20] Examining the normal Raman (NR) and resonance Raman (RR) spectra of BLM,[9,18] there is one weak band at 1487 cm^{-1}, one very strong band at 1542 cm^{-1}, and one very weak band at around 1638 cm^{-1}. The intensity ratio of these three bands is about 5:54:1. Assuming that these three bands have a Gaussian shape and have the same line width, adjusting the intensity ratio of these three

bands based on considering the enhancement by SERS and then shifting them all to low frequency of the same amount 22 cm^{-1}, (i.e.. 1487->1465 cm^{-1}, 1542->1520 cm^{-1}, and 1638->1616 cm^{-1}), we obtained a simulated spectrum which overlaps with the SERS spectrum fairly well (see Figure 4-2). The simulation method is offered by "Origin 4.0' program. The strong band at 1542 cm^{-1} has been assigned to the bithiazole moiety in BLM in NR and RR spectra study. It is reasonable there is a frequency shift between NR and SERS. Thus, the simulation curve confirms that the strong band at 1520 cm^{-1} in SERS is mainly attributed to the Raman scattering of the bithiazole moiety in BLM, but it also has contributions from two other vibrational modes in BLM. In table 4-I the SERS bands of BLM are listed and compared with that of NR and RR. Figure 4-3 shows the well-resolved SERS spectrum of Fe(III)-BLM complex at applied potential +0.02 V. In addition to the band around at 1520 cm^{-1} (shown as a shoulder) and 1323 cm^{-1}, the spectrum of ferric bleomycin contains two stronger bands at 1568 cm^{-1} and 1465 cm^{-1}, and one new weaker band at 830 cm^{-1}. The observation of bands at 1568 and 1465 cm^{-1} further confirm the results of the simulation in Figure 4-2. Figure 4-4 shows that the same vibration modes were also observed in the SERS spectrum of oxygen-ferric bleomycin (O_2-Fe(III)-BLM) with a little frequency shift at applied potential +0.02V. These bands are at 1574, 1465, 1326 and 830 cm^{-1}. For convenience of analysis, the corresponding bands from RR and SERS of BLM and Fe-BLM are listed in Table 4-I.

The features of the SERS spectra of BLM and Fe-BLM complex in the high-frequency region can be summarized as follows: (1) The relativity intensity of the band at 1520 cm^{-1} is more intensive in metal free BLM, but low or has disappeared in Fe-BLM complex. However, the relativity intensity of other bands at 1568, 1465 1323 and 830 cm^{-1} are enhanced in Fe-BLM complex, suggesting the latter four bands may be all involved in the bonding with the central iron, but

that the band at 1520 cm^{-1} is not. This is consistent with the assignment for the band 1520 cm^{-1} attributed to the bithiazole moiety in BLM and not bound to the center iron. The fact that intensities of those bands are enhanced in Fe-BLM complex may be related to the formation of the macrocycle ring; or transitions caused by charge transfer between ligands and center metal in metal-drug complex.[9] (2) the frequency of the vibrational mode corresponding to the band at 1568 cm^{-1} is sensitive to the ligation states of the center iron. At the same applied potential +0.02 V, this band is observed at 1568 cm^{-1} without oxygen and is shifted to 1574 cm^{-1} when oxygen is bound to iron, and can be considered to be at 1616 cm^{-1} in metal free BLM as the simulation curve shows. This vibrational mode is also sensitive to the redox state of the central iron ion. This property can be examined through the Table 4-II, which is a list of the data from potential dependent spectra of Fe-BLM. The potential dependent spectra of Fe-BLM were obtained by preparing the solution with ferric ion (Fe(III) from $Fe_2(SO_4)_3$) and BLM, holding the potential at +0.02 V, then changing the potential, step by step, to a relatively negative value, -0.2 V. As the potential is changed, the redox state of iron is changed. One can expect that the spectrum at relatively positive applied potential corresponds to Fe(III)-BLM species and that the spectrum at relatively negative applied potential corresponds to Fe(II)-BLM species. Table 4-II shows that the band at 1568 cm^{-1} shifts to 1560 cm^{-1} as the applied potential is changed from +0.02 V to -0.2 V. (3) The band at 1465 cm^{-1} is symmetric and has a relatively narrow line width. Its frequency is only weakly dependent on the redox state of iron (shifted from 1465 cm^{-1} to 1463 cm^{-1} when the applied potential changed from +0.02 V to -0.2 V), it is not sensitive to ligation states of iron. (4) The band at around 1320 cm^{-1} is somehow sensitive to the ligation states of the central iron (at 1320 cm^{-1}, in metal free BLM, 1323 cm^{-1} in Fe-BLM and 1326 cm^{-1} in O_2-Fe-BLM), and is a broaden band whether in

metal free BLM or in the metal complex. (5) The new weak band at 830 cm^{-1} is not sensitive to ether the redox or ligation states of iron but is more broaden than the band at 1465 cm^{-1}. These different characteristics suggest that all these Raman features may arise from different portions of the BLM molecule.

We limited our assignment of the spectral features of the SERS spectra of Fe-BLM to only the six nitrogen atoms in the bleomycin molecule mentioned before. Among them, the two amines and the carbamyl moiety and the imidazole can be excluded according to the result of the NR and RR spectra of Fe-BLM.[9,18] There remain two candidates for ligands to the iron atom to account for the observed new bands in the SERS of Fe-BLM: the amide nitrogen of β-hydroxyhistidine and the nitrogen of the pyrimidine ring. According to Takahashi's explanation,[9] the amide group can chelate metal ions. Coordination can occur at either the oxygen or the nitrogen atom. Research has shown that for polypeptides the C=O stretching vibration of the amide moiety (amide I mode) is located at 1660 cm^{-1} in metal-free state and shifts to 1625 cm^{-1} when the amide nitrogen is bound to a metal.[9,21] We can infer in the SERS experiment that this mode will shift further to lower frequency since there is a chance that both oxygen and nitrogen atom could be bound to metal atoms, one could bind to iron and another could interact with a Ag atom of the surface. Mascharak and co-workers[22,23,24] demonstrated that the IR spectrum of Fe-PMA, a synthetic model of the metal-binding region of bleomycin, has a mode assigned as a carbonyl stretching vibrational of a coordinated amide at 1630 cm^{-1} for the ferric state and 1590 cm^{-1} for the ferrous state. Takahashi and co-workers[9] observed a carbonyl stretching vibration of the β-hydroxyhistidinyl amide at 1608 cm^{-1} for the ferric state and 1594 cm^{-1} for the ferrous state. Thus, the absolute frequency and redox state dependence of this mode is similar to that of the band at 1568 cm^{-1} in the SERS of Fe-BLM, and we are prompted to assign

it to the carbonyl stretching vibration of the β-hydroxyhistidinyl amide. When the redox state of iron changes, there is a relatively small shift in the SERS spectrum (7 cm^{-1}) compared to that in RR (14 cm^{-1}), which can be explain as follows. Two resonance forms are possible for a deprotonated amide bound to a metal ion through the nitrogen atom:

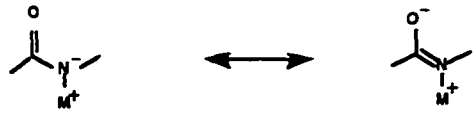

I II

the ferrous iron would favor form II due to its increased electron density, whereas the ferric complex would favor the negatively charged nitrogen of form I. The relatively low frequency of C-O stretching mode and small shift in SERS band is caused by increasing contribution of form II due to the interaction between the oxygen atom of the amide and the positively charged Ag surface. The same reason can be used to explain why there is a spectral shift in frequency of this vibration mode without and with oxygen (at 1567 cm^{-1} without oxygen, at 1572 cm^{-1} with oxygen). The oxygenated ferric complex would favor the form I much more than that of form II since the electron density of center iron will decrease when oxygen is bound to it.

The band at 1465 cm^{-1} has a relatively narrow line width, low sensitivity to the redox state of iron, suggesting that this vibrational mode arises from a different mode, probably an internal mode of vibration. The NR has shown that pyrimidine has a ring stretching mode at 1467 cm^{-1}.[20] Therefore, we assign the band at 1465 cm^{-1} as a pyrimidine internal mode. The skeletal vibration of polypeptide has a band around 900 cm^{-1} region, attributed to Cα-C-N stretching.[21] It has been found to be conformationally sensitive. The assignment of band at 830 cm^{-1} as a skeletal vibration is consistent with its lack

of sensitive to ligation and redox state but its sensitivity to conformationally change from metal-free BLM to Fe-BLM complex.

Low Frequency Region. The most direct way of probing the bonding about the iron atom is to monitor the modes attributable to the iron-ligand vibrations which occur below 700 cm^{-1}. Figure 4-5 and Figure 4-6 show the low frequency region of the potential dependent spectra of Fe-BLM and O_2-Fe-BLM complexes. There are two bands common to the both Fe-BLM and O_2-Fe-BLM: bands at 393 and 556 cm^{-1}; and two new bands only for the O_2-Fe-BLM. They are the bands at 413 and 754 cm^{-1}.

The Fe-OH_2 stretching vibration for $[Fe(H_2O)_6]^{2+}$ occurs at 389 cm^{-1}, and Fe-OH_2 wagging motion for $[Fe(H_2O)_6]^{2+}$ occurs at 575 cm^{-1}.[9] Thus, we propose that two common bands may be caused by the formation of complex ion $[Fe(H_2O)_6]^{2+}$ from extra iron ion in the solution. Brunner et al.[25] identified the Fe-O_2 stretching mode in oxyhemoglobin, which occurs at 567 cm^{-1}. For some metalloproteins, on visible excitation, a metal-oxygen stretching mode is observed shifted to low frequency near 500 cm^{-1}.[25] Comparing the structure of oxyhemoglobin with that of O_2-Fe-BLM, we propose that the new band at 413 cm^{-1} is an Fe-O_2 stretching mode. The relatively low frequency of this mode in O_2-Fe-BLM can be explain as follows: there are many groups around the iron atom in Fe-BLM which affect the bonding of oxygen to iron, or we may say the bonding structure is looser than that of oxyhemoglobin, so the bonding length is longer than that in oxyhemoglobin. The features of another new band at 754 cm^{-1} can be examined in the Figure 4-6. At a relatively positive potential of +0.00 V, this mode is not detected clearly for O_2-Fe(III)-BLM. When the potential changes to a relatively more negative value at -0.16 V or -0.3 V, this mode is then observed clearly. In oxyhemocyanin the oxygen-oxygen stretching mode was

observed in the RR spectrum at 742 cm^{-1},[25] and the position is characteristic of peroxides. Thus we assign the band at 754 cm^{-1} to the peroxide O-O stretching mode, which means that oxygen bound Fe-BLM should exist as a peroxide form O_2^{-2}-Fe(III)-BLM at the negative potential.

Time Resolved SERS. As we discussed above, the Raman character of the carbonyl stretching of the β-hydroxyhistidinyl amide is sensitive to the ligation state and redox state of the central iron. It is these properties which allow us to be able to study the mechanism of drug activation by monitoring the changes of this band in a potential induced electrochemical reaction. We have utilized potential step controlled time-resolved SERS to observe the intermediates of Fe-BLM and O_2-Fe-BLM system under electrochemical reduction on the Ag electrode. Time-resolved SERS was carried out as following: The initial potential was set at +0.02 V and an original SERS spectrum was taken at this potential. Then we applied a reduction potential step from +0.02 V to -0.65 V on the electrode. An electrochemical reduction reaction of Fe(III)-BLM to Fe(II)-BLM should be generated. The signal of the potential step is also used to trigger the gated diode array detector and the OMA system. Using the data acquisition mode 8 offered by OMA, continuous scans were taken just following the potential step at given time intervals and saved automatically in the memory. Then the original spectrum is subtracted from each scan. The data acquisition time for each scan of the TRSERS' spectra reported here was set at 450 ms. Figure 4-7 shows the difference spectra for time resolved SERS of Fe-BLM, and Figure 4-8 shows the difference spectra of time dependent SERS of O_2-Fe-BLM. In Table 4-III are the data for the difference spectra of time resolved SERS of Fe-BLM system and O_2-Fe-BLM system.

We first focus on studying the changes of the carbonyl stretching of the β-

hydroxyhistidinyl amide at 1568 cm^{-1} band at +0.02 V in Fe-BLM system. This frequency is an indicator of, or corresponds to Fe(III)-BLM species. Since this mode is sensitive to chemical alteration of the central iron atom, it could be used as a potential structure and mechanism monitor. There is a product band at 1535 cm^{-1} in the time resolved difference spectra of Fe-BLM, which is by a drop in frequency of the band at 1568 cm^{-1} in original. The degree of drop is 33 cm^{-1}. Since only the potential is changed in this experiment, we infer this 33 cm^{-1} low shift in the band frequency corresponds to the reaction where Fe(III)-BLM is reduced to Fe(II)-BLM. The product band 1535 cm^{-1} disappears in about 4s, which means that this product formed during the potential step may desorb from the Ag surface under a potential at -0.65 V.

More interesting phenomena were observed when oxygen was added to the Fe-BLM. In the time resolved SERS difference spectra of O_2-Fe-BLM, the product band experienced continual changes. After the potential is jumped to -0.65 V, the first observation of an intermediate band appears at 1546 cm^{-1} in the first 450 ms. It shifts to 1535 cm^{-1} in about 2.7s. Then this band, 1535 cm^{-1} shifts back to 1543 cm^{-1} in about 1.8s. The final product seems stable on the electrode surface, since the band 1543 cm^{-1} can be observed for a long time without changing frequency and intensity. It may not be desorbed during the experiment.

So, we have one simple case and one complicated case. In the Fe-BLM system only one reaction occurs during the potential step TRSERS experiment. It is a one electron transfer from the Ag electrode to Fe(III)-BLM to form Fe(II)-BLM. The rate of electron transfer is fast enough so that we can only observe the product band in the first 450 ms. The shift down of 33 cm^{-1} in frequency is responsible to this process. But in the case of O_2-Fe-BLM, the process corresponding to those observations could be a four step reaction as shown

below:

$$O_2\text{.Fe(III).BLM} \xrightarrow[E]{e^-} O_2\text{.Fe(II).BLM} \xrightarrow[C]{} O_2^-\text{.Fe(III).BLM} \xrightarrow[E]{e^-} O_2^-\text{.Fe(II).BLM} \xrightarrow[C]{} O_2^{-2}\text{.Fe(III).BLM}$$

The first step is one electron transfer from electrode to O_2-Fe(III)-BLM to form O_2-Fe(II)-BLM. The rate of the first electron transfer is fast enough, as in the case of Fe-BLM, so that we see the product band at 1546 cm^{-1} in the first 450 ms. The second step is an intramolecular charge transfer by which the O_2-Fe(II)-BLM converts to O_2^--Fe(III)-BLM. The structure of O_2-Fe(II)-BLM may be more stable than its "resonance" species, O_2^--Fe(III)-BLM. Therefore the majority species on electrode is O_2-Fe(II)-BLM in the first 450 ms after the potential jump. We only observed the O_2-Fe(II)-BLM band in the first 450 ms TRSERS spectrum. Once O_2^--Fe(III)-BLM was formed, it obtains a second electron from the electrode under the applied potential of -0.65 V to form O_2^--Fe(II)-BLM. The rate of the second electron transfer could be very fast and close to that of first one. The accumulation of O_2^--Fe(II)-BLM species enable us to observe the second intermediate band, 1535 cm^{-1}. Finally, through another intramolecular charge transfer, the O_2^--Fe(II)-BLM intermediate could be converted to its "resonance" structure O_2^{-2}-Fe(III)-BLM as a final product of this reaction which is thought to be stable on the electrode at applied potential -0.65 V. The 1543 cm^{-1} band finally observed may correspond to this species. The intramolecular charge transfer step allowed us to observe a band shift from 1536 cm^{-1} to 1543 cm^{-1}.

The first drop in frequency caused by the potential jump is 28 cm^{-1}. This value is close to that obtained in Fe-BLM system. It is reasonable to suggest the first species we detect could be O_2-Fe(II)-BLM. The stable SERS spectra of the low frequency region of O_2-Fe-BLM shows us a characteristic band of peroxide

O-O stretching as we discussed in previous section. We suggest that the final species observed could be O_2^{-2}-Fe(III)-BLM. Recalling this vibration mode has a frequency drop when the central iron Fe(III) is converted to Fe(II), we may propose the following mechanism: (1) The first intermediate band at 1546 cm^{-1}, which shifts down 28 cm^{-1} in frequency from the original one at 1574 cm^{-1}, corresponds to the formation of O_2-Fe(II)-BLM. (2) There is an intramolecular charge transfer process between species O_2-Fe(II)-BLM and its "resonance" structure O_2^--Fe(III)-BLM. Since O_2-Fe(II)-BLM is more stable than O_2^--Fe(III)-BLM, therefore the majority of species is O_2-Fe(II)-BLM. (3) Once O_2^--Fe(III)-BLM is formed, it is very quickly converted to the intermediate species, O_2^--Fe(II)-BLM by accepting another electron from the electrode. The rate of this step is fast enough so we can not detect the intermediate species O_2^--Fe(III)-BLM. This step causes the second shift in frequency, the band at 1546 cm^{-1} shifts to 1535 cm^{-1}, corresponds to the formation of O_2^--Fe(II)-BLM. (4) The O_2^--Fe(II)-BLM can convert to its more stable "resonance" form O_2^{-2}-Fe(III)-BLM through a intramolecular charge transfer step. We observed the band shifts from 1536 cm^{-1} back to 1543 cm^{-1} since Fe(II) converts to Fe(III). This species, O_2^{-2}-Fe(III)-BLM, may be the so called activated BLM found by Burger and co-workers.[14]

Cyclic voltammetry. To further probe that proposed mechanism, experiments with cyclic voltammetry were also carried out. The cyclic voltammetry is designed to show the charge transfer process between molecules and electrode. With oxygen, Fe-BLM can be converted to one or more reactive intermediates which involves reductive activation of dioxygen[2]. To facilitate the study of oxygen activation by Fe-BLM and the characterization of the resulting activated species, Hecht et al.[26] developed an electrochemical system for reductive activation of dioxygen + Fe(III)-BLM. We have designed a potential

initiating reduction step which was probed by TRSERS discussed above. The reaction involved in the potential step was determined by cyclic voltammetry which was carried out in the same sample cell, electrodes, electrolyte, and pH value. Figure 4-9a shows the cyclic voltammograms of the background solution (0.05 M K_2SO_4, pH=4.3) at different scan rates with and without oxygen. Aerobically (curve b in Figure 4-9), the cyclic voltammograms exhibited a reduction wave at -0.35 V, vs. Ag/AgCl with salt bridge, for $(O_2+H^+)/H_2O$ redox couple. Figure 4-10 shows the cyclic voltammograms of metal free BLM at different scan rates without oxygen. No apparent redox reaction can be detected in the potential scan range, from 0.00 V to -1.0 V. Figure 4-11 shows the cyclic voltammograms of Fe-BLM at different scan rates without oxygen. There is a reduction wave observed (at -0.41 V), and a reoxidation wave observed (at -0.35 V) in the reverse sweep. The difference is about 60 mV, with $E_{1/2}$=-0.38 V vs. Ag/AgCl with salt bridge. No apparent changes are observed when the potential scan rate is changed from 50 to 200 mV/s. The shapes of these CV curves correspond to a one-electron, reversible, Fe(III)-BLM/Fe(II)-BLM redox couple with considerable capacity background current.

Figure 4-12 shows the cyclic voltammograms of O_2-Fe-BLM at different scan rates, which correspond to a two electron transfer, irreversible process. The cyclic voltammogram in an aerobic system (O_2-Fe-BLM) exhibited increased current for the first reduction wave at -0.44 V relative to the anaerobic system (Fe-BLM), shows a second reduction wave at more negative potential value -0.61 V, and one wide reoxidation wave around -0.36 V, which corresponds to first reduction wave. That the increased current of the first reduction wave (-0.44 V) is not equal but larger than the sum of currents from the Fe(III)-BLM/Fe(II)-BLM couple and oxygen reduction wave suggests that the O_2 was really bound to the Fe-BLM. The second reduction wave at -0.61 V suggests that the O_2-Fe(II)-BLM,

once formed in the first reduction wave, can undergo further reduction at the electrode surface.[26] But the second reduction wave is wide and 'flat', suggesting there may be a slow chemical step before it. The absence of the second reoxidation wave in the reverse sweep of the cyclic voltammogram suggests that there are chemical reactions following the second electron transfer steps. The broad reoxidation wave (at -0.36 V) observed in the reverse sweep, which corresponds to the first reduction wave, suggesting again there is a slow chemical step before the reoxidation step. But the very low oxidation current compared with the reduction current, suggests there may be another side reaction exists. Considering that Fe(II) has reducing power, a disproportionation reaction may happen. Thus, one possible mechanism is the flowing:

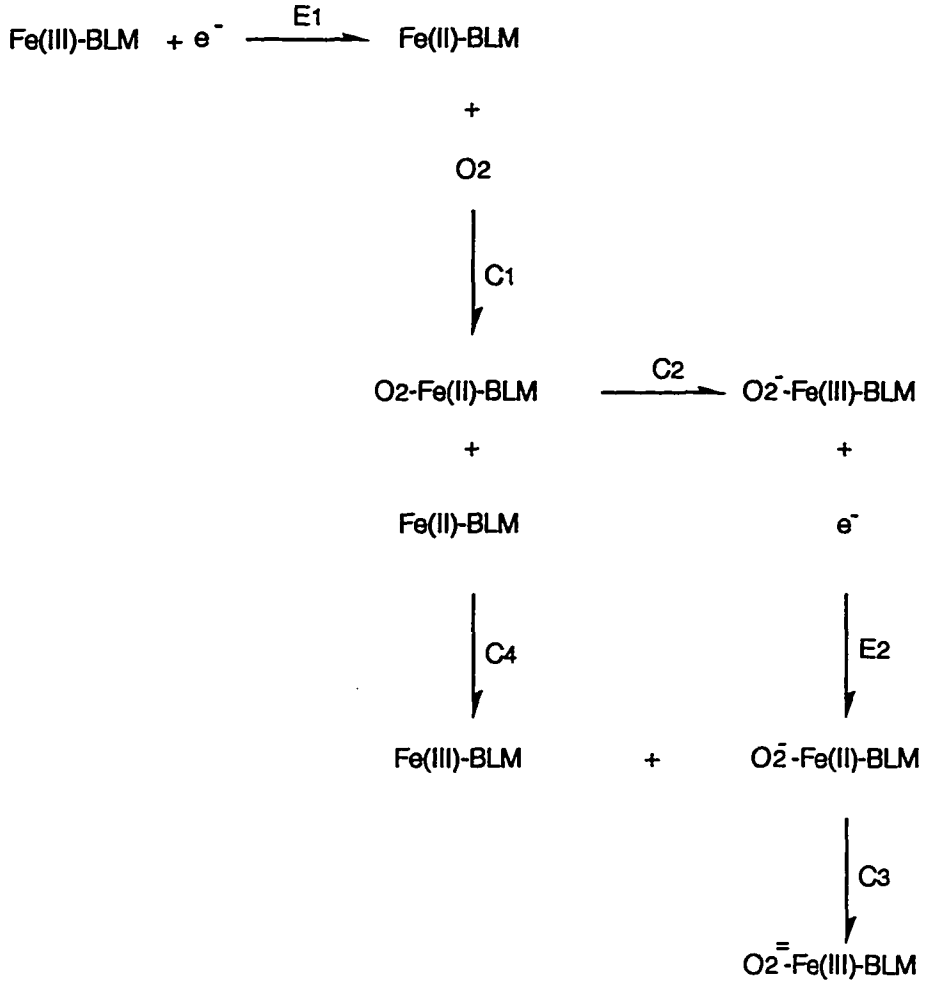

Since the final product can be formed during the chemical reaction, one can expect that when the scan rate is slow the second reduction wave will be difficult to detect. This is confirmed by the results of the low scan rate cyclic voltammetry.

4.4. Conclusions

The results obtained by the SERS and the potential dependent SERS experiments further confirm the β-hydroxyhistidinyl amide and pyrimidine as ligands bound to the central iron ion in both the Fe-BLM and the O2-Fe-BLM complexes. The results obtained by TRSERS and CV experiments suggest that two one electron reduction steps, not a two electrons reduction, are involved in the process of forming the activated bleomycin. The "activated bleomycin" is in the oxidized form: $O_2^{=}$-Fe(III)-BLM and it is relatively stable on the Ag electrode.

Table 4-I: Comparison of NR, RR and SERS of BLM.

Attributed to the portion in BLM:	NR* cm^{-1}	RR** cm^{-1}		SERS cm^{-1}			
	BLM	BLM	Fe-BLM	BLM	Simulated	Fe-BLM	O2-Fe-BLM
C=O of histidine	1638		1611		1616	1568	1574
Bithizole	1542	1540	1540	1520	1520	1520	
Pyrimidine	1487	1487	1479		1465	1465	1465
	1328	1328	1327	1320		1323	1326
	840					829	830

*: From reference 18. **: From reference 9.

Table 4-II: Potential Dependent SERS of Fe-BLM Wavenumber List (cm^{-1}).

Appl. Potential (v)	Band (I) (cm^{-1})	Band (II) (cm^{-1})	Band (III) (cm^{-1})	band (IIII) (cm^{-1})
-0.2	1560	1463	1323	830
-0.18	1560	1463	1323	830
-0.16	1560	1464	1323	830
-0.14	1566	1463	1322	830
-0.12	1565	1463	1323	830
-0.10	1565	1465	1323	830
-0.08	1567	1463	1322	830
-0.06	1567	1465	1323	830
-0.04	1567	1465	1323	829
-0.02	1568	1463	1323	829
0.00	1568	1465	1323	830
+0.02	1568	1465	1323	829

Table 4-III: Frequency shifting in time resolved SERS of Fe-BLM and O_2-Fe-BLM at applied potential -0.65 V.

Time duration	Frequency of C=O of β-hydroxyhistidinyl in	
(s)	O_2-Fe-BLM	Fe-BLM
	(cm^{-1})	
0.45	1546	1535
0.90	1544	1535
1.35	1544	1535
1.80	1541	1535
2.25	1541	1535
2.70	1536	1535
3.15	1536	1535
3.60	1536	1535
4.05	1535	
4.50	1535	
4.95	1543	
5.40	1543	

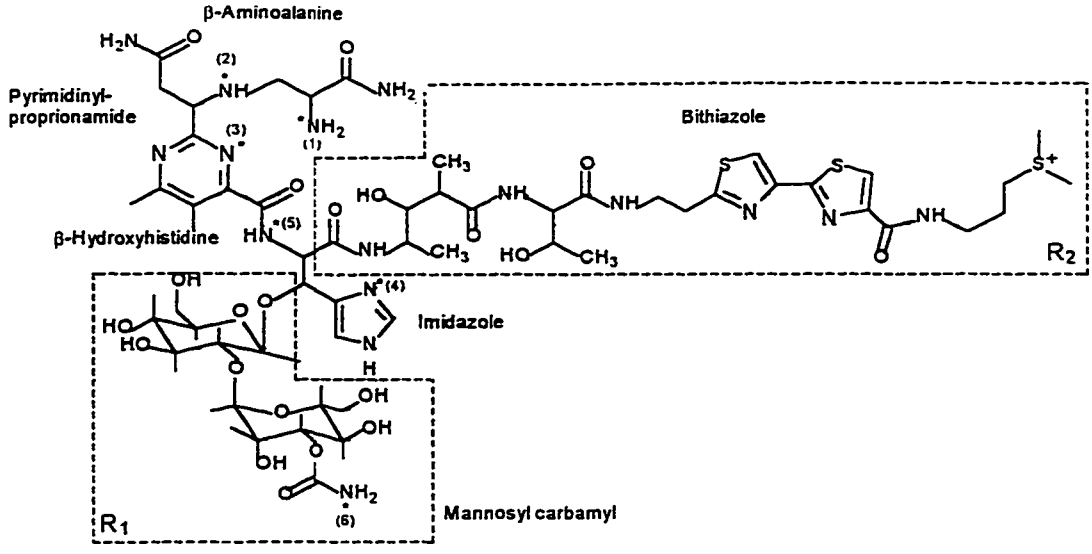

(a): Structure of Bleomycin A2. Asterisks denote proposed ligands

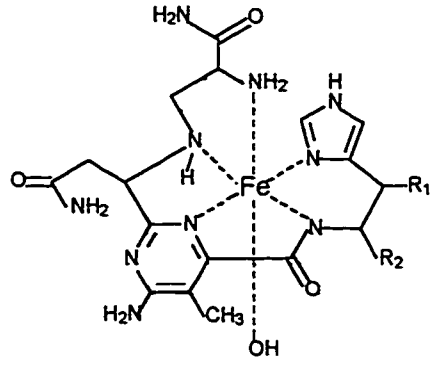

(b): One of proposed Structure of Fe-BLM

Figure 4-1

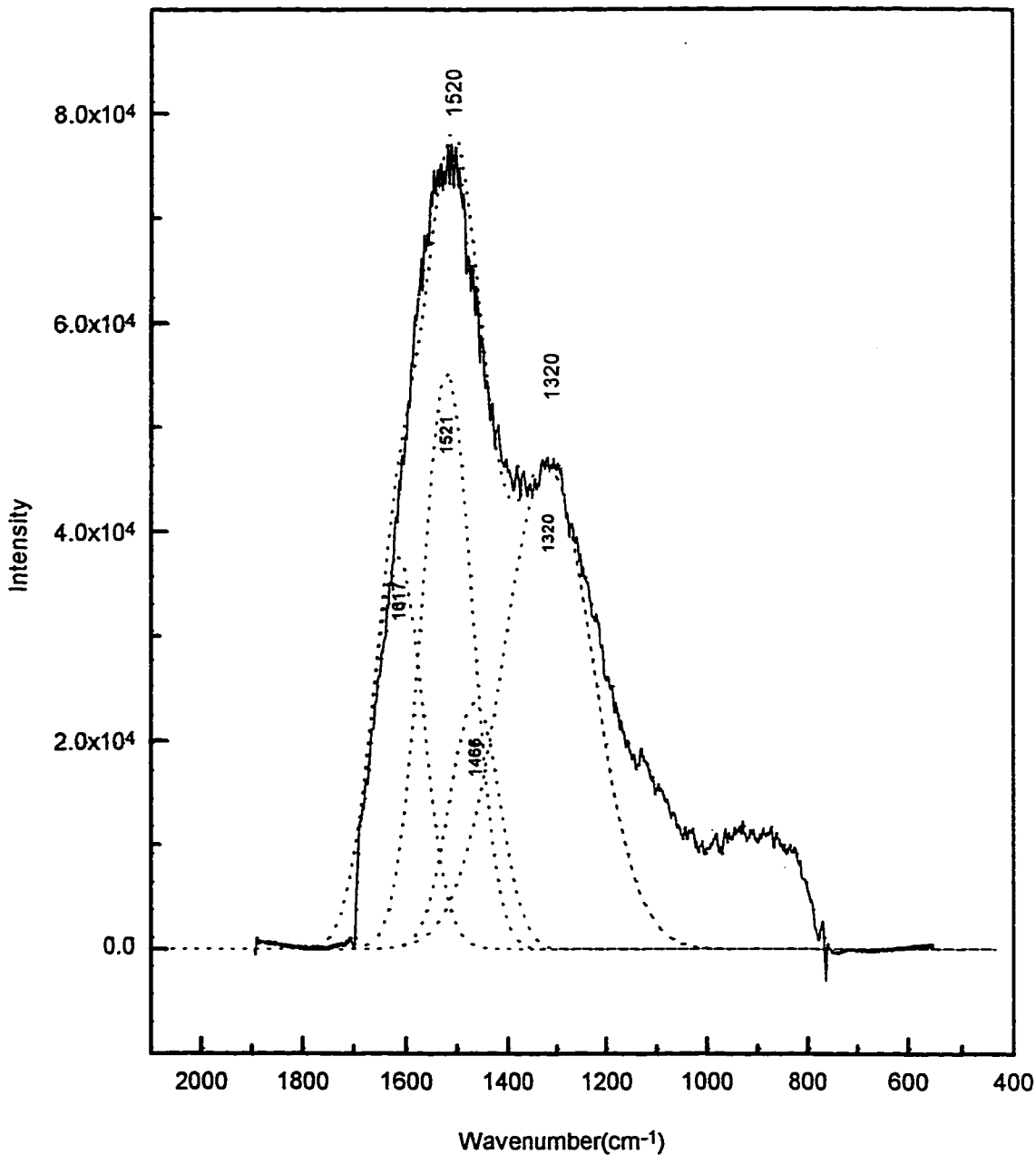

Figure 4-2: SERS spectrum of metal free BLM adsorbed on a roughened Ag electrode, at +0.02 V (_), and simulated curve based on NR of BLM (...). The roughened electrode was put in the $2x10^{-4}$ M BLM/0.05 M K_2SO_4 solution under N_2, and pH value is 4.3.

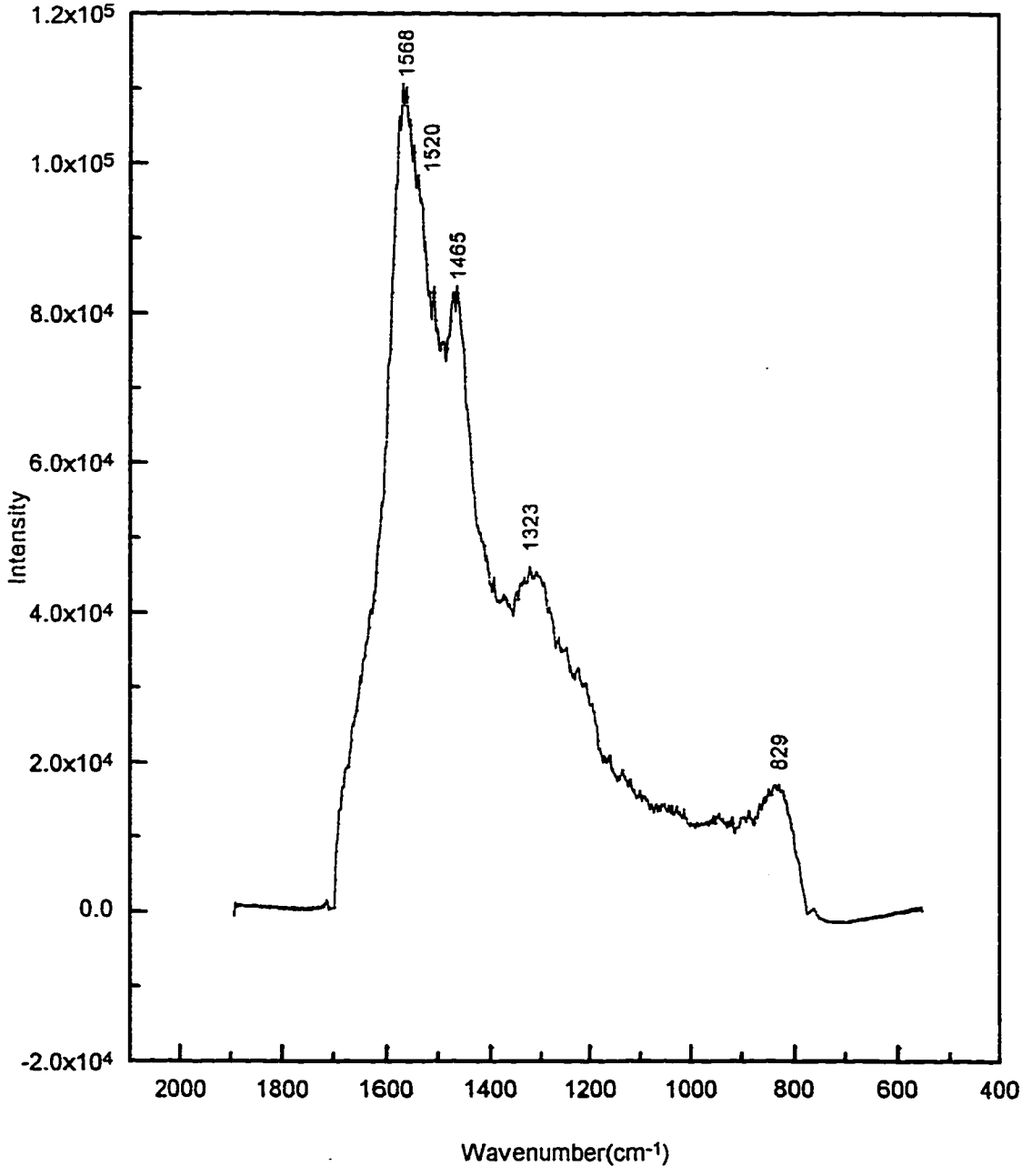

Figure 4-3: SERS spectrum of Fe-BLM, at +0.02 V under N_2 and pH value is 4.3. Experiment conditions are same as Fig. 4-2.

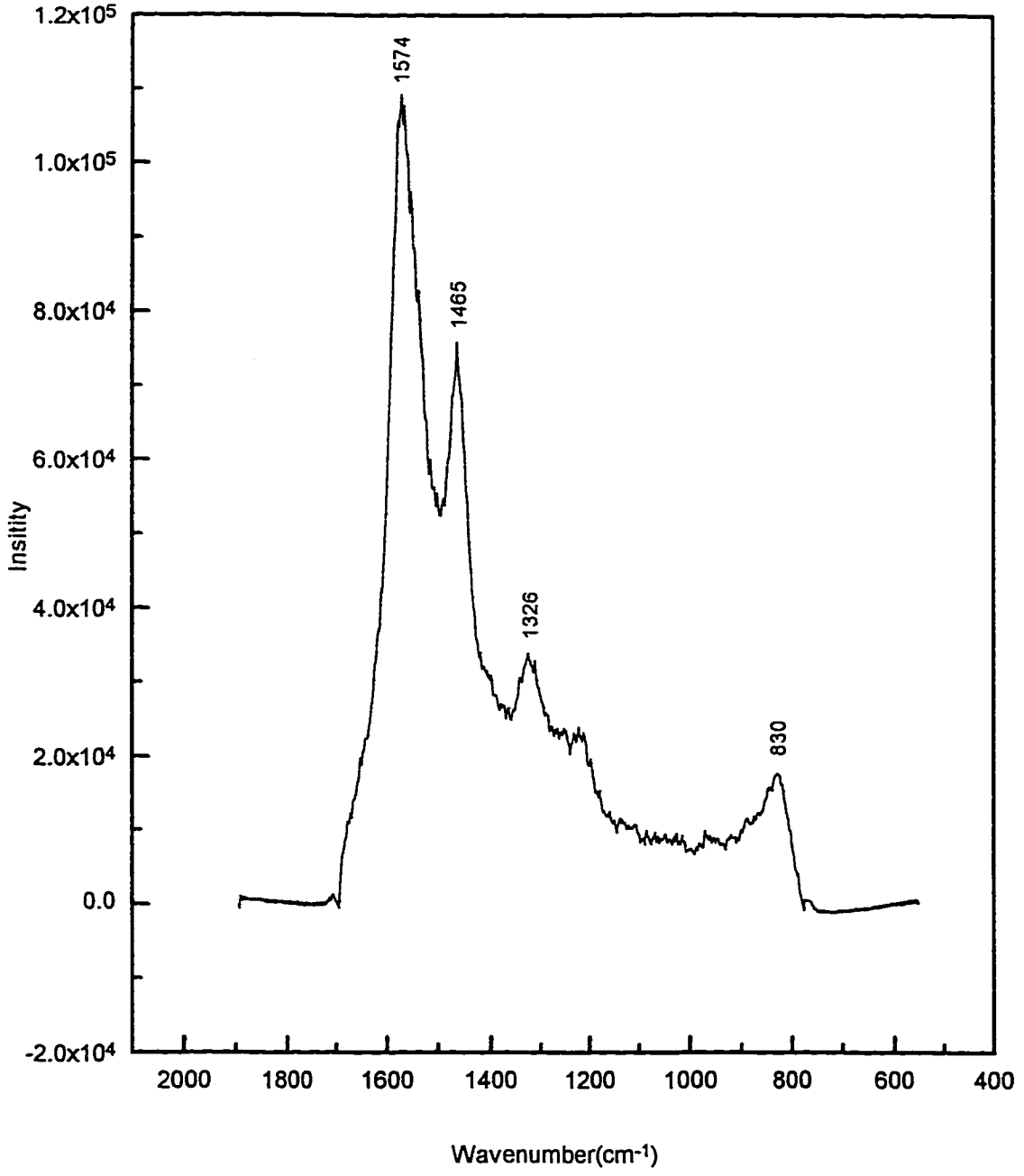

Figure 4-4: SERS spectrum of O_2-Fe-BLM, at +0.02 V under O_2 and pH value is 4.3. Other experiment conditions are same as Fig.4-2.

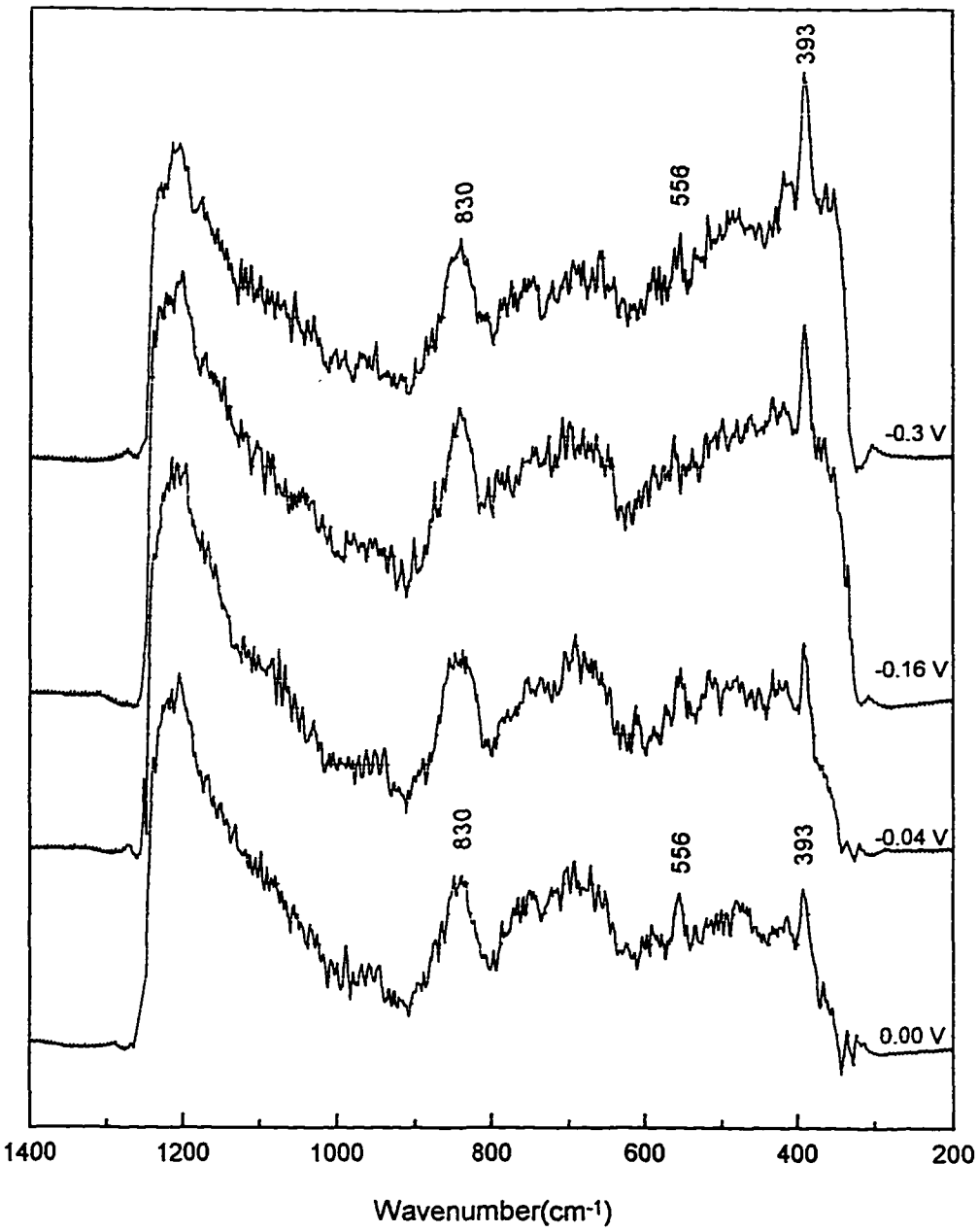

Figure 4-5: Low Frequency SERS of Fe-BLM at Different Potential.
Other experiment conditions are same as indicated in Fig.4-3.

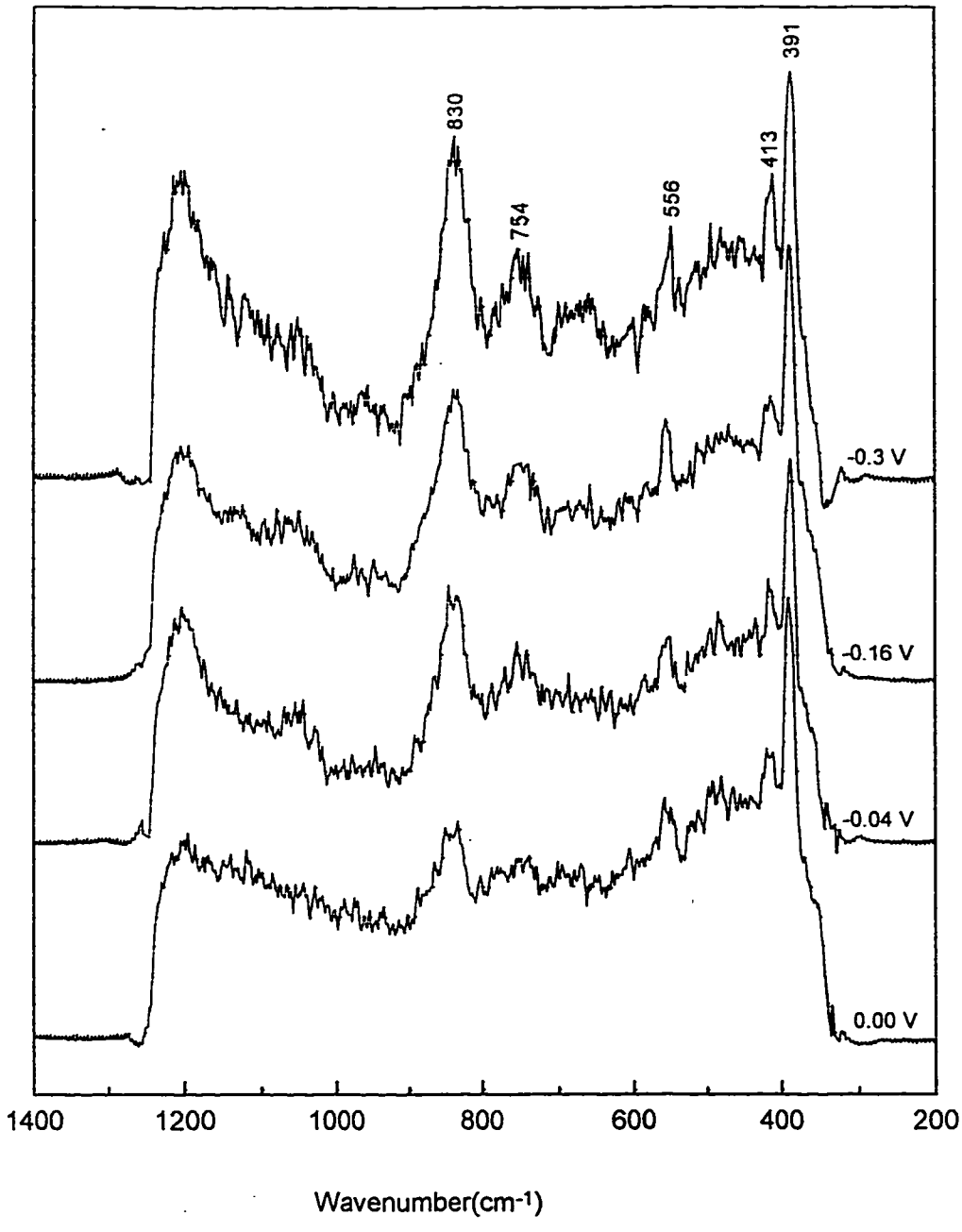

Figure 4-6: Low Frequency SERS of O_2-Fe-BLM at Different Potential. Other experiment conditions are same as indicated in Fig.4-4.

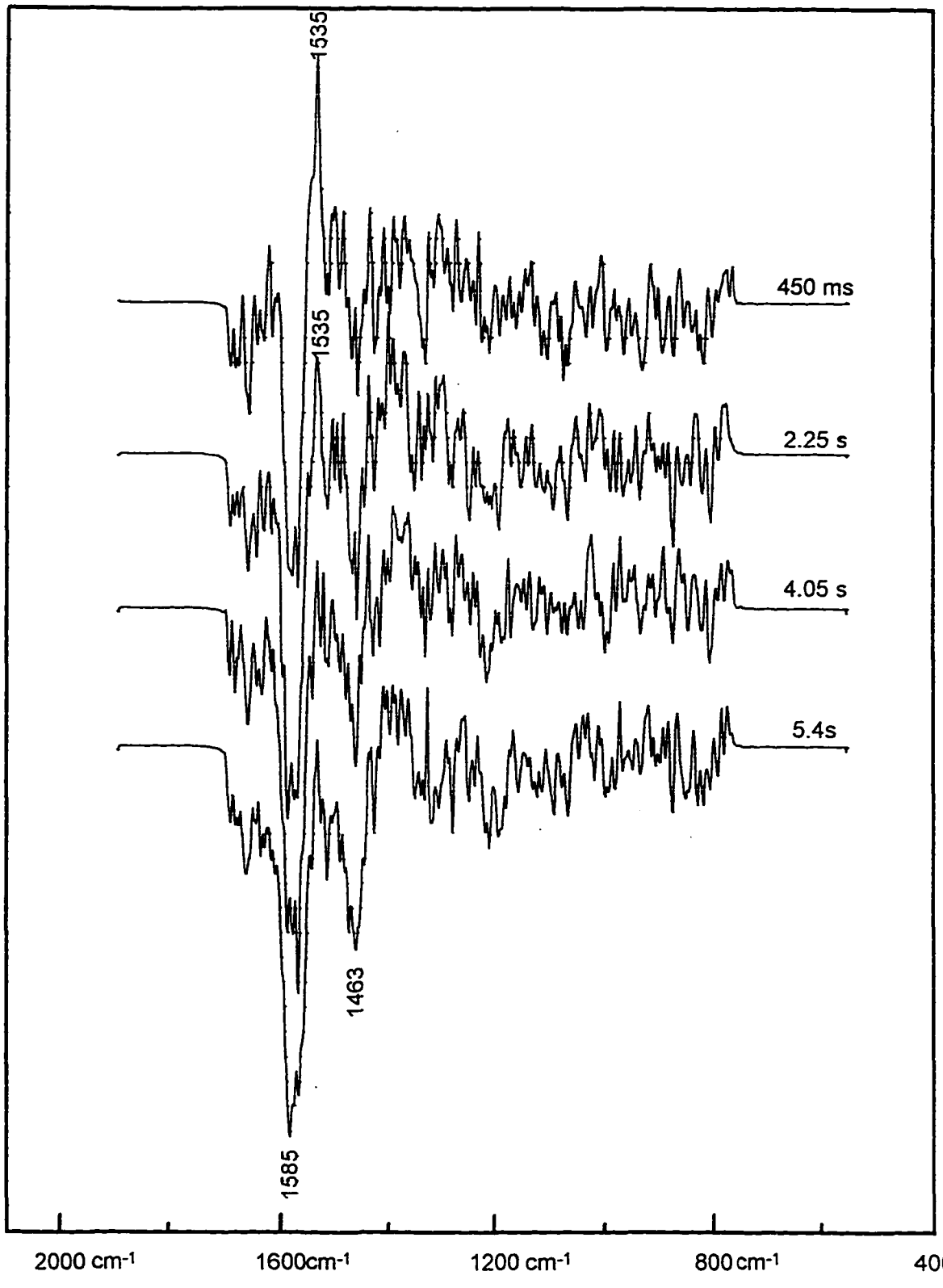

Figure 4-7: Difference TRSERS spectra of Fe-BLM. The spectra were obtained at -0.65 V under N_2, after the applied potential steped from +0.02 V to -0.65 V. The integration time of each scan is 450 ms. Other experiment conditions are same as Fig. 4-3

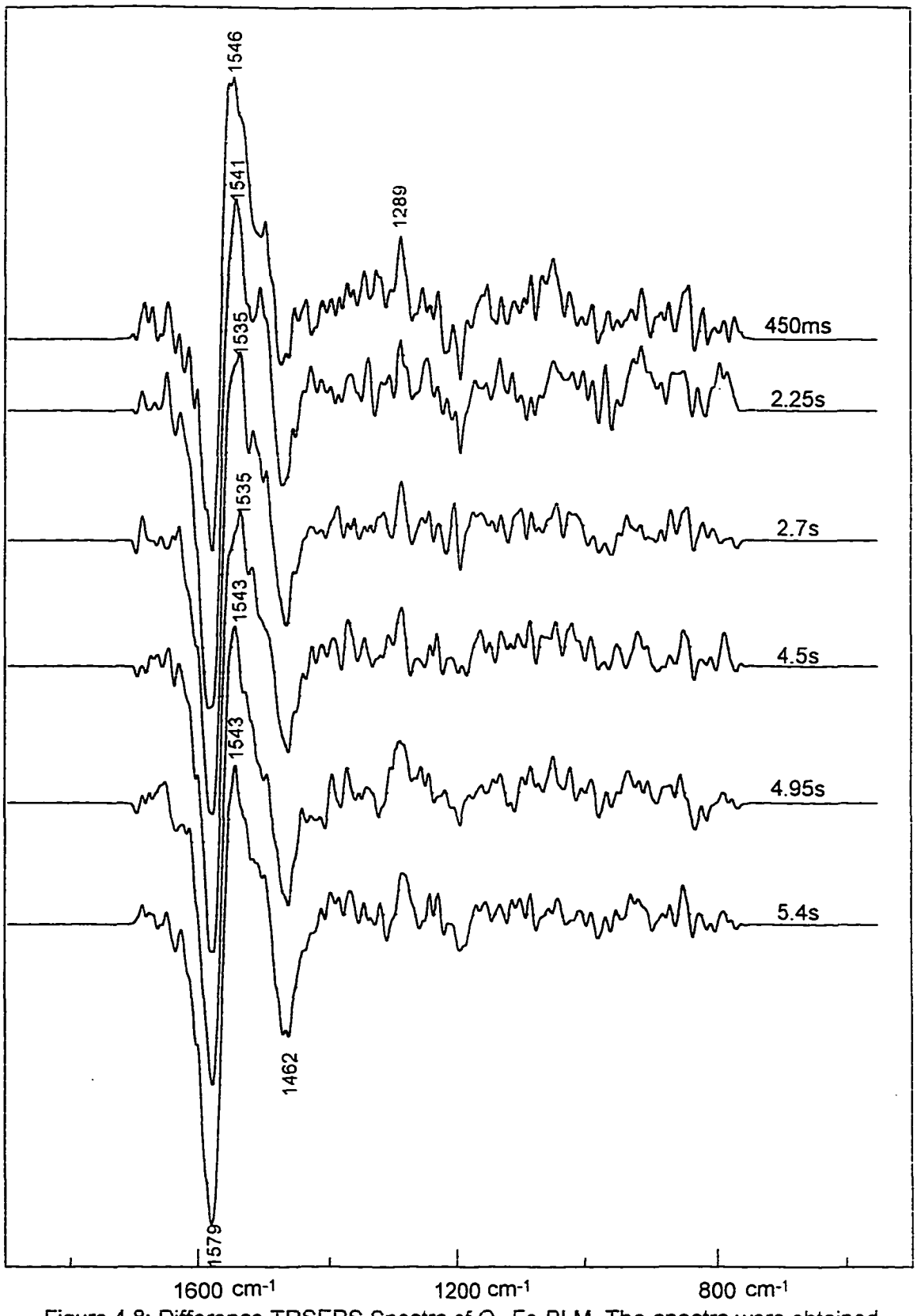

Figure 4-8: Difference TRSERS Spectra of O_2-Fe-BLM. The spectra were obtained at -0.65 V, under O_2. Other conditions are same as indicated in Fig.4-7.

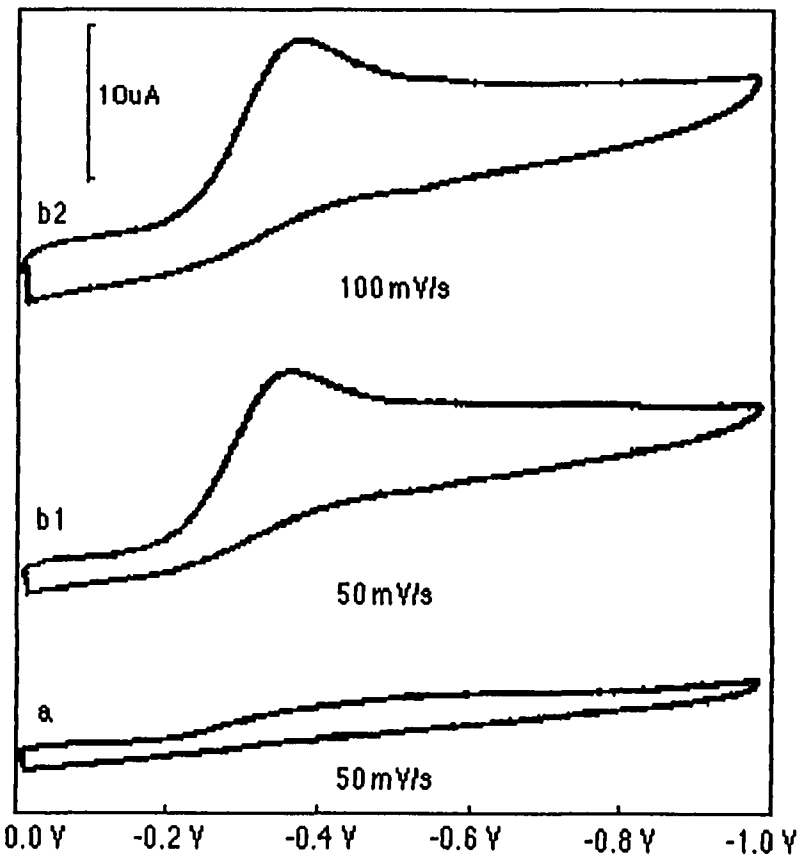

Figure 4-9: Cyclic voltammograms of 0.05 M K_2SO_4 in the (a) absence and (b) presence of O_2.

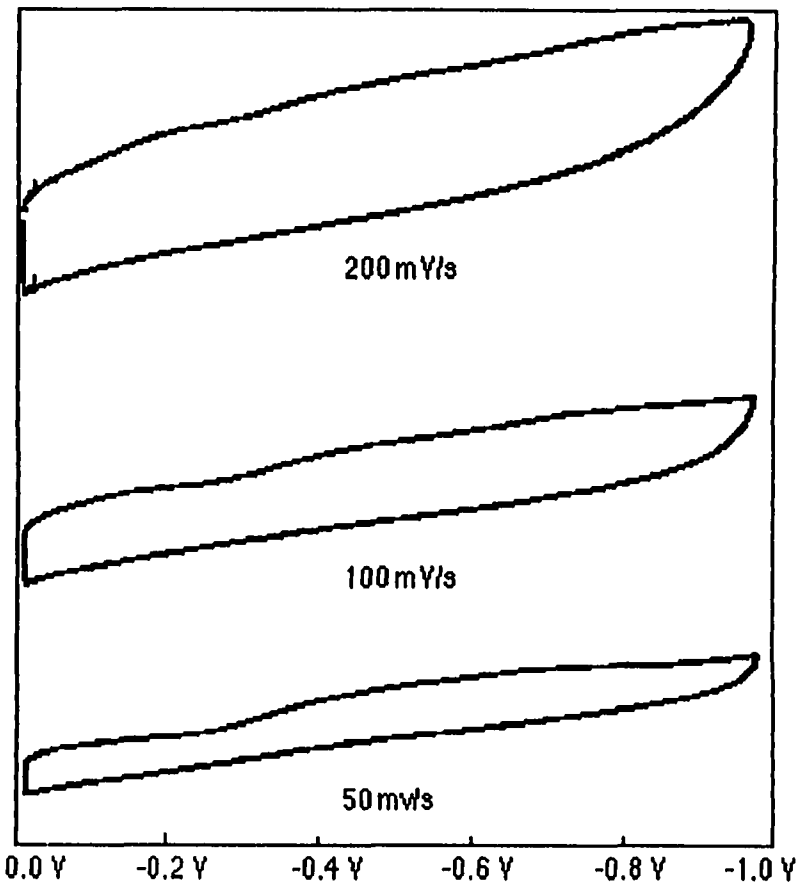

Figure 4-10: Cyclic voltammograms of metal free BLM ($5x10^{-4}$ M BLM/0.05 M K_2SO_4) in the absence of oxygen.

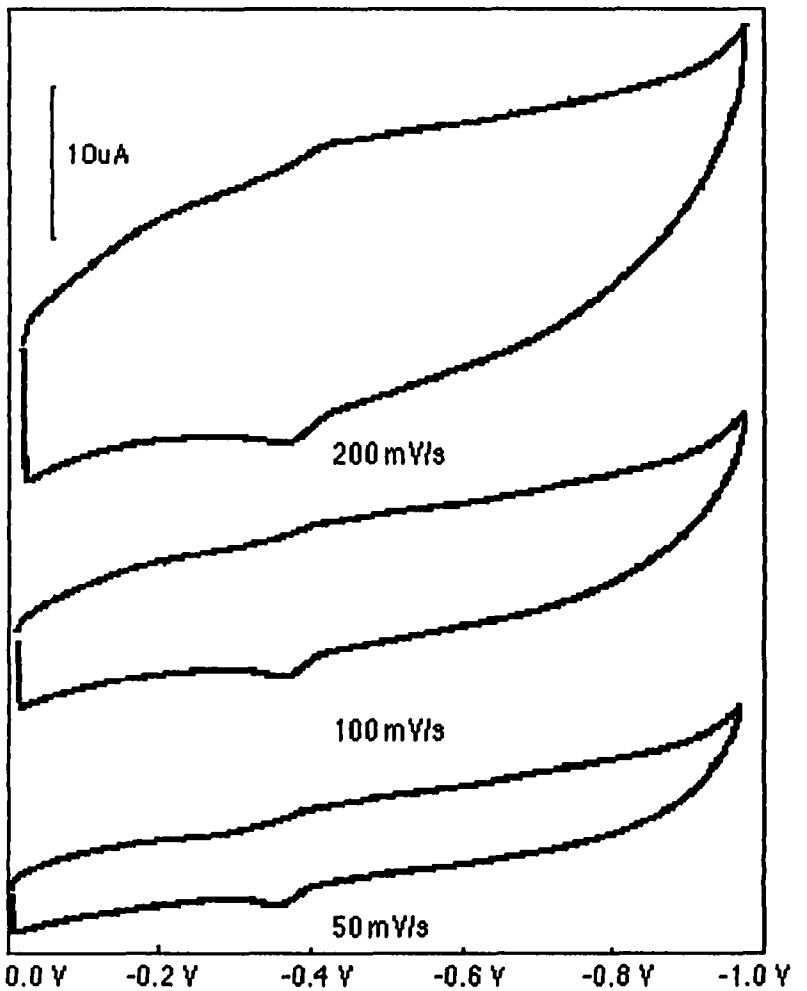

Figure 4-11: Cyclic voltammograms of Fe-BLM obtained in5x10^{-4} M Fe-BLM/0.05 M K_2SO_4.

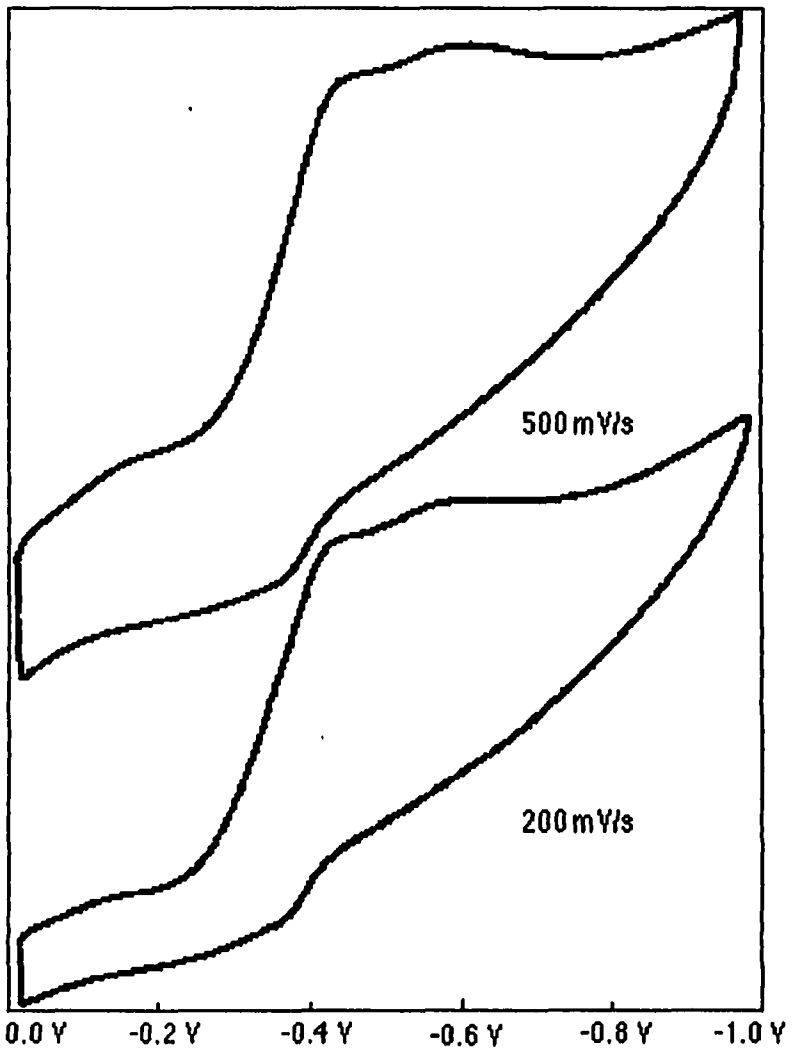

Figure 4-12: Cyclic voltammograms of O_2-Fe-BLM obtained in 5x10^{-4} M Fe-BLM/0.05 M K_2SO_4 with O_2.

Chapter V

Raman and Surface Enhanced Raman Scattering of 3-Hydroxyflavone on a Ag Electrode

5.1 Introduction

Over 4000 chemically unique flavonoids have been identified in plant sources.[1] These low-molecular-weight substances, found in all vascular plants, are phenyl-benzopyrones (phenylchromones) with an assortment of basic structures. One of these compounds is 3-hydroxyflavone (3-HF, Figure 5-1a). The flavonoids are involved in photosensitization and energy transfer. They display a remarkable array of biochemical and pharmacological actions, some of which suggest that certain members of this group of compounds may significantly affect the function of multiple mammalian cellular systems.[1-7]

As a member of the flavonoid family, 3-hydroxyflavone has been extensively examined for many years for structural and chemical properties by means of IR, UV, PMR and NMR.[1-2,8-9] Specifically, it has been used as a prototype molecule for studies of the mechanism of excited-state intramolecular proton transfer and photoisomerization since 1979 by means of electronic spectroscopy and nanosecond to picosecond time-resolved fluorescence measurements.[10-13] Much information on the molecular vibrations of 3-HF has been provided by IR.[14-19] The published IR data in the double bond and hydroxy stretching regions reveal certain unusual features in 3-HF and some substituted derivatives, which could not be rationalized by the usual frequency structure correlations. The carbonyl absorption in flavanone (Fig. 5-1b) is at 1695 cm^{-1} but in flavone (Fig. 5-1c) it is at 1649 cm^{-1}, showing the frequency decrease resulting from the increased conjugation of the carbonyl group with the pyrone ring through the C=C bond at 2,3 position. Compared with 1649 cm^{-1} of flavone, the carbonyl frequency of 3-HF is further lowered to 1610 cm^{-1} and overlaps with the frequency of the C=C band. There is some controversy about what causes this shift to lower frequency. It has been suggested that there is

strong chelation between the C=O and OH groups.[14-16] In the C-H and O-H stretching region (2000 to 4000 cm^{-1}) the IR spectrum of 5-hydroxyflavone (5-HF, Fig. 5-1d) does not contain a definite band readily assignable to O-H stretching, clearly establishing 5-HF as an intramolecular hydrogen bonding compound. The IR spectra of 3-HF in the C-H and O-H stretching region, however, were reported differently by various researchers.[14-16] Thus, Jose et al.[15] concluded that there is no strong hydrogen bonding in 3-hydroxyflavone and the low frequency characteristics of the C=O and C=C bands arise from structural features.

Although infrared spectra of 3-HF have been extensively studied, there have been no Raman studies reported so far. IR and Raman spectroscopy differ in the means by which photon energy is transferred to the molecule and in the instrumentation used. Thus, the information extracted exhibits different characteristics. The information content of the infrared and Raman spectroscopy are often complementary, and both are often necessary for a complete vibrational analysis of a molecule. The low solubility of 3-HF has hindered the use of Raman spectroscopy. Fortunately, the discovery of surface enhanced Raman scattering has provided a way to increase the Raman scattering efficiency. SERS spectra can be obtained from solution of low concentration even at $1x10^{-5}$ M. In this chapter we report normal Raman (NR) and surface enhanced Raman scattering (SERS) spectral characteristics for 3-HF. For the purpose of analysis, FTIR of 3-HF also has been carried out. The explanation for the lower frequency shift of C=O stretching is discussed. In next chapter we report the photochemical properties of 3-HF examined by a time resolved SERS scattering technique.

5.2 Experimental Section

The experimental set up for normal Raman and SERS studies has been described in previous papers.[20] A Spectra Physics Model 164 argon ion laser line at 488 nm was used as a Raman excitation source. Spectra were recorded with a Spex Model 1402 double monochromator with a resolution of 2 cm^{-1}. Photon-counting detection was used. The laser power was approximately 30 mW in the SERS experiment and only 5 mW in the NR experiment. 3-HF was purchased from the Aldrich Chemical Company Inc., used as received.

The NR spectrum of solid 3-HF has been obtained in the region of 100 to 4000 cm^{-1} directly from a pure sample without any matrix. SERS spectra of 3-HF were obtained at different pH values and different applied potentials with an activated Ag electrode which had 3-HF adsorbed on it. For acidic conditions, 3-HF was first dissolved in a small amount of CH_3OH, then diluted by a 0.1 M K_2SO_4 solution for which the pH value was adjusted with a 0.1 M H_2SO_4 solution. For basic conditions a 0.1 M NaOH solution was used to adjust the pH of a 0.1 M K_2SO_4 sample solution. In SERS experiments, the sample cell consisted of a silver working electrode, a Pt counter electrode, and a saturated calomel electrode (SCE) as the reference. All potentials reported in this chapter are quoted vs SCE. For activating an Ag electrode, the polished Ag electrode was roughened by an oxidation-reduction cycle (ORC) pretreatment which was accomplished in the solution of 3-HF ($2x10^{-5}$ M) in 0.1 M K_2SO_4 aqueous solution by applying a potential pulse from -0.4 V to 0.5 V for 2 seconds. 3-HF was adsorbed on the Ag electrode surface during the ORC. Non-adsorbed 3-HF molecules were then washed from the electrode by distilled water. After the *ex-situ* ORC pretreatment, the activated Ag electrode was placed in 0.1 M K_2SO_4 aqueous solution for carrying out SERS experiments at various

potentials. ORC pretreatment and potential control during the SERS experiments were carried out by using an EG&G PARC Model 175 universal programmer and an EG&G PARC Model 173 potentiostat. FTIR spectra of 3-HF were recorded with a Nicolet Model Impact 400 FTIR spectrometer.

5.3 Results and Discussion

Figure 5-1 shows the structure and atomic numbering of the phenylchromone ring of 3-HF. For convenience in analysis and discussion, we designate the benzo ring in the chromone system as ring A, the phenyl ring as ring B and the pyrone ring as ring C.

Figure 5.2 shows a comparison of the NR and FTIR spectra of solid 3-HF. In Figure 5-2a the NR spectrum of 3-HF in the 800 to 1700 cm^{-1} spectral region is displayed for a pure solid sample, while in Figure 5-2b the FTIR spectrum in the same region for a KBr pellet is shown. Figure 5-3 shows a comparison of NR and FTIR spectra of solid 3-HF in the high frequency region of 2000 to 4000 cm^{-1}. The SERS spectrum of 3-HF adsorbed on a roughened silver electrode is given in Figure 5-4a, at an applied potential of -0.45 V with only K_2SO_4 aqueous solution in the bulk when excited with 488 nm laser light. The spectral region is from 200 to 1700 cm^{-1}. Figure 5-4b shows the NR spectrum of solid 3-HF again in the same region for comparison.

The FTIR spectrum of 3-HF obtained in our work is consistent with the IR results previously reported by Looker and Hanneman.[14] Since 3-HF possesses no symmetry the FTIR and NR spectra are quite similar in appearance. Thus, the assignment of the Raman bands have been made mainly by comparisons with the previous IR studies of flavone and

hydroxyflavone derivatives. According to previous IR results,[14-19] the presence of a hydroxy group in the 3-position lowers the frequencies of both the carbonyl and C_2=C_3 stretching mode, so that the band at 1610 cm^{-1} in FTIR (1594 cm^{-1} in NR and SERS) represents the decreased double bond character of the carbonyl group and the aromatic character of the pyrone ring, i.e. the overlapping of C=O with C=C. The band at 3070 cm^{-1} in NR is attributed to an unsaturated C-H stretching. The band at 1351 cm^{-1} in FTIR (1352 cm^{-1} in NR and 1354 cm^{-1} in SERS) is attributed to an O-H in-plane deformation. The bands in the region from 1400 to 1600 cm^{-1} are associated with aromatic in-plane skeletal vibrations. There are two benzene nuclei in 3-HF. No attempt had been made to assign frequencies to a specific ring system in previous studies. Thus, normal mode calculations have been carried out in the present chapter to provide further assistance for making detailed band assignments. The normal mode calculations were carried out with a restricted simplex Normal Coordinate Calculation (NCC) Program wriitten in our laboratory by Vivoni.[21] In this program, the NCC routines of Diem[22] were adapted with a restricted Nelder-Mead simplex optimization method. A valence force field was used in the calculation. Interactions between normal vibrational modes are considered in the program and reflected in interaction constants. The molecular geometry parameters and force constants used in our normal mode calculation of 3-HF are adapted and modified from references 23, 24, 25, 26 and 27. In Table 5-I are listed the assignments of the vibrational bands for 3-HF. The calculated normal mode wavenumber and percentage of energy distribution (PED) from each normal mode are also listed in this table. The calculated results are consistent with the experimental results. In Table 5-II are listed the optimized force constants obtained with the calculation.

Although 3-HF molecular vibrational frequencies observed by both FTIR

and NR techniques are nearly the same, the relative vibrational band intensities and shapes differ markedly at the paired FTIR/NR bands of 1562/1566, 1627/1619 and 3070/3211 cm^{-1}. Hence both spectra are needed to derive a complete picture of the vibrational behavior of 3-HF. We are especially concerned with whether there is strong intramolecular hydrogen bonding in 3-HF. Intramolecular hydrogen bonding would be expected for those compounds, e.g. 3-HF, that simultaneously contain an OH group and an accessible basic site, so that a hydrogen bond can be easily formed via a five- or six-member ring structure. There are two types of intramolecular hydrogen bonding, namely, single-bridge and chelation. In single-bridge, the bonding is due to the mutual attraction between the OH proton and the lone-pair or p electrons on the basic site. In the case of chelation, the OH group is involved in a molecular resonance structure when the OH group is on the ß carbon of a C=C conjugated with a C=O group. Infrared spectroscopy has proven to be an excellent technique to study hydrogen bonding. Research has shown that the effect of hydrogen bond formation is to lower the O-H stretching frequency and increase the IR intensity. Generally, the stronger the hydrogen bond, the more the O-H stretching frequency is shifted to lower frequency. It has been reported[28] that free O-H stretching in phenol compounds appears as a single band in the region from 3640 to 3660 cm^{-1} in the vapor phase, and around 3610 cm^{-1} in dilute CCl_4 solution. The single-bridge intramolecular hydrogen bonding, not a strong interaction, lowers the O-H stretching frequency to the region from 3300 to 3400 cm^{-1}, and the corresponding IR band of υ(O-H) is sharp with medium intensity. On the other hand, the chelated intramolecular hydrogen bonding, a strong interaction, results in an even lower O-H stretching frequency to the region from 2500 to 3200 cm^{-1}, and the corresponding IR band of υ(O-H) is sometimes extremely broad. Shaw and Simpson[16] reported that all the 3-

hydroxyflavones examined showed only "feeble" absorption bands at about 3360 cm^{-1}. As mentioned above, the single-bridge hydrogen bonding is not a strong interaction and the band at 3360 cm^{-1} is in the single-bridged O-H stretching frequency region. Thus, based on the observation of a feeble absorption band at 3360 cm^{-1}, some researchers concluded that a weaker hydrogen bonding formed in 3-HF. However, this type of single-bridge hydrogen bonding should not give rise to a feeble absorption, but a sharp IR band with medium intensity. Looker and Hanneman reported a strong and very broad band observed in the region from 2500 to 3300 cm^{-1}.[14] Similar to their results, we observed a broad band centered at 3211 cm^{-1} ($\Delta\upsilon$>200 cm^{-1}) in the FTIR spectrum of 3-HF (see Fig. 5-3b). However, the spectral features of unsaturated C-H stretching are often in this region. This obstruction leads to uncertainty in the assignment. Fortunately, the weak Raman scattering from the O-H stretching mode provides a good window for observing the unsaturated C-H moieties. The normal Raman spectrum of 3-HF shows only a fairly sharp band at 3070 cm^{-1} ($\Delta\upsilon$<30 cm^{-1}, Fig. 5-3a) in the region from 2000 to 4000 cm^{-1}, which can be assigned unequivocally to the C-H stretching. The SERS spectrum of 3-HF at -0.45 v shows C-H stretching and O-H stretching bands at 3070 and 3200 cm^{-1} separately (Fig. 5-5). Thus, the broad band at 3211 cm^{-1} in the FTIR is definitely the result of interference from a very strong and broad O-H stretching band, suggesting there is a chelation hydrogen bonding in the molecule of 3-HF. The possible OH chelation with C=O in the resonance structures of 3-HF is shown as follows:

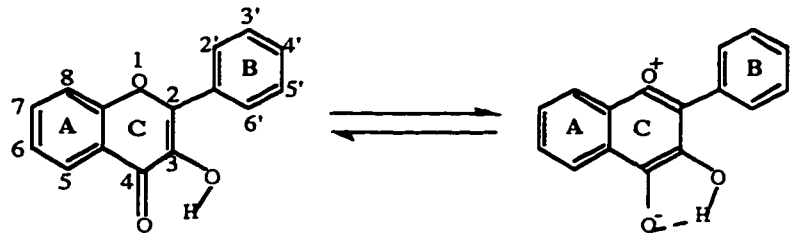

I II

Increasing the contribution of form II in the resonance structures of 3-HF will cause the frequency of the carbonyl stretching to shift to lower wavenumber. Furthermore, three very strong NR bands at 1619, 1594 and 1566 cm^{-1} are observed in the region from 1500 to 2000 cm^{-1}. The band at 1619 cm^{-1} has a contribution from C=O (39%)/C=C (30%) and the band at 1594 cm^{-1} from C=O (39%)/C=C (33%). Such strong intensity can not just be caused by the overlap of C=O stretching with that of C=C, suggesting some structural features. Generally, a Raman band due to a multiple chemical bond, e.g., a C=C vibration, give rise to intense stretching modes, and those Raman features arising from the normal coordinates involving two or more in-phase bond stretching motions are also more intense. Thus, for aromatic compounds the in-phase "breathing" mode which includes three C=C vibration bonds is usually the most intense. On this basis the increasing contribution from form II in the resonance structures of 3-HF may be responsible for the strong intensity observed at band 1619 and 1594 cm^{-1}.

Except for the absence of bands at 1619 and 1566 cm^{-1}, the SERS spectra of 3-HF is similar to that of both FTIR and NR spectra with a few differences in the molecular vibrational frequencies (see Table 5-I). It is reasonable that there are 7 to 14 cm^{-1} lower frequency shifts in the SERS bands of 1457 (1470 in NR), 1430 (1444 in NR) and 1404 cm^{-1} (1412 cm^{-1} in NR), which are all assigned to the aromatic ring in-plane stretching, when the SERS

spectra of 3-HF are obtained under the potential of -0.45 V. Although the vibrational frequencies of the two spectra are similar to each other, the relative intensities of some SERS bands differ considerably from the NR spectra of 3-HF. Two intense bands, namely those at 1619 and 1594 cm^{-1} represent the character of the carbonyl group and the pyrone ring in the NR spectrum . One (at 1619 cm^{-1}) disappears and the other (at 1594 cm^{-1}) shows much lower relative intensity in the SERS, suggesting a stronger interaction between the C=O group and the electrode surface. In addition, the relative intensities of SERS bands at 1498, 1430 and 1404 cm^{-1}, all assigned to the phenyl ring (ring B) in-plane skeletal stretching, increased; whereas, the intensities of SERS bands assigned to the benzo-ring (ring A) in-plane skeletal stretching show little change. The relative intensities of the C-H deformation of B-ring (bands at 1000, 946, 900 cm^{-1}) increased in the SERS, whereas that of C-H deformation of A-ring (band at 992 cm^{-1}) did not. Furthermore, three unsaturated C-H stretching bands at 2860, 2910 and 3070 cm^{-1} have been observed in the SERS spectrum (see Fig. 5-5) but only one at 3070 cm^{-1} in NR spectrum is observed. This indicates that the two benzene nuclei in 3-HF have different orientation with respect to the electrode surface. All these observations suggest that the main heteroatom ring systems (ring A and the pyrone ring C) in the molecule of 3-HF are probably parallel to the electrode surface, while the phenyl ring (ring B) is at an angle to the surface.

In the high frequency region, SERS spectra of H_2O obtained on a Ag electrode have shown that the stretching band of υ(O-H) is at 3536 cm^{-1} under -0.5 V and at 3556 cm^{-1} under -0.2 V.[29] In the SERS of 3-HF, however, no band was found from 3400 to 3600 cm^{-1} in the high frequency region under -0.45 V (Figure 5-5), but a weak band at 3200 cm^{-1}, representing the O-H stretching from 3-HF, was observed. This provides evidence that an

intramolecular hydrogen bond exists in 3-HF even in solution. In potential dependent SERS experiments the applied potential is changed from -0.1 V to -0.9 V. The SERS characteristics of 3-HF display no change until the applied potential is more negative than -0.7 V, showing that 3-HF is quite a stable species on the Ag electrode surface for these negative potentials. When the applied potential is more negative than -0.7 V, e.g. at -0.75 V, the υ(O-H) band at 3200 cm^{-1} disappears, but a weak broad band at about 3366 cm^{-1} is observed in the high frequency region. This indicates that the intramolecular hydrogen bond may be weakened by the highly negative charged surface (Figure 5-5).

Furthermore, the relative intensities of SERS bands at 770, 984, 998, 1404 and 1430 cm^{-1} are changed when the potential is more negative than -0.7 V (Figure 5-6). Examing these bands, it is discovered that the changes in these bands make the appearance of the SERS spectrum at -0.75 V more NR features. For example, the band at 778 cm^{-1} in the NR disappears in the SERS under -0.45 V, but reappears at 770 cm^{-1} in the SERS under -0.75 V. The paired bands at 984 and 998 cm^{-1} in SERS under -0.75 V correspond to the paired bands at 992 and 1000 cm^{-1} in the NR spectrum. These have been assigned to the deformation of C-H in ring A and the deformation of C-H in ring B, respectively. In NR, the band at 992 cm^{-1} is more intense relative to that of its paired band at 1000 cm^{-1}. On the contrary, the band at 1000 cm^{-1} has been shown to be more intense than that of its paired band at 992 cm^{-1} in the SERS under -0.45 V since ring B of 3-HF is at an angle with respect to the electrode surface. However, it reverts in SERS under -0.75 V with the band at 984 cm^{-1} becoming more intense relative to that of its paired band at 998 cm^{-1}. The same changes were also observed at the paired bands of 1404 and 1430 cm^{-1}. In the SERS under -0.45 V, the band at 1430 cm^{-1} shows stronger intensity than that

of the band at 1404 cm^{-1}; but in the SERS under -0.75 V and in the NR (corresponding bands at 1412 and 1444 cm^{-1}), these two bands show almost same intensity. Thus, it seems the spectra lose some SERS characteristics when obtained under more negative potentials than -0.7 V. One possible explanation lies in the fact that the potential of zero charge (PZC) of Ag is around -0.7-0.8 V.[29,30] The highly active SERS sites are metastable and liable to decompose as the applied potential approachs the PZC due to the rearrangement of the surface atoms (or clusters) that occur near this critical potential point.[29] Losing the active SERS sites not only weakens the SERS signals, but also causes reorientation of 3-HF on the surface, so that we observe more NR characteristics for potentials more negative than -0.7 V. SERS spectra also have been examined at different pH values under an applied potential of -0.45 V. Unlike intermolecular hydrogen bonding, the intramolecular hydrogen bonding is relatively unaffected by the solute-solvent interaction. The spectra obtained at pH values of 4.7 and 10.8 are nearly the same (not shown in this chapter). This further confirms that there is chelated intramolecular hydrogen bonding in the molecule 3-HF even in a polar solvent. The observation of pH independent phenomenon is also consistent with the fact that 3-HF acts as both a very weak acid and a very weak base (K_a=2.5X10^{-10}, K_b=1.3X10^{-17})[31].

In conclusion it is pointed out that the hydroxy in the 3-position of flavone is strongly hydrogen bonded to the C=O group in a chelation form, whether in the pure solid state or in the solution. The lower frequency shift of C=O may be due to the importance of resonance structures.

Table 5-I: Calculated and Observed frequencies of 3-HF

No.	Vibrational assignment PED of main contribution	Calc. Freq. (cm^{-1})	Obs. Freq FTIR (KBr)	NR (solid)	SERS (K_2SO_4)
1	υ(O-H) 100%	3213	3211_s		3200_{vw}
					3070_{vw}
2	υ(C-H) 99%	3071		3070_m	2910_w
					2860_w
3	υ(C=O) 39%, υ(C_2=C_3) 30%	1702	1627_{sh}	1619_{vs}	
4	υ(C=O) 39%, υ(C_2=C_3) 33%	1609	1610_s	1594_{vs}	1594_s
5	υ(Ring A) 25%, υ(Ring B) 12%	1544	1562_s	1566_{vs}	
6	υ(Ring A) 32%, υ(Ring B) 24%	1521			
7	υ(Ring B) 32%, υ(Ring A) 24%	1494	1491_{sh}	1490_m	1498_s
8	υ(Ring A) 54%, υ(Ring B) 16%	1485	1481_s	1482_w	1482_{sh}
9	υ(Ring A) 62%	1467	1471_s	1470_s	1457_s
10	υ(Ring B) 87%	1446	1445_m	1444_s	1430_s
11	υ(Ring B) 30%, υ(C_3-OH) 10%	1417	1416_s	1412_s	1404_s
12	δ(O-H) 43%, υ(C-O_1) 15%	1352	1351_s	1352_s	1354_m
			1321_w	1320_{sh}	1316_s
13	υ(Ring A) 28%, δ(C-H of Ring A) 22%	1309	1306_s	1308_s	1298_{sh}
14	υ(Ring A) 22%, υ(Ring B) 15%	1288	1286_s	1278_m	
15	υ(Ring B) 25%, δ(C-H of Ring B) 29%	1259	1247_w	1246_m	1248_s
			1224_w	1226_m	
16	υ(Ring B) 31%, δ(C-H of Ring B) 24%	1206	1211_s	1212_w	1218_{sh}
17	υ(C-O_1) 22%, δ(C-H of Ring B) 14%	1178	1184_w	1188_s	1186_s
			1155_w	1148_m	1150_s
18	δ(C-H of Ring B) 39%, δ(CCC) 25%	1122	1130_s	1134_w	1116_w
19	δ(CCC) 24%, δ(C-H of Ring B) 12%	1073	1078_m		1078_{vw}
20	δ(CCC) 21%, υ(C-O_1) 19%	1046	1034_m	1034_w	1028_{vw}
21	δ(C-H of Ring B) 76%	1004		1000_s	1000_s
22	δ(C-H of Ring A) 61%	990	989_m	992_s	992_s
23	δ(C-H of Ring B) 53%, δ(C-H of Ring A) 13%	925	930_w		946_{vw}
24	δ(C-H of Ring A) 36%, υ(Ring A) 15%	919			
25	δ(C-H of Ring B) 37%, δ(C-H of Ring A) 13%	912	898_s		900_m
26	δ(C-H of Ring B) 47%, δ(C-H of Ring A) 23%	866	864_m		
27	δ(C-H of Ring A) 31%, δ(C-H of Ring B) 22%	856	839_w	838_s	842_s

Table 5-II: Force constants optimized in the normal mode calculation*

No.	Type of force constants	mdyne/Å	No.	Type of force constants	mdyne/Å
1	K(C_9-C_{10})	4.3583	21	H(C_4-C_{10}-$C_{9,5}$)	0.9000
2	K(C_3-C_4) & K(C_4-C_9)	3.0000	22	H(C_3-C_4-C_{10})	0.6000
3	K(C_2=C_3)	7.1682	23	H(C-C-H) of ring A	0.6108
4	K(C_2-O_1) & K(C_9-O_1)	4.7604	24	O(C....)	0.4667
5	K(C-C) of ring A	4.8813	25	O(O=....)	0.1152
6	K(C-H)	5.1340	26	O(OH....)	0.2436
7	K(C_4=O)	9.7110	27	O(H....)	0.3033
8	K(C_3-OH)	4.7523	28	T(O_1-C_2=C_3-OH)	0.0957
9	K(O-H)	5.7843	29	T(O=C_4-C_3-OH)	0.0800
10	K(C_2-$C_{1'}$)	3.0000	30	F(O...H)	0.0842
11	K(C-C) of ring B	4.6534	31	F(O..H..O)	0.2303
12	H(O_1-C_9-$C_{8,10}$)	0.6500	32	S-S: ortho- interaction**	0.0399
13	H(C-C-C)	1.0342	33	S-S: meta- interaction**	-0.1706
14	H($C_{3,10}$-C_4=O)	1.4499	34	S-S: para- interaction**	-0.1301
15	H($C_{2,4}$-C_3-OH)	0.6100	35	S-S: (C_3-O, O-H)	0.2124
16	H(O_1-C_2=C_3)	1.4163	36	S-S: (C_3-O, C_3-$C_{4,2}$)	0.0383
17	H(C_2=C_3-$C_{4,1'}$)	1.2001	37	S-S: (C_4=O, C_4-$C_{3,10}$)	0.2494
18	H(C_2-O_1-C_9)	1.7301	38	S-S: (C_4=O, O-H)	0.0913
19	H(C-C-H) of ring B	0.6325			
20	H(C_3-O-H)	0.5354			

* K: stretching; H: in plane bending; O: out of plane bending; T: torsion; F: non-bonded interaction; S-S: interaction between two stretching modes

** different interactions between two stretching modes in pyrone ring

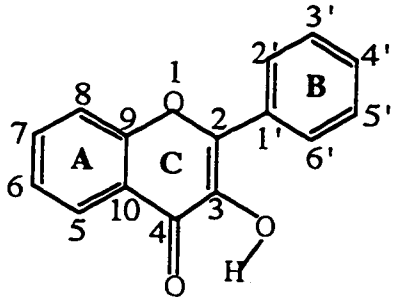

a: 3-HF

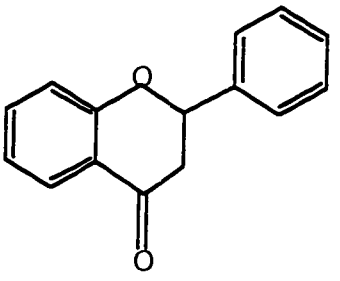

b: Flavanone

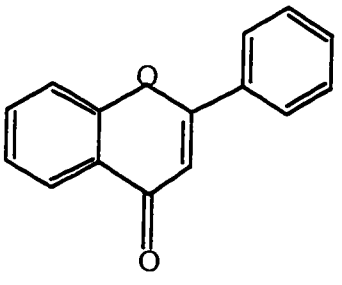

c: Flavone

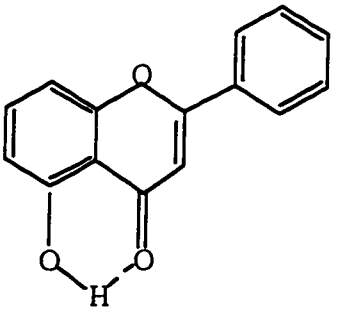

d: 5-HF

Figure 5-1: The Structures of 3-Hydroxyflavone and some flavonoids

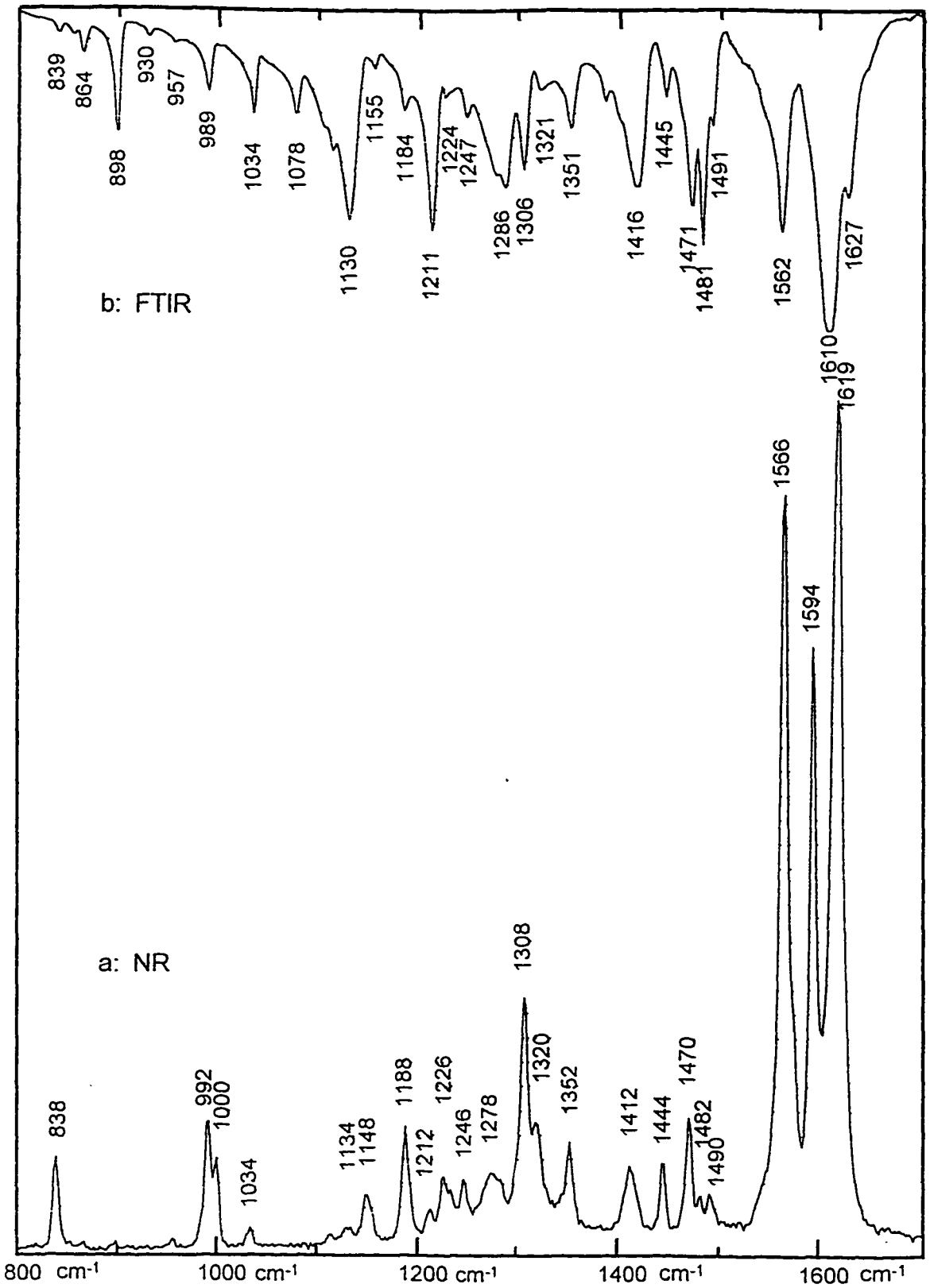

Figure 5-2: The comparison of (a) NR for a pure solid sample of 3-HF, and (b) FTIR for a KBr pellet of 3-HF

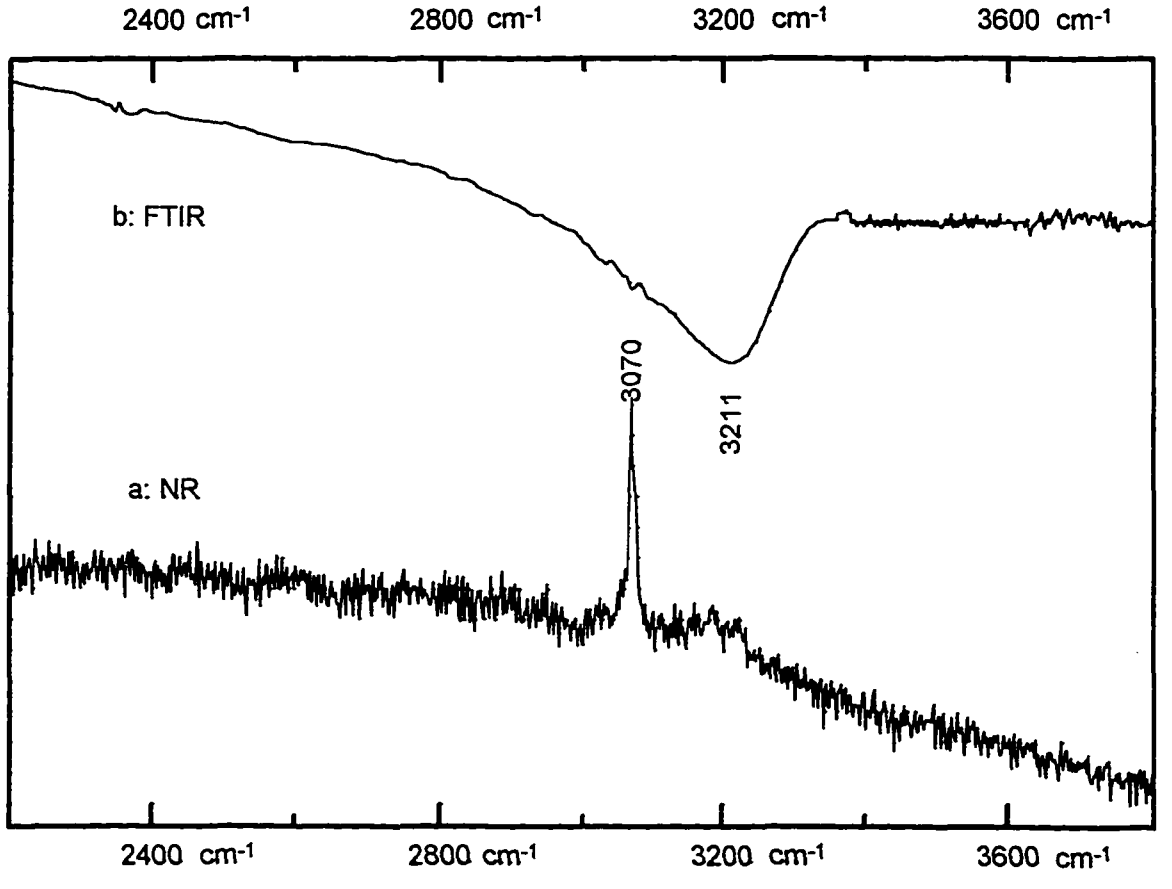

Figure 5-3: (a) NR and (b) FTIR of 3-HF in the high frequency region.
Samples are as same as indicated in Figure 5-2.

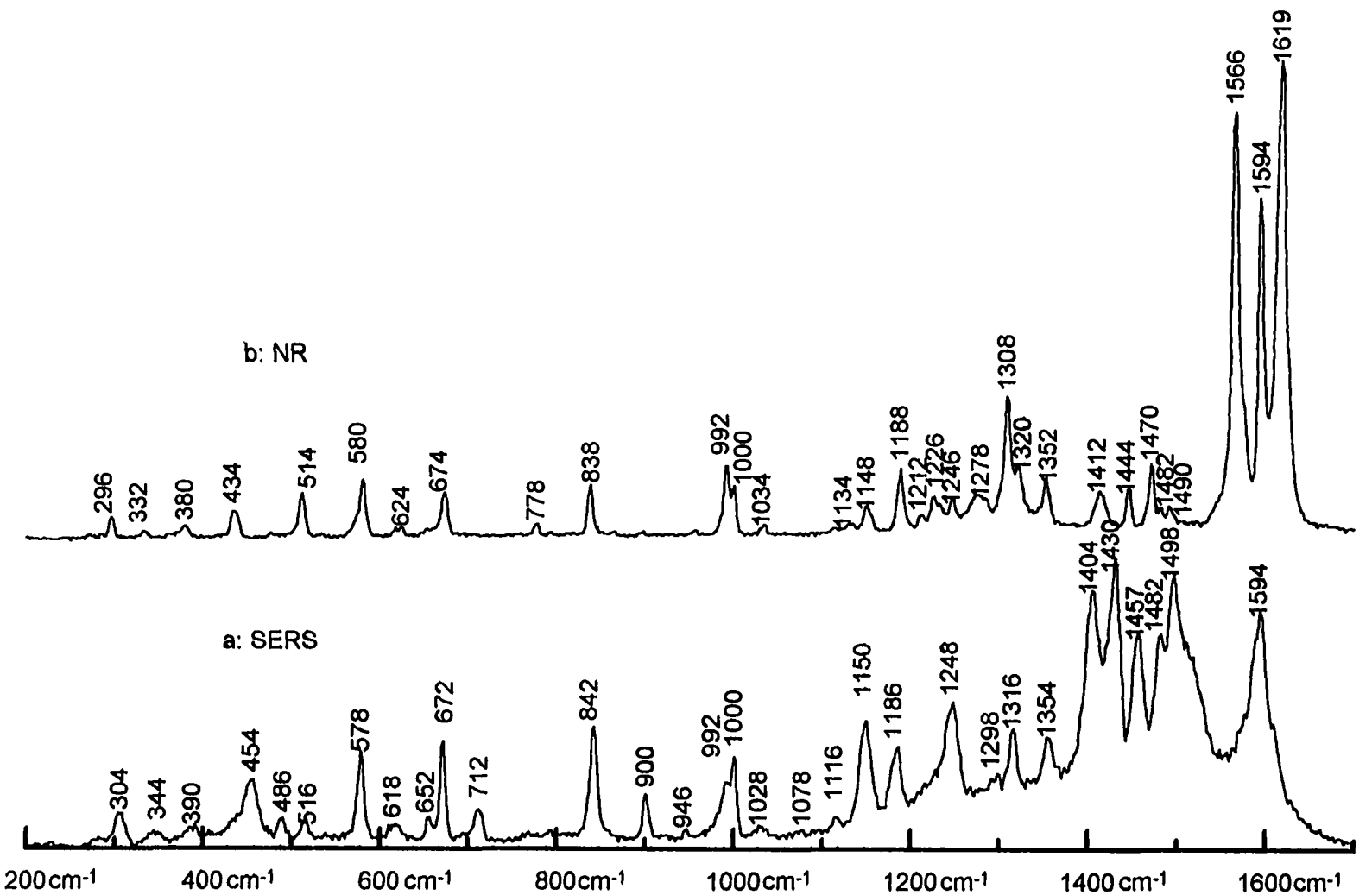

Figure 5-4: The comparison of SERS and NR of 3-HF. (a) SERS spectrum of 3-HF adsorbed on a roughened Ag electrode at applied potential -0.45 V vs SCE in pH 4.7 K_2SO_4 (0.1 M) solution. (b) NR spectrum of pure solid 3-HF.

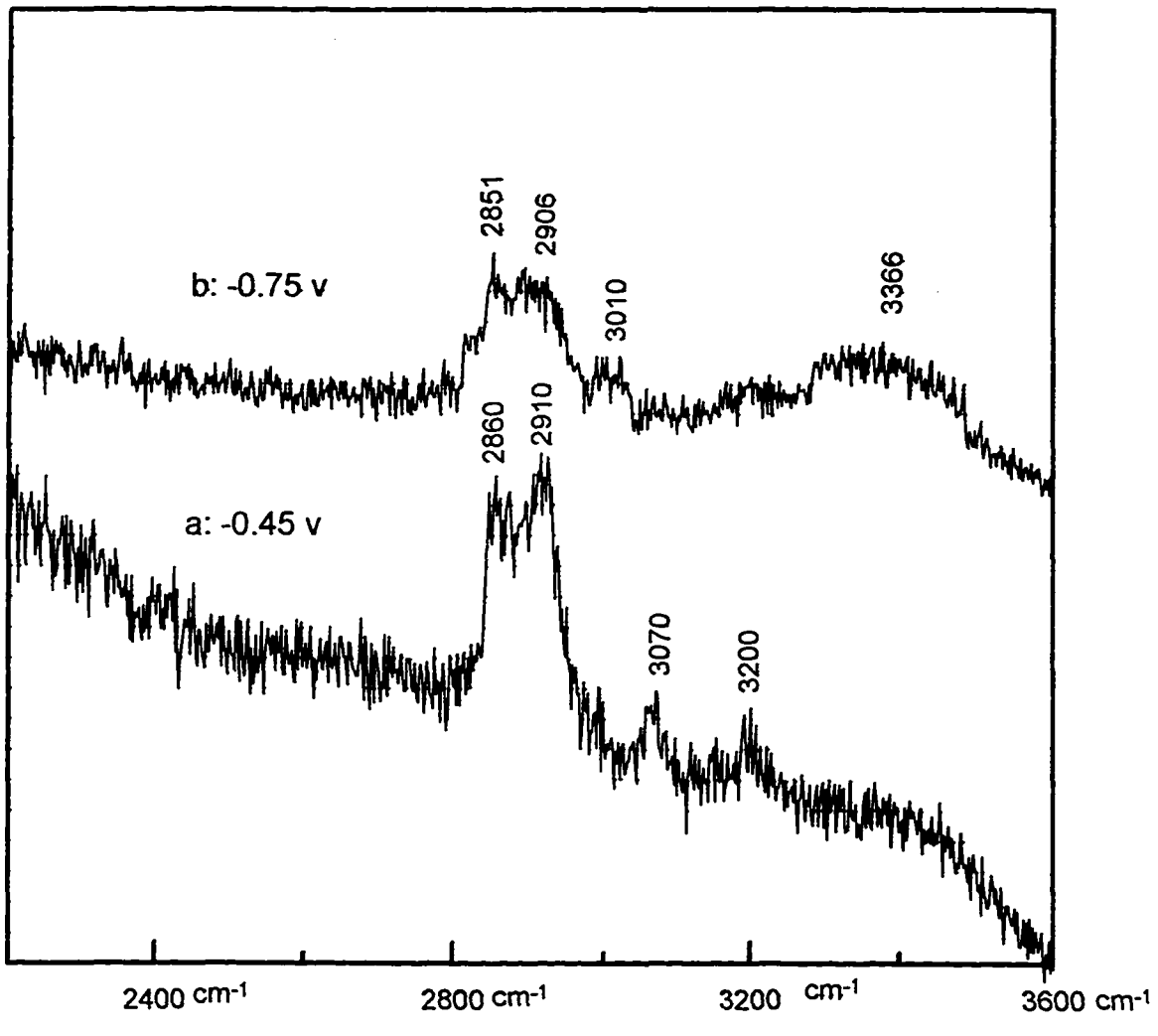

Figure 5-5: Potential Dependent SERS of 3-HF in the High Frequency.
(a) at applied potential -0.45 V, (b) at applied potential -0.75 V
Experiment conditions are same as indicated as Figure 5-4.

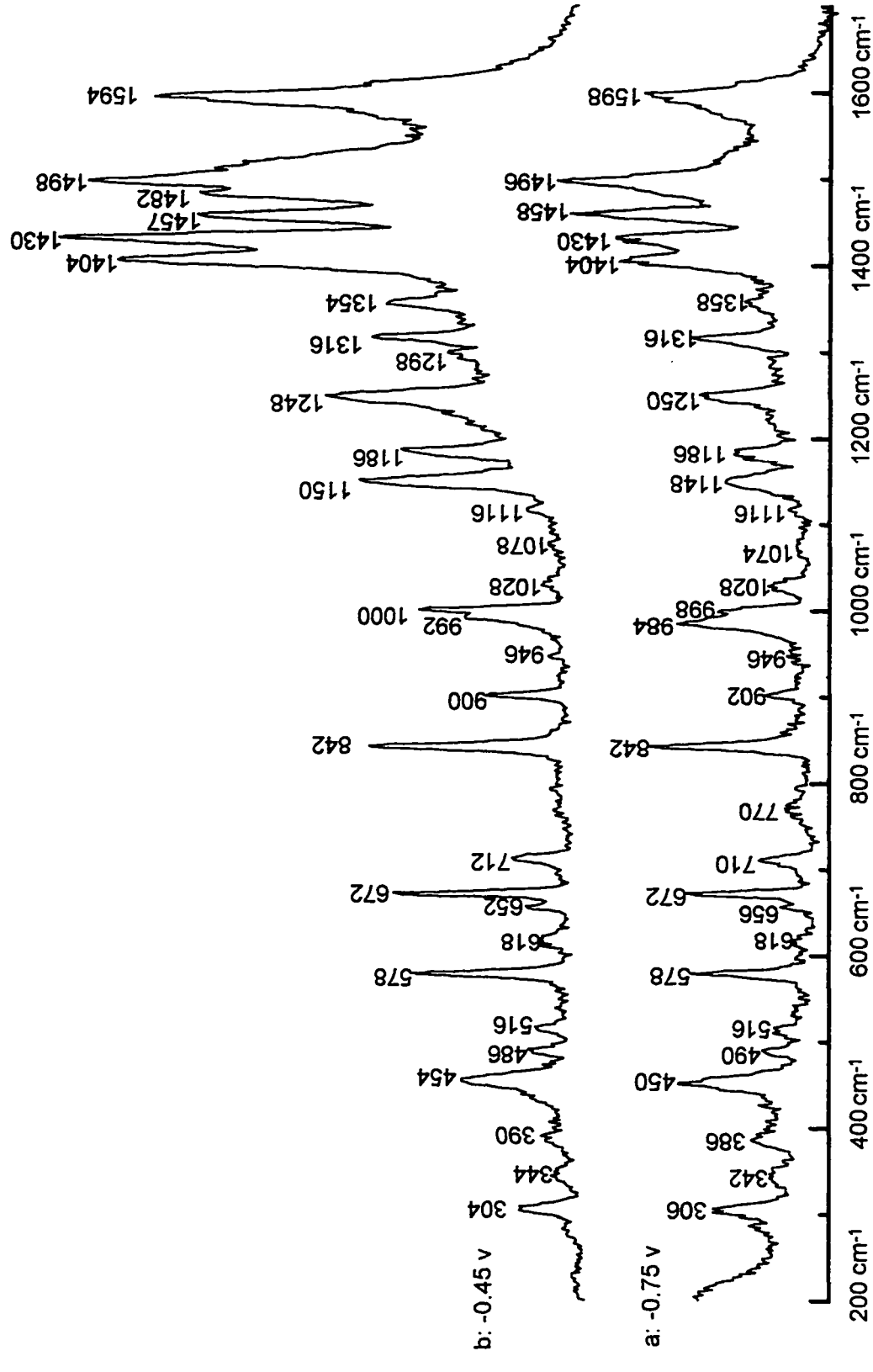

Figure 5-6: SERS of 3-HF at different potential (a) -0.75 V, and (b) -0.45 V.

Chapter VI

Time Resolved Surface Enhanced Raman Scattering Studies Of 3-hydroxyflavone On A Ag electrode

6.1 Introduction

Proton-transfer reactions occupy an important role in chemistry. Numerous investigations of proton transfer and photoisomerization in hydrogen-bonding systems have been reported.[1-4] The study of proton-transfer reactions is facilitated when both acid and base moieties are on the same molecule, e.g. 3-hydroxyflavone (3-HF). In 1979, Sengupta and Kasha[5] first proposed the mechanism of excited-state proton transfer (ESPT) to explain the dual luminescence phenomena (blue band at 413 nm and green band at 543 nm) of 3-hydroxyflavone. They described the behavior of 3-HF in terms of excited-state intramolecular proton transfer along the intra-molecular hydrogen bond. The mechanism of proton transfer in 3-HF is shown in Scheme 6-I. Since then, 3-HF has been studied extensively as a prototype molecule exhibiting excited state intramolecular proton transfer.[6-10] Most of the studies on 3-HF rely on steady-state electronic spectroscopy and nanosecond to picosecond time-resolved fluorescence measurements that permit detailed kinetic analyses of excited-state photo-tautomerization. Many steady-state and kinetic measurements have been made on 3-HF in a wide variety of solvent environments and temperatures in order to elucidate the mechanism of the proton transfer. In nonpolar environments, only tautomeric fluorescence (green band at 543 nm) is observed even at low temperature, implying a rapid ESPT process. The rate of the ESPT is believed to be on the order of femtoseconds.[11] In hydrogen-bonding solvents, observation of the normal (blue band at 413 nm) as well as the tautomeric (green band at 543 nm) fluorescence is observed. This indicates that proton transfer occurs slowly under these conditions. The rate of the ESPT in polar surroundings may be on the order of picoseconds.[11-13]

In spite of the ultrafast rate of the proton transfer in the excited state, Itoh et al.[14] reported several transient absorption and two-step laser excitation measurements to demonstrate that a long-lived ground-state tautomer of 3-HF at room temperature (approximately microseconds) is unexpectedly involved in the reverse proton transfer. It is striking that the rate for the ground-state reverse proton transfer (GSRPT) of 3-HF is reported to be more than 6 orders of magnitude smaller than the rate of the excited-state proton transfer. Contradictory to the previous results, Aartsma and co-workers[15] put a lower limit of $3x10^{10}$ s^{-1} for the rate of the reverse proton transfer by means of picosecond time-resolved absorption spectroscopy coupled with a stimulated emission pumping technique. But in 1989 Chou and Brewer et al.[16] re-examined the ground-state reverse proton transfer of 3-HF again by transient absorption and two-step laser excitation measurements. They reported that the life time of the ground-state tautomer at room temperature could be about 14 μs in thoroughly degassed solution, but about 0.3 μs when oxygen is present at high concentrations ($1x10^{-3}$ M). Since the rate of the reverse proton transfer may be the rate-determining step for the entire proton-transfer cycle, it may play a key role in determining the photo-chemical reactivity of 3-HF. Hence, a detailed study of the ground-state reverse proton transfer of 3-HF is desirable on the basis of the above controversial results.

The time resolved surface enhanced Raman spectroscopy (TRSERS) technique is an idea tool for short time resolved surface photochemistry of adsorbates at a Ag electrode.[17] Theoretically, a fs time scale Raman process could enable surface enhanced Raman scattering (SERS) experiments to follow the fastest reaction processes. An observation of intramolecular proton transfer in a photoinduced reaction of FMN adsorbed on a Ag surface has been observed by Zhang, Lombardi and Birke et al. with ns time scale TRSERS.[18]

In chapter 5, we have reported SERS spectral characteristics for 3-HF.[19] Here we use TRSERS to examine the mechanism of the ground-state reverse proton transfer of 3-HF. In order to ascertain the dynamics of the reverse proton transfer, a detection system that utilizes a gated diode array detector is applied in the TRSERS measurements. This detection system permits an entire spectrum to be recorded within a single pump-probe cycle and a repetitive pump-probe mode used to generate reasonable signal to noise ratio for short time resolution. With this detection system, our data show unequivocal evidence of the existence of a long-lived tautomer species in the relaxation of proton transfer in 3-HF.

6.2 Experimental Section

3-HF was purchased from the Aldrich Chemical Company Inc. and used as received. Reagent grade CH_3OH was purchased from Baker and $AgNO_3$ was purchased from Aldrich Chemical Company Inc.. All aqueous solutions were prepared with deionized distilled water.

In SERS and TRSERS experiments, the sample cell consisted of a silver working electrode, a Pt counter electrode, and a saturated calomel electrode (SCE) as the reference. All potentials reported in this chapter are quoted vs SCE. Two methods have been used to activate a Ag electrode. One procedure has been described as in the chapter 5. In that procedure the polished Ag electrode was roughened by an oxidation-reduction cycle (ORC) pretreatment in the aqueous solution of 3-HF ($2x10^{-5}$ M) in 0.1 M K_2SO_4 by applying a potential pulse from -0.4 V to 0.5 V for 2 seconds. 3-HF was adsorbed on the Ag electrode surface during the ORC. In the second procedure electrodeposition was used to roughen the Ag electrode surface. The polished

Ag electrode was dipped in the 1:1 (v/v) Of MeOH-0.05 M $AgNO_{3\,aq}$ solution in the presence of 3-HF ($2X10^{-5}$ M). Then a reduction potential of -0.4 V was applied on the working electrode (Ag) for 10-12 seconds. Ag^+ ions in the solution were reduced and deposited on the Ag electrode with 3-HF molecules together. Nonadsorbed 3-HF molecules were then washed out from the electrode surface by distilled water. After the ex-situ pretreatment, the activated Ag electrode was placed, in the absence of 3-HF, in 0.1 M K_2SO_4 aqueous solution in order to carry out SERS and TRSERS experiments at various potentials. The SERS spectra of 3-HF obtained from the two procedures are exactly the same in the region of 100-2000 cm^{-1}, but the intensity of Raman signals for the second procedure is stronger. Thus, in the TRSERS experiment the second procedure has been used for activating the electrode.

The SERS experimental setup is similar to that described in the previous publications[20] except that spectra were recorded by a Triplemate monochromator with optical multichannel analyzer (OMA). The pump-probe TRSERS instrumental setup has been described in detail in the earlier reports from our laboratory.[21] In the TRSERS experiments, we use a 337 nm nitrogen laser pulse to induce a proton transfer reaction of 3-HF on the electrode surface. Adsorbed 3-HF was excited by a nitrogen laser pulse of 1 mJ/pulse and a 5 ns pulse width. Excited 3-HF, or its photoproduct intermediates generated by 337 nm laser pulse were then probed by the 488 nm line of the Ar^+ ion laser. The excitation was followed by a delayed probe in which the detector was gated. The exciting nitrogen laser pulse energy density on the electrode surface was adjusted by changing the focus of the impinging light or the nitrogen gas pressure of the nitrogen laser pulse. The time delay between the pump and probe was adjusted by a programmable delay pulse generator and the gate of

the multichannel detector was opened by a 500 ns gate pulse for gathering the transit SERS signal.

6.3 Results and Discussion

For convenience of analysis and discussion, the structure and atom numbering of 3-HF, and each ring name have been shown in the scheme 6-I.

Figure 6-1 is the stationary SERS spectrum of 3-HF obtained by a Triplemate-OMA system at a potential of -0.45 V and pH value of 4.7, which represents the Raman character of the 3-HF species in the normal ground state. The assignment of Raman bands of 3-HF has been given in chapter 5.[19] Figure 6-2 is a comparison of spectra that were taken before and after photoexcitation (delay time is 75 ns, acquisition time 500 ns). As discussed later, Fig. 6-2b represents the Raman character of the 3-HF species in the tautomer ground state. Figure 6-3 shows the time evolution of the photoproduct spectra measured at delay times from 75 ns to 8 μ s. Figure 6-4 is the stationary SERS spectrum of 3-HF obtained after the photoexcitation experiment. It is exactly overlapped with the spectrum in Fig. 6-1, suggesting a reversible photoreaction cycle in which the final product is converted back to normal 3-HF under an applied potential of -0.45 V. In Table 6-I are listed in detail the vibrational frequency changes at various delay times.

Comparing the stationary SERS spectra with the TRSERS results, the following spectral features were observed:

(a) The band at 1595 cm^{-1} in the stationary spectrum, which has been assigned to the carbonyl stretching mode coupled with C_2=C_3 stretching, splits in to 1601 and 1585 cm^{-1} bands at delay time 75 ns in the TRSERS spectrum, and this splitting disappears at delay time about 1.5 μ s.

(b) The band at 1355 cm^{-1} in the stationary spectrum, which has been assigned to the O-H in-plane deformation, disappears at delay time 75 ns and reappears at delay time about 1 μs in TRSERS.

(c) New bands at 1344, 1285, 1264, 1106, 1063, and 977 cm^{-1} appear at delay time 75 ns and disappear at delay time around 1.5 to 4 μs in TRSERS spectra. Their intensities change with delay time.

(d) Two new bands at 966 and 1048 cm^{-1} appear at delay time 500 ns, and disappear at delay time about 2 μs. Their intensities also change when measured at different delay times.

(e) Frequency shifting were observed. The band at 1405 cm^{-1} shifts to 1420 cm^{-1}, then back to 1404 cm^{-1}; the band at 1030 cm^{-1} first shifts to 1038 cm^{-1}, then to 1023 cm^{-1}, then back to 1031 cm^{-1}; the band at 842 cm^{-1} shifts to 858 cm^{-1}, then back to 842 cm^{-1}.

The relative transient band intensities mentioned in (c) have been measured by choosing the band at 1430 cm^{-1} as the normalizing band, which has been assigned to the phenyl ring in-plane stretching only (the percentage of energy distribution (PED) is as high as 87%). This band shows no change during the TRSERS study since the phenyl ring in the molecule 3-HF is not involved directly in the ESPT process. The log intensity of some transient bands have been plotted as function of time and are shown in Figure 6-5. The fitting functions and corresponding correlation coefficients were also given in the Figure 6-5. It clearly shown that bands at 1344, 1285, 1264, 1106, 1063 and 977 cm^{-1} have almost the same linear decay time. But the new bands at 966 and 1048 cm^{-1} mentioned in (d) behave in different way.

From the above observations, it seems that two dynamic processes are involved during the ground state tautomer decay. The observations of the first process include (a), (b) and (c) as described as above. In general it is found

that photoexcitation increases the acidity of aromatic alcohols and the basicity of aromatic ketones,[22] and this results in an energetically favorable excited-state proton-transfer reaction in 3-HF. The band at 1355 cm^{-1} represents the O-H bending mode (PED 43%).[19] The observation that this band disappeared in the 575 ns TRSERS spectrum supports the conclusion that an excited state proton transfer has taken place. Note that the times quoted for spectra are the delay time plus the acquisition time. A more interesting phenomenon is the observation that this band reappears in the 1.5 μs TRSERS spectrum, suggesting a second conclusion that a reverse ground state proton transfer is taking place within this time domain.

The splitting of the band at 1595 cm^{-1} to 1601 cm^{-1} and 1585 cm^{-1} indicates electron density changing at the bonds of C=O and C_2=C_3 on going from normal 3-HF to the photoproduct intermediates. Unlike the normal ground state, the positive charge on the carbonyl group increased in the tautomer 3-HF (in the form C=O^+-H), so that the conjugation of the carbonyl group with the pyrone ring through the C=C bond at 2,3 position decreased. Thus the lower conjugation of C=O and C_2=C_3 may be responsible for the band at 1595 cm^{-1} splitting in to two bands, one at a little higher frequency, and another one at a little lower frequency. That the splitting of the band at 1595 cm^{-1} is observed only within about 1.5 μs supports the second conclusion again that the ground state reverse proton transfer is taking place within this time domain.

Furthermore, those transient bands at 1344, 1285, 1264, 1106, 1063 and 977 cm^{-1}, which are all observed at the 575 ns, show almost the same linear decay time. The average lifetime of these transient bands calculated from the slope of plots in Figure 6-5 is 1.4 μs. Among these transient bands, one band may correspond to a new deformation mode of C=O^+-H. Other bands may correspond to some compound bands splitting into their components. This is

caused by the distribution of electron density changes due to the structural difference between the normal and the tautomer states and the several resonance structures existing in the tautomer ground state (Figure 6-6).[23] According to above analysis, we infer that the TRSERS spectra represents the Raman character of the 3-HF species in a tautomer ground state. From our results, the life time of the tautomer 3-HF is in the μs time range (1.4 μs). During this time the photoisomerization reaction takes place on or near the electrode surface.

The observation of the second process concerns a new transient Raman band at 966 cm^{-1}, which appears at 500 ns and disappears at about 2 μs in the TRSERS spectra, as shown in Figure 6-3. This band may correspond to one kind of peroxide intermediate formed in the proton transfer cycle. 3-HF in the tautomer ground state has a strong electrophilic C=O$^+$-H functional group and the high nucleophilicity of the C=C-O$^-$ functional group may cause its high reactivity toward oxygen. The frequency of -O-O- stretching for the peroxide derivatives is around 900-950 cm^{-1} in normal Raman spectra.[24,25] The proposed mechanism of the photooxygenation of 3-HF in the tautomer ground state is the following:[16]

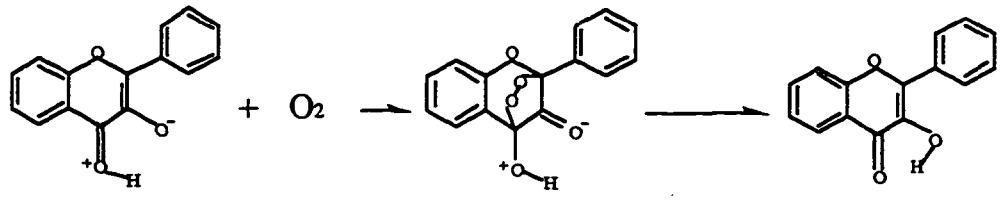

Tautomer **Peroxide** **Normal**

Further experimental evidence suggesting the formation of a peroxide intermediate comes from the observation of frequency shifts for some bands at 1405 cm^{-1}, 1030 cm^{-1}, and 845 cm^{-1}, and another transient band found at 1048

cm^{-1}, which behaves the same as the band at 966 cm^{-1}, appearing at 500 ns and disappearing at 2 μs. The compound band at 1405 cm^{-1}, which has been assigned to the phenyl ring stretching and C_3-O stretching, shifts to 1420 cm^{-1} in 500 ns TRSERS spectrum, then gradually shifts back to 1405 cm^{-1} in about 4 μs. This 15 cm^{-1} shift indicates an increase of the bond order in these vibrational modes during the relaxation of 3-HF from tautomer to normal ground state. Thus, the higher bond order of C_3-O in the peroxide form of 3-HF supports the formation of peroxide intermediate. Yet the reaction center of oxygen to 3-HF is on the pyrone ring, thus, the perturbation of the peroxide which forms also causes two other frequency shifts at the compound band of 1030 cm^{-1}, and at 845 cm^{-1}. The former band has been assigned to the deformation of C-C-C and stretching of C-O_1 on the pyrone ring, and the latter band has been assigned mainly to the deformation of C-H on the benzo-ring.[19] The lower conjugation of the benzo-ring with the pyrone ring in the peroxide form causes a simple frequency shift of 13 cm^{-1} for the band at 845 cm^{-1}, starting at 500 ns, shifting to 858 cm^{-1}, and shifting back to 847 cm^{-1} at about 2 μs. The shift happens in the same time domain as that of the transient band at 966 cm^{-1}, which we have discussed already.

The observation of frequency shift at the compound band at 1030 cm^{-1} is more complicated since the components of this band, C-C-C deformation and C-O_1 stretching, are just on the pyrone ring. It is expected at first that the frequency of the band at 1030 cm^{-1} should shift to low frequency when peroxide forms because the bond order of the C-C-C moiety of the pyrone ring decreases in the peroxide form. However, when the shift starts at 500 ns, it first shifts up to higher frequency at 1038 cm^{-1}, then shifts down to lower frequency at 1023 cm^{-1} at 1.5 μs. An explanation of this complicated frequency shift is proposed as follows. The perturbation of the peroxide form causes the compound band at

1030 cm^{-1} not just to shift frequency but also to split into its components. The C-O_1 stretching component appears at 1048 cm^{-1}, which is a new transient band, and C-C-C deformation component appears at 1038 cm^{-1}, which is at a little higher frequency due to the interference by the band at 1048 cm^{-1}, which is just forming. Then the band of the C-C-C deformation mode shifts, as expected, to lower frequency at 1023 cm^{-1} during the development of peroxide formation. When the transient band at 1048 cm^{-1} disappears at 2 μs, the compound band shifts back to its original frequency at 1030 cm^{-1}.

In conclusion the existence of a long-lived tautomer species in the relaxation of the proton transfer of 3-HF has been demonstrated by TRSERS. The life time of tautomer on the Ag electrode is about 1.4 μs. The TRSERS spectral results also support the formation of a photooxygenation product in the peroxide form during the ground state reverse proton transfer reaction of 3-HF.

Table 6-I: Time dependent SERS of 3-HF

Before /	After photoexcitation: Delay time								
cm^{-1}	75(ns)	500(ns)	1(us)	1.5(us)	2(us)	4(us)	8(us)	16(us)	12(min)
	1601	1597	1602						
1595_s				1592	1593	1592	1591	1591	1593
	1585	1588	1588						
1497_s	1497	1502	1498	1496	1500	1497	1498	1494	1494
1484_{sh}	1483	1483	1486	1473	1484	1490	1484	-------	-------
1457_s	1459	1458	1452	1457	1457	1459	1455	1458	1457
1430_s	1430	1433	1429	1428	1429	1429	1427	1429	1429
1405_s	1405	1420	1414	1407	1410	1404	1406	1407	1404
o	1377	1382	1377	1373	1379	-------	-------	-------	-------
1355_m*	-------	-------	1355	1355	1355	1355	1354	1355	1355
o	1344	1344	1341	1332	1345	1332	-------	-------	-------
1317_s	1316	1318	1314	1316	1319	1312	1316	1315	1317
1299_{sh}	1302	-------	1304	1302	1303	1295	1299	1298	1299
o	1285	1286	1287	1277	1287	-------	-------	1287	-------
o	1264	1253	1251	-------	-------	-------	-------	-------	-------
1248_s	1245	1241	1239	1248	1248	1248	1249	1249	1248
1217_{sh}	1215	1205	1206	1218	1216	1211	1211	1215	1217
1184_s	1179	1182	1180	1184	1185	1183	1184	1186	1184
1149_s	1141	1149	1148	1149	1149	1151	1149	1154	1148
1115_{vw}	1119	1124	1114	1119	1122	1119	1130	1123	1115
o	1106	1105	1104	1103	1107	1109	-------	-------	-------
1076_{vw}	1081	1080	1089	1084	1078	1081	1077	1083	1079
o	1063	1063	1063	1072	1068	-------	1064	1063	-------
o	-------	1048	1049	1046	1052	-------	-------	-------	-------
1031_{vw}	1030	1038	1035	1023	1038	1037	1030	1031	1031
999_s	997	1002	995	993	995	998	998	998	999
o	977	978	978	979	970	-------	-------	-------	-------
o	-------	966	962	956	960	-------	-------	-------	-------
o	928	-------	-------	-------	-------	-------	-------	-------	-------
904_m*	910	915	910	908	904	909	898	910	904
845_m	842	850	858	853	847	846	843	842	845

*: Band disappeared from the original spectrum after photoexcition

o: New bands formed after photoexcition

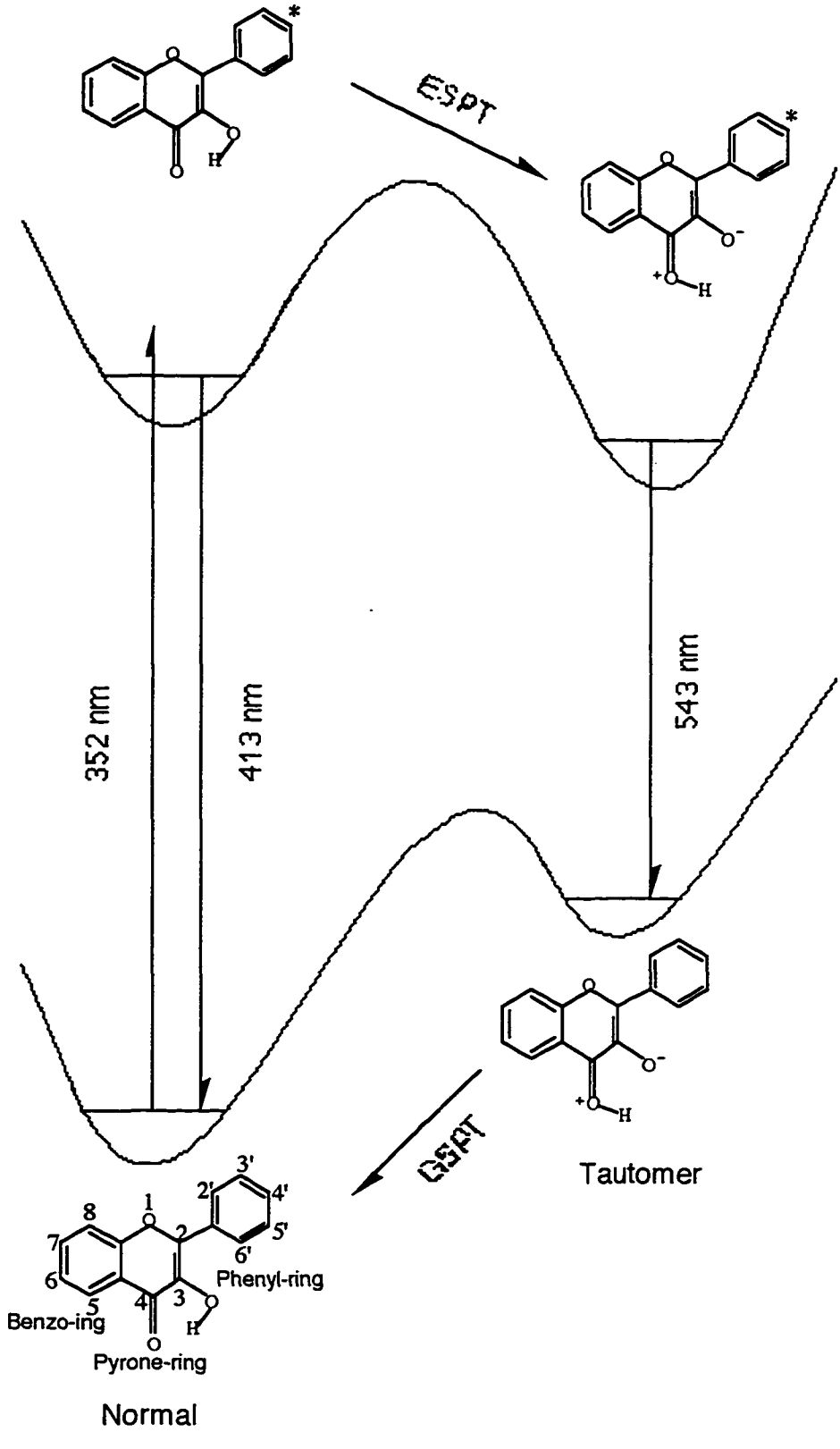

Scheme 6-I: The Mechanism of Proton Transfer in 3HF

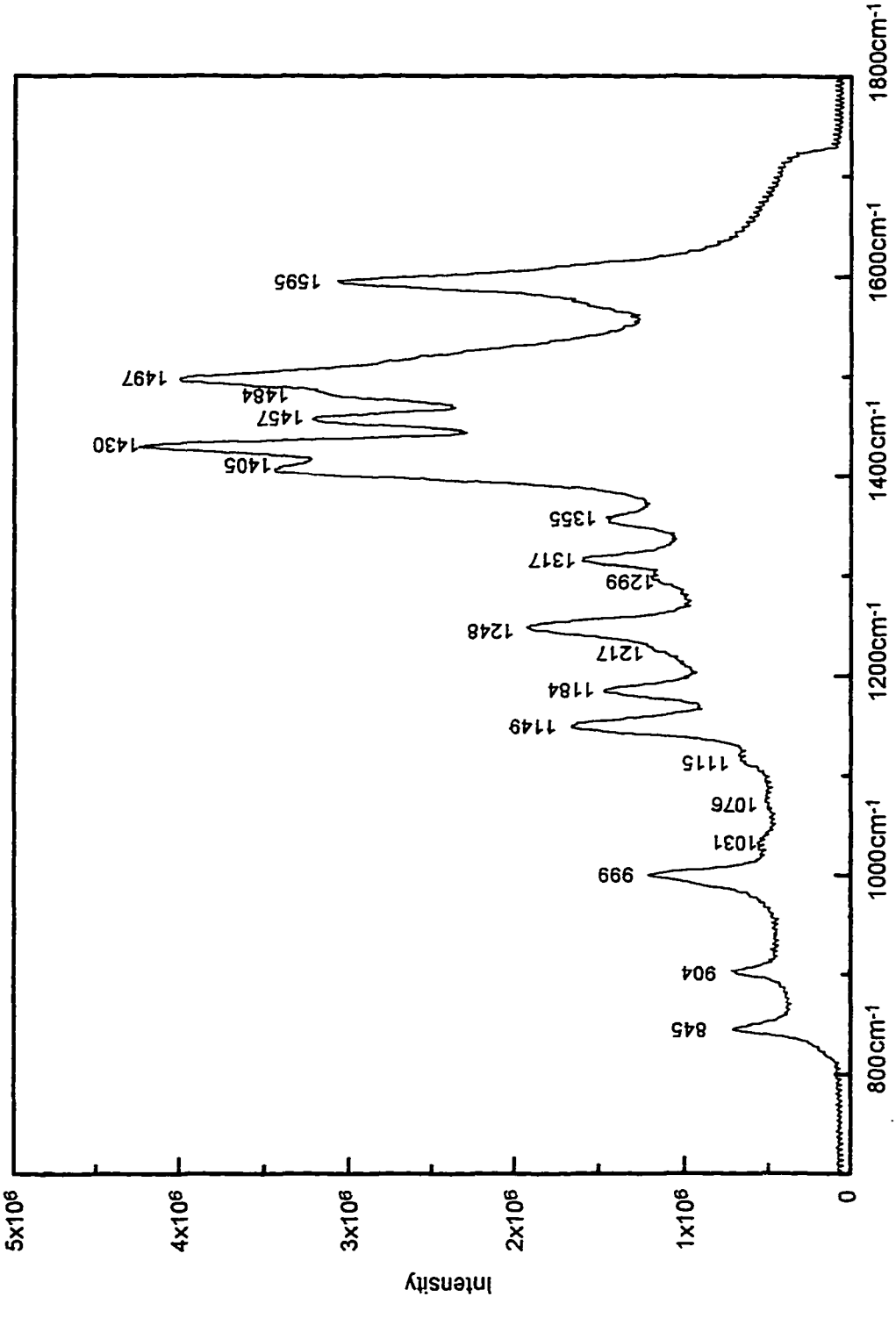

Figure 6-1: SERS of 3-HF adsorbed on a roughened Ag electrode at potential of -0.45 V vs SCE in pH 4.7 K_2SO_4 (0.1 M) solution.

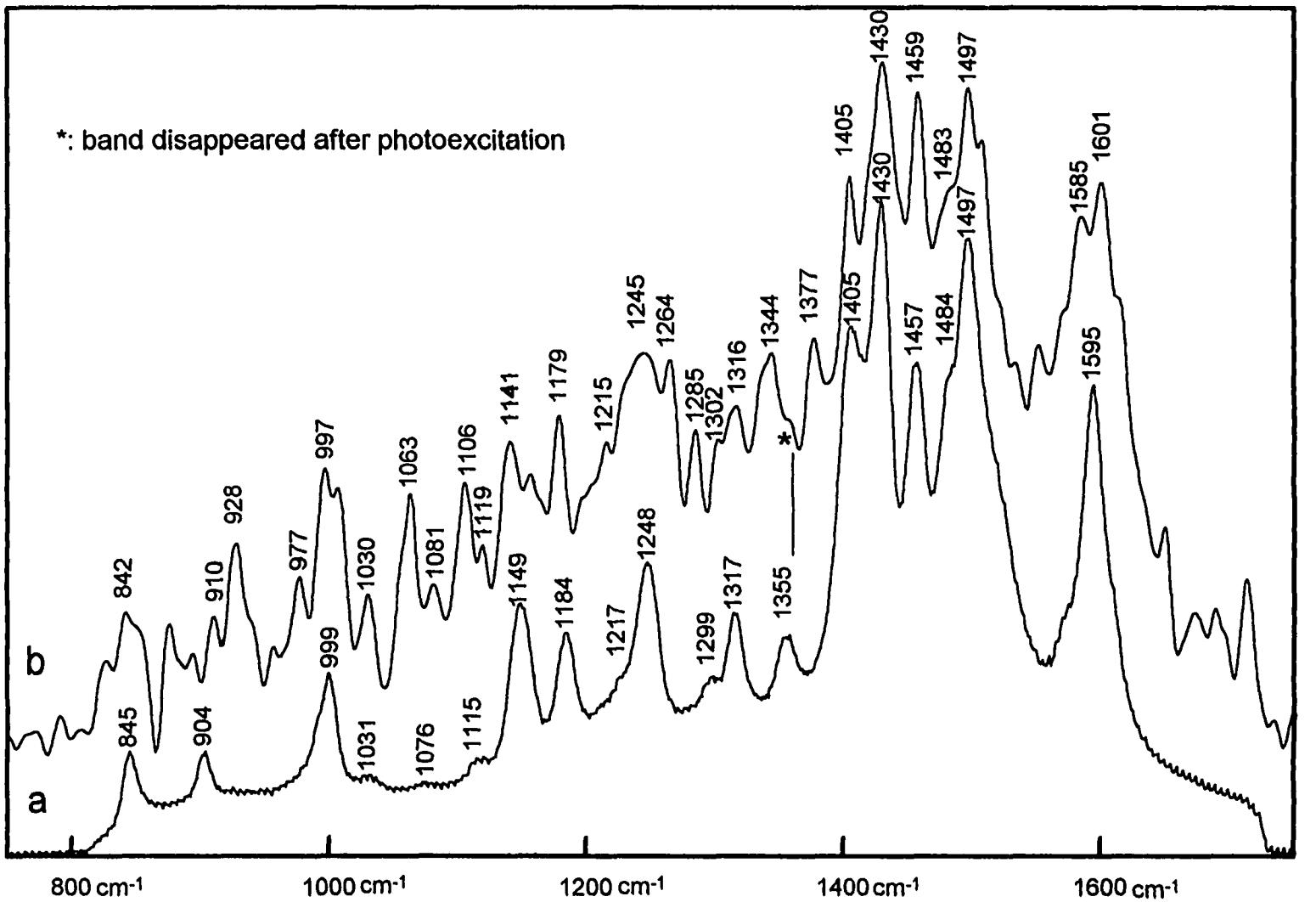

Figure 6-2: TRSERS spectra of 3-HF adsorbed on a roughened Ag electrode at potential of -0.45 V vs SCE in pH 4.7 K_2SO_4 (0.1 M) solution. (a) before photoexcitation. (b) 75ns after photoexcitation. Integration time is 500ns

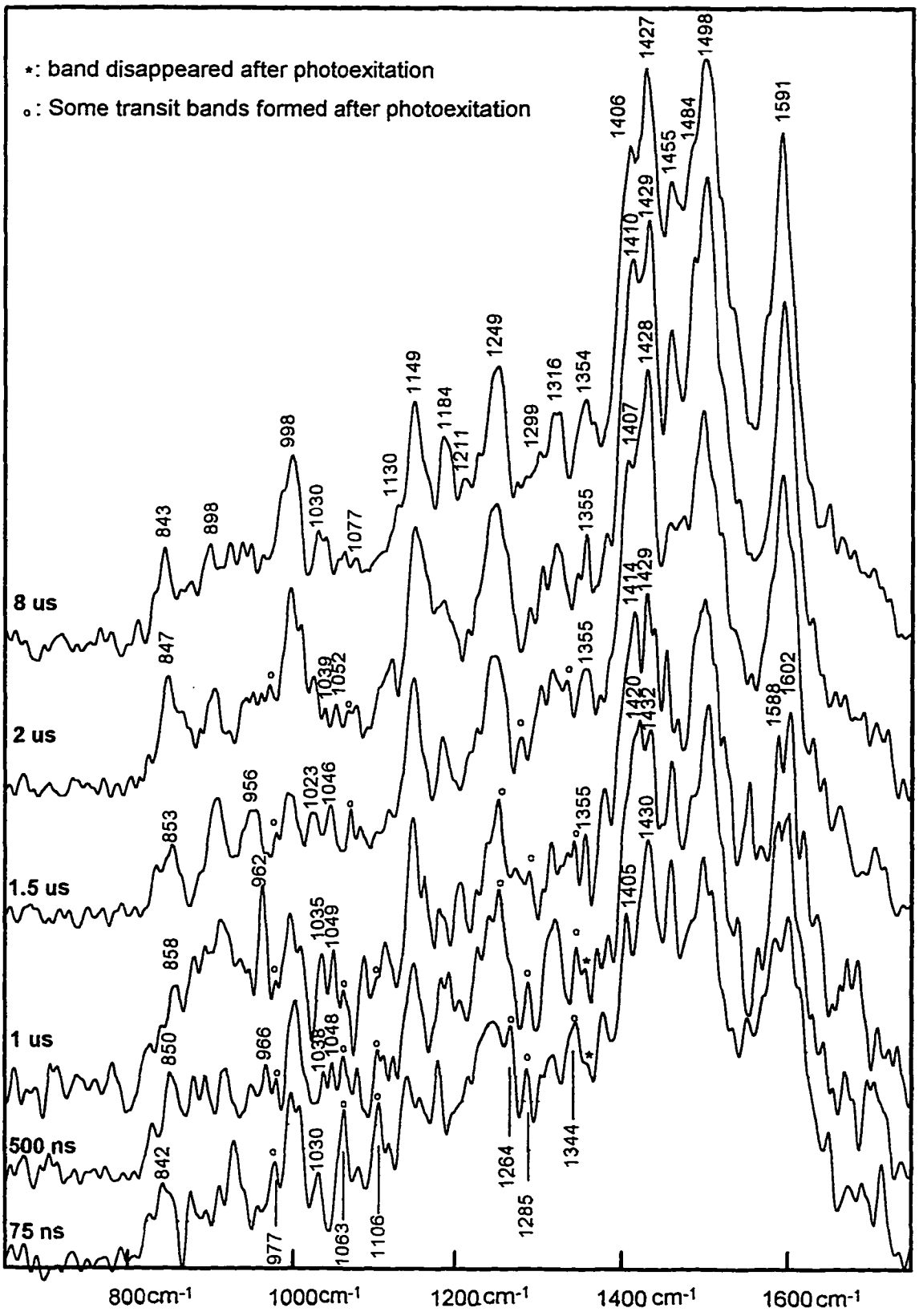

Figure 6-3: Time evolution of the photoproduct spectra of 3-HF, same condition as Fig.6-2

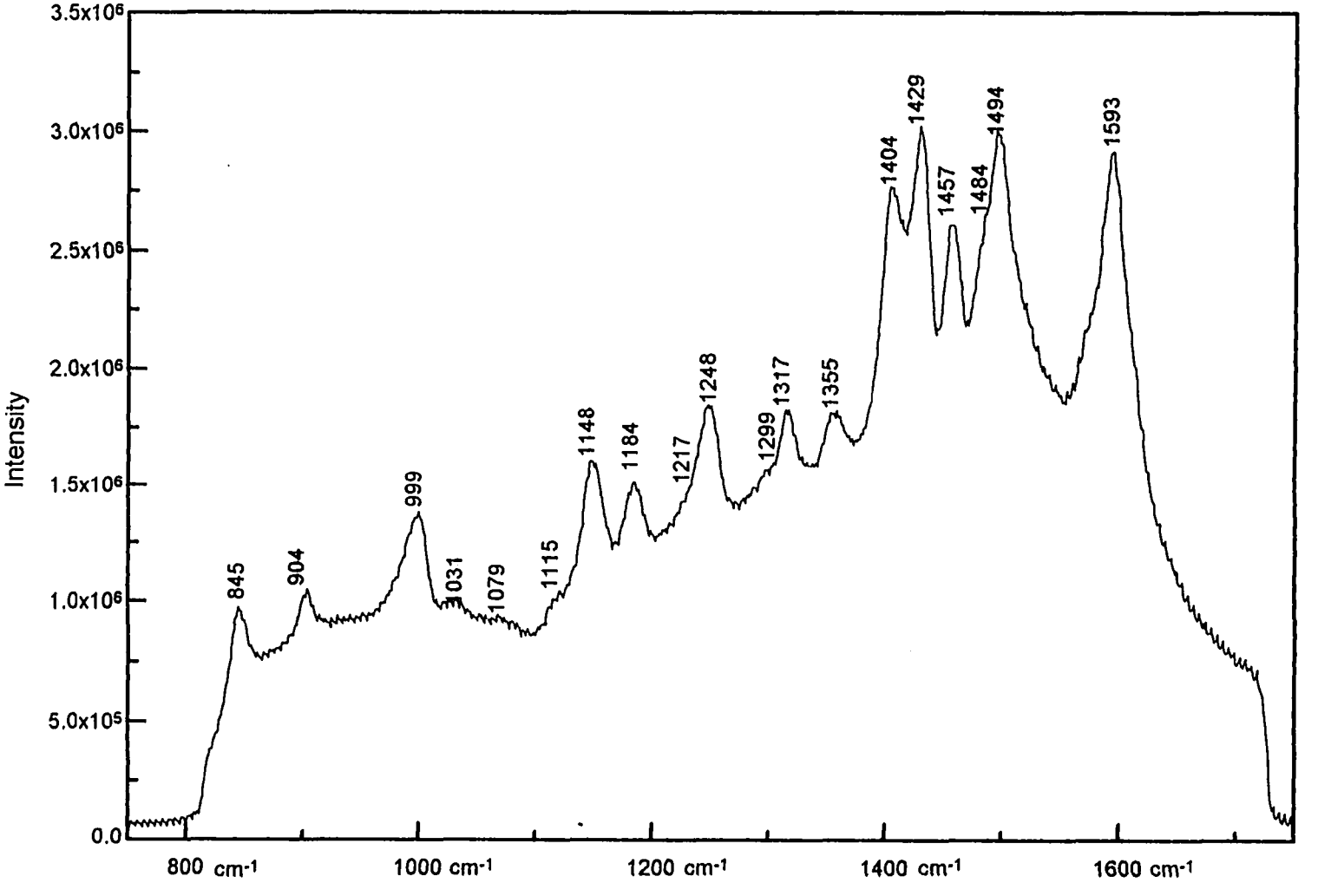

Figure 6-4: SERS of 3-HF obtained after photoexcitation experiment, same conditions as Fig.6-1.

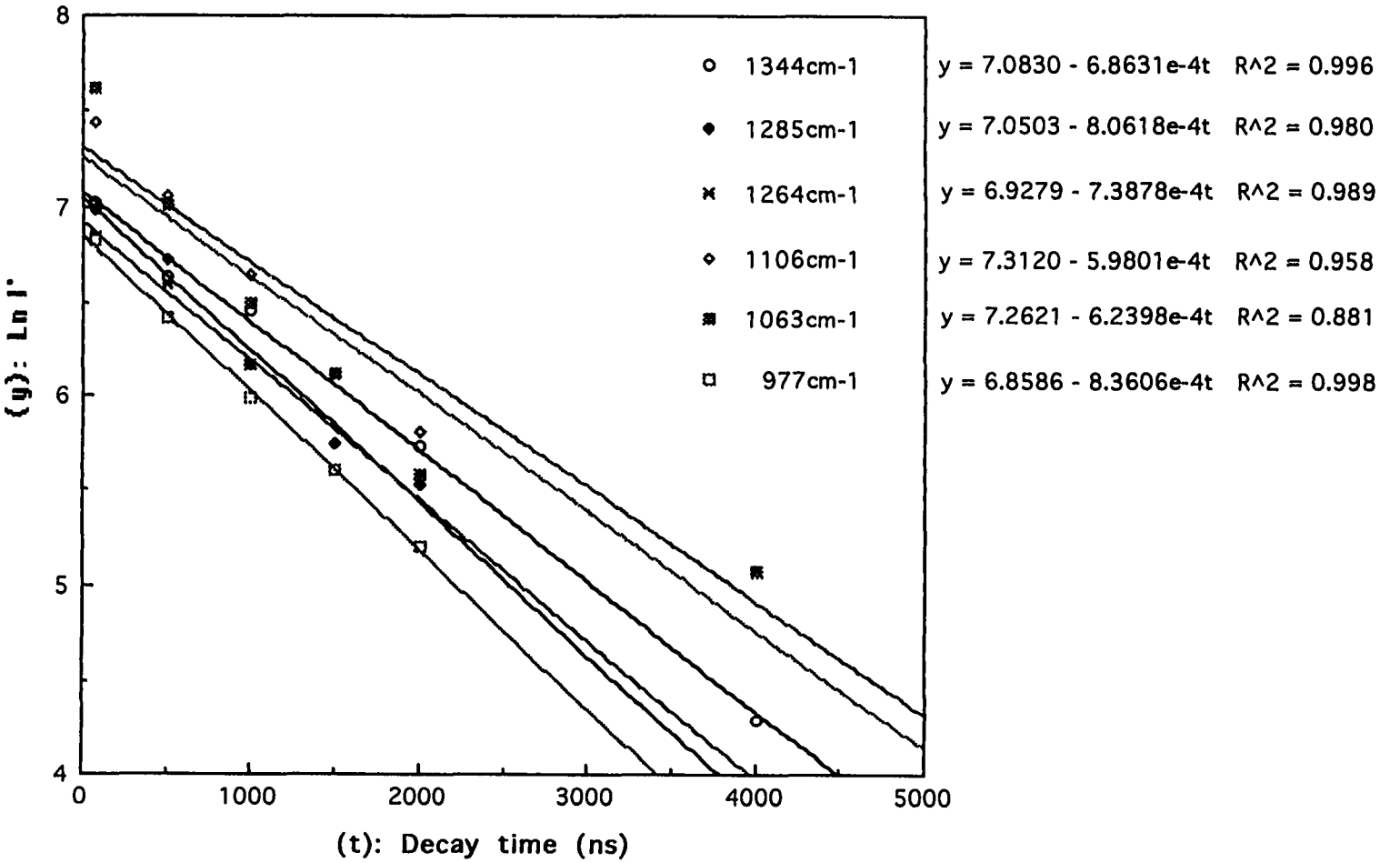

Figure 6-5: Log intensity of some transient bands plotted against delay time observed for photoproduct 3-HF.

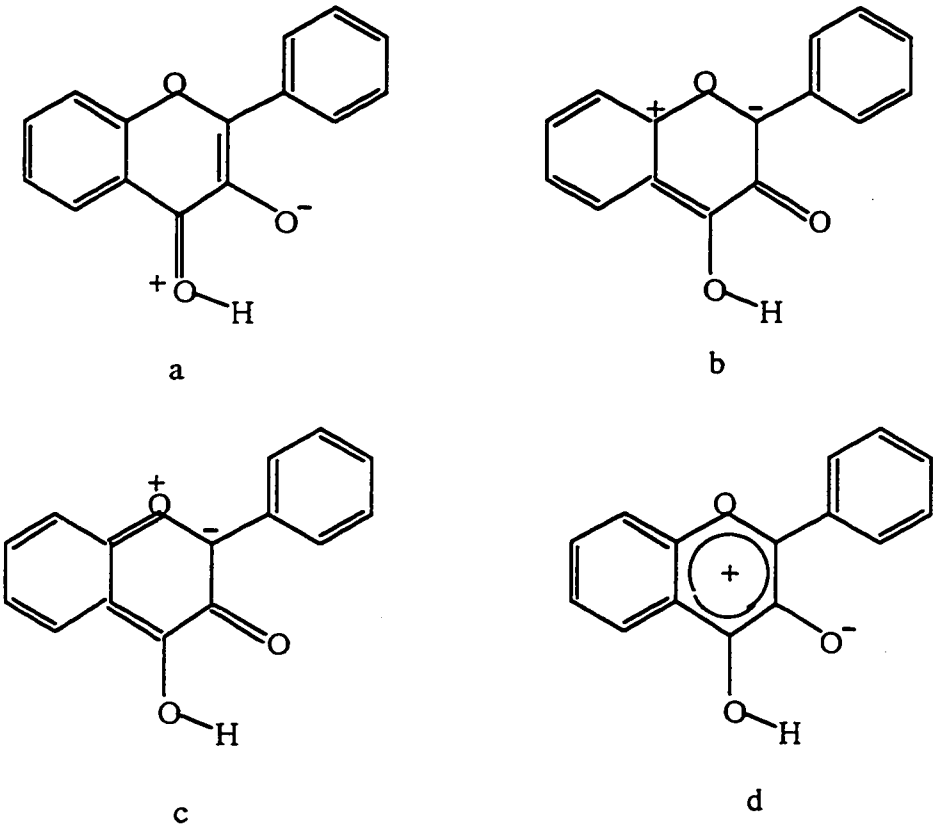

Figure 6-6: The Resonance Structures of 3-HF in The Tautomer Form

BIBLIOGRAPHY

Chapter 1

(1) R. L. Birke, and J. R. Lombardi: "Investigation of Radical Ions with Time-Resolved Surface Enhanced Raman Spectroscopy", in 'Molecular Engineering' 4, Kluwer Academic Publishers, Netherlands, 1994, pp. 277-310.

(2) R. K. Chang, "Surface Enhancement Mechanisms", in 'Time-Resolved Vibrational Spectroscopy', Academic Press, Inc., 1983, pp. 369-375.

(3) R. K. Chang, and B. L. Laube, CRC Crit. Rev. Solid State Mater. Sci., 12 (1984) 1.

(4) D. A. Weitz, M. Moskovits, and J. A. Creighton, in R. B. Hall and A. B. Ellis (Eds.), 'Chemistry and Structure at Interfaces-New Laser and Optical Techniques', VCH, Deerfield Beach, FL, 1986, p. 197.

(5) Wei Zhang, "Time Resolved Surface Enhanced Raman Scatteing Studies of Surface Photochemistry and Electrochemistry", Ph. D. Thesis, 1995, City Univ. of New York.

(6) R. K. Chang, and T. E. Furtak (eds.): 'Surface Enhanced Raman Scattering', Plenum Press, New York, (1982)

(7) R. L. Birke, T. Lu, and J. R. Lombardi: "Surface-Enhanced Raman Spectroscopy", in R. Varmi and J. R. Selman (eds.), 'Techniques for the Characterization of Electrodes and Electrochemical Process', John Wiley and Son, Inc., New York (1991), pp. 211-277.

(8) M. A. El-sayed, Pure & Appl. Chem., Vol. 57, No. 2, pp. 187-193, 1985, Printed in Great Britain.

(9) Ping Gao, David Gosztola and Michael J. Weaver, Analytica chimica Acta, 212 (1988) 201-212.

(10) T. M. Cotton, J. Am. Chem. Soc. 102, 7960 (1980).

(11) R. L. Garrell, J. Bioactive, and Compatible Polymers, Vol. 6, 1991, p. 296

(12) R. K. Chang, "Spectroscopic & Diffraction Techniques in Interfacial Electrochemistry", Eds by C. Gutierrez and C. Melendres, Klumer Academic Publishers, 1990.

(13) C. Shi, W. Zhang, R. L. Birke, and J. R. Lombardi: J. Electroanalytical Chemistry and Interfacial Electrochemistry, in press (1997).

(14) C. Shi, W. Zhang, R. L. Birke, and J. R. Lombardi: J. Phys. Chem. 95, 6276 (1991).

(15) W. Zhang, A. Vivoni, J. R. Lombardi, and R. L. Birke: J. Phys. Chem. 99, 12846 (1995).

(16) G. C. Pimental (ed.): "Opportunities in Chemistry", National Academy Press, Washington, S. 86 ff. (1985).

Chapter 2

(1) G. Herzberg: " Molecular Spectra and Molecular Structure," 2nd Ed., van Nostrand Reinhold Company, New york, 1950.

(2) J. I. Steinfeld: "Molecules and Radiation, An Introduction to Molecular Spectroscopy," The MIT Press, Cambridge, Massachusetts, 1985.

(3) P. R. Carey: "Biochemical Applications of Raman and Resonance Raman Spectroscopies", Academic Press, New York London, 1982

(4) J. R. Lombardi, R. L. Birke, T. Lu, and J. Xu: J. Chem. Phys. **84**, 4174 (1986).

(5) A. C. Albrecht: J. Chem. Phys. **3 4**, 1476 (1961)

(6) R. L. Paul, A. J. McQuilan, P. J. Hendra, and M. Fleischmann: J. Electroanal. Chem. 66, 248 (1975).

(7) M. L. A. Temperini, H. C. Chagas, and O. Sala: Chem. Phys. Lett. 79(1), 75 (1981).

(8) J. R. Lombardi, and R. L. Birke: Surf. Sci. 95, 1259 (1980).

(9) M. Fleischmann, I. R. Hill, and G. Sundholm: J. Electroanal. Chem. 157(2), 359 (1983).

(10) M. Fleischmann, I. R. Hill, and G. Sundholm: J. Electroanal. Chem. 158(1), 153 (1983).

(11) M. Kim, and K. Itoh: J. Electroanal. Chem. 188(1-2), 137 (1985).

(12) D. Thierry, and C. Jeygrad: J. Electrochem. Soc. 132(5), 1009 (1985).

(13) K. C. Grabar, R. G. Freeman, M. B. Hommer, and M. J. Natan, J. Anal. Chem. 1995, 67, 735-743.

(14) B. H. Loo, Y. G. Lee and Z. Yazid: Chem. Phys. Lett. 114(4), 405 (1985).

(15) S. M. Heard, F. Grieser, and C. G. Barraclough: Chem. Phys. Lett. 95(2), 154 (1983).

(16) R. R. Smardzewski, R. J. Colton, and J. S. Murday: Chem. Phys. Lett. 68(1), 53 (1979).

(17) J. E. Rowe, C. V. Shank, D. A. Zwemer, and C. A. Murray: Phys. Rev. Lett. 44(26), 1770 (1980).

(18) H. Seki, and M. R. Philpott: J. Chem. Phys. 73(10), 5376 (1980).

(19) I. Pockrand, J. Billmann, and A. Otto: J. Chem. Phys. 78(11), 6384 (1983).

(20) H. Seki: J. Elecroanal. Chem. 150(1-2),425 (1983).

(21) K. Manzel, W. Schulze, and M. Moskovits: Chem. Phys. Lett. 85(2), 183 (1982).

(22) C. G. Blatchford, O. Siiman, and M. Kerker: J. Phys. Chem. 87(14), 2503 (1983).

(23) P. C. Lee, and D. Meisel: Chem. Phys. Lett. 99(3), 262 (1983).

(24) J. A. Creighton, M. S. Alvarez, D. A. Weitz, S. Garoff, and M. W. Kim: J. Phys. Chem. 87(24), 4793 (1983).

(25) S. M. Heard, F. Grieser, C. G. Barraclough, and J. V. Sanders: J. Phys. Chem. 89(3), 389 (1985).

(26) J. C. Tsang, J. R. Kirtley, and J. A. Bradley: Phys. Rev. Lett. 43, 772 (1979).

(27) J. C. Tsang, and J. R. Kirtley: Solid State Commun. 30(10),617 (1979).

(28) J. C. Tsang, J. R. Kirtley, T. N. Thesis, and S. S. Jha: Phys. Rev. B: Condens. Matter [3], 25(8), 5070 (1982).

(29) J. C. Tsang, P. Avouvis, and J. R. Kirtley: J. Electron Spectrosc. Relat. Phenom. 29,343 (1983).

(30) M. Fleischmann, P. J. Hendra, and A. J. McQuillian: Chem. Phys. Lett. **2 6**, 163 (1974).

(31) Jia Xu, "Surface Enhanced Raman Spectroscopy on Electrodes: Enhancement mechanisms and Application to the Studies of Flavin Molecules", Ph. D. Thesis, 1987, City Univ. of New York.

(32) T. M. Davine: in 'Electrochemical and Optical Techaniques for the Study and Monitoring of Metallic Corrosion', M. G. S. Ferreira and C. A. Melendres (eds.), Kluwer Academic Publishers, 389-437 (1991).

(33) S. Maskevich, N. Strekal, I. Artsukevich, I. Chernikevich, G. gachko, and V. Oskirko, in Fifteenth International Conference on Raman spectroscopy, Volume II, Eds by P. Stein and S. A. Asher, 1996, p.74.

(34) J. F. Arenas, M. S. Woolley, J. C. Otero, and J. I. Marcos, in Fifteenth International Conference on Raman spectroscopy, Eds by P. Stein and S. A. Asher, 1996, p.626.

(35) P. S. Wooley, B. J. Keely, and R. E. Hester, in Fifteenth International Conference on Raman spectroscopy, Eds by P. Stein and S. A. Asher, 1996, p.660.

(36) M. K. Weldon, V. R. Zhelyaskov, and M. K. Morris, in Fifteenth International Conference on Raman spectroscopy, Eds by P. Stein and S. A. Asher, 1996, p.678.

(37) M. Nissum, P. W. Jensen, and O. F. Nielsen, in Fifteenth International Conference on Raman spectroscopy, Eds by P. Stein and S. A. Asher, 1996, p.674

(38) R. P. Van Duyne, in: Chemical and Biochemical Applications of Lasers, Bol. 4, Ed. C. B. Moore (Academic Press, New York, 1978), pp. 101-185

(39) J. A. Creighton, M. G. Albrecht, R. E. Hester, and J. A. D. Matthew: Chem. Phys. Letters 55 (1978) 55.

(40) D. L. Jeanmaire, and R. P. Van Duyne: J. Electroanal. Chem. 84 (1977) 1.

(41) B. Pettinger, and U. Wenning and D. M. Kolb, Ber. Bunsenges: Physik. Chem. 82 (1978) 1326.

(42) M. G. Albrecht, and J. A. Creighton: J. Am. Chem. Soc. 99 (1977) 5215.

(43) M. Fleischmann, P. J. Hendra, A. J. McQuillan, R. L. Paul and E. S. Reid: J. Raman Spectrosc. 4 (1976) 269.

(44) S. Efrima, and H. Metiu: Chem. Phys. Letters 60 (1978) 59;

(45) S. Efrima, and H. Metiu: J. Chem. Phys. 70 (1979) 1602, 2297, 1939.

(46) M. R. Philpott: J. Chem. Phys. 62 (1975) 1812.

(47) F. W. King, R. P. Van Duyne, and G. C. Schatz: J. Chem. Phys. 69 (1978) 4472.

(48) G. L. Eesley, and J. R. Smith: Solid State Commun. 31 (1979) 815.

(49) R. M. Hexter, and M. G. Albrecht: Spectrochim. Acta 35A (1979) 233

(50) A. Otto: Surface Sci. 75 (1978) L392.

(51) A. Otto, in: Proc. Conf. on Vibrations in the Adsorbed Layer, Jülich, Germany, 1978,p.162.

(52) S. L. McCall, and P. M. Platzman: Bull. Am. Phys. Soc. 24 (1979) 340.

(53) E. Burstein, Y. J. Chen, C. Y. Chen, S. Lundquist and E. Tosatti: Solid State Commun. 29 (1979) 567.

(54) A. Otto, J. Timper, J. Billmann, G. Kovacs and, I. Pockrand: Surface Sci. 92 (1980) L55.

(55) R. K. Chang: "Raman Spectroscopic Techniques in Interfacial Electrochemistry", in C.Gutiérrez and C. Melendres (eds.), Spectroscopic and Diffraction Techniques in Interfacial Electrochemistry, Kluwer Academic Publishers, Netherlands, pp. 155-180.

(56) J. A. Creighton: "The Selection Rules for Surface-Enhanced Raman

Spectroscopy", in R. J. H. Clark and R. E. Hester (eds.), Spectroscopy of Surfaces, Hohn Wiley and Sons Ltd, 1988, pp.37-89.

(57) R. L. Birke, and J. R. Lombardi: "Surface Enhanced Raman Scattering", in J. R. Gale (ed.), Spectroelectrochemistry: Theory and Practice, Plenum Press, New York, 1988, pp263-348.

(58) R. L. Birke, T. Lu, and J. R. Lombardi: "Surface-Enhanced Raman Spectroscopy", in R. Varmi and J. R. Selman (eds.), Techniques for the Characterization of Electrodes and Electrochemical Process, John Wiley and Son, Inc., New York (1991), pp. 211-277.

(59) J. I. Gersten, and A. Nitzan: in "Surface Enhanced Raman Scattering", (R. K. Chang and T. E. Furtak, eds.), Plenum Press, New York, (1982), p. 89.

(60) H. Metiu: in "Surface Enhanced Raman Scattering", (R. K. Chang and T. E. Furtak, eds.), Plenum Press, New York, (1982), p. 1.

(61) B. J. Messinger, K. U. Von Raben, R. K., Chang, and P. W. Barber: Phys. Rev. B 24, 649 (1981).

(62) M. Kerker, D. S. Wang, and H. Chew: Appl. Opt. 19, 4159 (1980).

(63) A. Otto: in "Light Scattering in Solids III", (M. Cardona and G. Güntherodt, eds.),Springer-Verlag, Heidelberg.

(64) G. J. Schulz: in "Principles of Laser Plasmas" (George Bekefi, ed.), Wiley, New York, (1976), p. 33.

(65) J. Tang, and A. C. Albrecht: in "Raman Spectroscopy, Theory and Practice", (H. A. Szymanski, ed.), Vol. 2, Plenum Press, New York, pp.33-68.

(66) M. Bridoux, and M. Delhaye: (1976). Adv. Infrared Raman Spectrosc. 2, 140.

(67) D. L. Jeanmaire, and R. P. Van Duyne: J. Electroanal. Chem. 1975, 66,

235.

(68) S. K. Schwab, R. L. McCreery and F. T. Gamble: Anal. Chem. 1986, 58, 2486.

(69) R. T. Packard, and R. L. McCreery: Anal. Chem. 1987, 59, 2631.

(70) C. Shi, "Applications of Time-Resolved Surface Enhanced Raman Spectroscopy in Electrochemical Process", Ph. D. Thesis, 1992, City Univ. of New York.

(71) J. D. Ingle, JR., and S. R. Crouch: "Spectrochemical Analysis", Prentice Hall, Englewood Cliffs, New Jersey 07632.

(72) R. L. Birke, and J. R. Lombardi: "Investigation of Radical Ions with Time-Resolved Surface Enhanced Raman Spectroscopy", in Molecular Engineering 4, Kluwer Academic Publishers, Netherlands, 1994, pp. 277-310.

(73) Wei Zhang, "Time Resolved Surface Enhanced Raman Scatteing Studies of Surface Photochemistry and Electrochemistry", Ph. D. Thesis, 1995, City Univ. of New York.

(74) J. E. Pemberton, and R. P. Buck: J. Electroanal. Chem. 136, 201 (1982).

(75) W. H. Li, and Z. Q. Tian: Chinese Chemical Letters Vol. 4, No. 9, pp. 829-830, 1993.

(76) C. K. Chen, T. F. Heinz, D. Ricard, and Y. R. Shen: Chem. Phys. Letts. 83, 455 (1981).

(77) M. Takahashi, and M. Ito: J. Electron Spectry., 54/55 (1990) 913.

(78) M. Takahashi, and M. Ito: Springer Proceedings in Physics, Vol. 68 Ed.: H. Takahashi, Time Resolved Bibrational Spectroscopy V. Springer-Vcrlag Berlin Heidelberg 1992.

(79) K. Kneipp, and H. Kneipp: Spectrochim. Acta, 1993, 49A (2), 167

(80) K. Kneipp: J. Molec. Struct., 1990, 218, 357

(81) K. Kneipp, W. Jahr, and G. Roewer: Chem. Phys. Lett., 1989, 163, 105

(82) H. G. Zhang, F. Z. Liu, T. J. He, and H. W. Xin: Chemical Journal of Chinese University, 1993, 14 (2), 261

(83) H. G. Zhang, H. W. Xin, T. J. He, and F. C. Liu: Spectrochim. Acta, 1991, 47A (7), 927

(84) R. Dornhaus, M. B. Long, R. E. Benner, and R. K. Chang: Surface Science 93 (1980) 240-262.

(85) M. R. Philpott, F. Barz, J. G. Gordon II, and M. J. Weaver, J. Electroanal. Chem., 150 (1983) 399-414.

(86) P. Gao, D. Gosztola, and M. J. Weaver, Anal. Chim. Acta 212, 201 (1988)

(87) J. F. Owen, T. T. Chen, R. K. Chang, and B. L. Laube, J. Electroanal. Chem., 150 (1983) 389.

(88) T. M. Cotton, and M. Vovra, Chem. Phys. Lett., 106 (1984) 491.

(89) L. N. Mackey, and T. Kuwana: Bioelectrochem. Bioenerg. 3, 596 (1976).

(90) C. J. Schoot, J. J. Ponjee, H. T. van Dam, R. A. Van Doorn, and P. T. Bolwijn: Appl. Phys. Lett. 23, 64 (1973).

(91) H. T. van Dam, and J. J. Ponjee: J. Electrochem. Soc. 121, 1555 (1974).

(92) R. Jasinski: J. Electrochem. Soc. 124, 533 (1979).

(93) R. C. Ciesliski, and N. R. Armstrong: J. Electrochem. Soc. 127, 2605 (1980).

(94) F. F. Fan, B. Reichman, and A. Bard: J. Am. Chem. Soc. 102, 1488 (1980).

(95) A. Regis and J. Corset: J. Chim. Phys. 78, 687 (1981).

(96) C. A. Melendres, P. C. Lee, and D. Meisel: J. Electrochem. Soc. 130, 1523 (1983).

(97) T. Lu, R. L. Birke, and J. R. Lombardi: Langmuir 2, 305 (1986).

(98) Q. Feng, and T. M. Cotton: J. Phys. Chem. 90, 983 (1986).

(99) A. Yasuda, H. Kondo, M. Itbashi, and J. Seto: Electroanal. Chem. 210, 265 (1986).

(100) T. Lu and T. M. Cotton: J. Phys. Chem. 91, 5978 (1987).

(101) Q. Feng, W. Yue, and T. M. Cotton: J. Phys. Chem. 94, 2082 (1990).

(102) M. Osawa, K. Nishijima, and W. Suetaka, Surf. Sci. 1986,104,270.

(103) M. Osawa, and W. Suetaka, J. Electroanal. Chem. 1989,270,261.

(104) Y. Misono, K. Shibasaki, N. Yamasawa, Y. Mineo, and Koichi Itoh, J. Phys. Chem. 1993, 97, 6054-6059.

(105) S. Sun, R. L. Birke, J. R. Lombardi, K. P. Leung, and A. Z. Genack: J. Phys. Chem. 92, 5965 (1988).

(106) G. L. McIntire, D. M. Chiappardi, R. L. Casselberry, and H. N. Blount: J. Chem. Phys. 86, 2632 (1982).

(107) A. J. Fry: in S. Patai (ed.), The Chemistry of Amino, Nitroso, Nitro Compounds and Their Derivatives, Part I, John Wiley and Son, New York (1982), p. 320.

(108) I. Rubinstein: J. Electroanal. Chem. 183, 379 (1985).

(109) P. Gao, D. Gosztola, and M. J. Weaver: J. Phys. Chem. 92, 7122 (1988).

(110) C. Shi, W. Zhang, R. L. Birke, and J. R. Lombardi: J. Phys. Chem. 94, 4767 (1990).

(111) C. Shi, W. Zhang, R. L. Birke, and J. R. Lombardi: J. Phys. Chem. 95, 6276 (1991).

(112) C. Shi, W. Zhang, R. L. Birke, and J. R. Lombardi: J. Electroanalytical Chemistry and Interfacial Electrochemistry, in press (1997).

(113) P. Gao, and M. L. Patterson, M. A. Tadayyoni, M. J. Weaver: Langmuir 1985, 1, 173.

(114) P. Gao, and M. J. Weaver: J. Phys. Chem. 89, 5040 (1985).

(115) T. M. Cotton, J. H. Kim, and R. A. Uphaus: Microchemical Journal, 42, 44-71 (1990).

(116) D. Franzke, and A. Wokaun, J. Phys. Chem. 96, 6377-6381 (1992).

(117) P. F. Heelis: Chem. Soc. Rev. 11, 15 (1982).

(118) J. Yamase: Photochem. Photobiol. 34, 11 (1981).

(119) N. S. Lee, Y. Z. Hsieh, M. D. Morris and L. M. Schopfer: J. Am. Chem. Soc., 109(5), 1358 (1987).

(120) C. Shi, W. Zhang, R. L. Birke, and J. R. Lombardi: J. Phys. Chem. 96, 10093 (1992).

(121) W. Zhang, A. Vivoni, J. R. Lombardi, and R. L. Birke: J. Phys. Chem. 99, 12846 (1995).

Chapter 4

(1) J. C. Dabrowiak, F. T. Greenway, S. F. Santillo, S. T. Crooke, and J. M.Essery, ACS Symposium Series, No. 140, 'Inorganic Chemistry in Biology and Medicine', Eds by A. E. Martell, American Chemical Society; **1980.**

(2) E. A. Sausville, J. Peisach, and S. B. Horwitz, Biochemistry; **1978,** 17, 2740.

(3) R. M. Burger, T. A. Kent, S. B. Horwitz, E. Munck, and J. Peisach, J. Biol. Chem.; **1983,** 258, 1559.

(4) R. M. Burger, J. S. Blanchard, S. B. Horwitz, and J. Peisach, J. Biol. Chem.; **1985,** 260 (29), 15406.

(5) R. M. Burger, J. Peisach, W. E. Blumberg, and S. B. Horwitz, J. Biol. Chem.; **1979,** 254, No.21, 10906.

R. M. Burger, S. B. Horwitz, J. Peisach, and J. B. Wittenberg, J. Biol. Chem.; **1979,** 254 (24), 12299.

(6) M. A. J. Akkerman, E. W. J. F. Neijman, S. S. Wijmenga, C. W. Hilbers, and W. Bermel, J. Am. Chem. Soc.; **1990,** 112, 7462.

(7) T. Takita, Y. Muraoka, T. Nakatani, A. Fuji, and Y. Iitaka, J. Antibiot.; **1978,** 31, 1073.

(8) Y. J. Sugiura, Am. Chem. Soc.; **1980,** 102, 5208.

(9) S. Takahashi, J. W. Sam, J. Peisach, and D. L. Rousseau, J. Am. Chem. Soc.; **1994,** 116, 4408.

(10) N. J. Oppenheimer, L. O. Rodriguez, and S. M. Hecht, Proc. Natl. Acad. Sci. USA; **1979,** 76, 5616.

(11) E. A. Sausville, J. Peisach, and S. B. Horwitz, Biochem. Biophys. Res. Commun.; **1976,** 73, 814.

(12) E. A. Sausville, J. Peisach, and S. B. Horwitz, Biochemistry; **1978,** 17, 2740.

(13) E. A. Sausville, R. W. Stein, J. Peisach, and S. B. Horwitz, Biochemistry; **1978,** 17, 2746.

(14) R. M. Burger, J. Peisach, and S. B. Horwitz, J. Biol. Chem.; **1981,** 256(22), 11636.

(15) C. M. Hosten, R. L. Birke, and J. R. Lombardi, J. Phys. Chem.; 1992, 96, 6685.

(16) R. L. Birke, J. R. Lombardi, and L. A. Sanchez, 'Surface Enhanced Raman Spectroscopy'; Kadish, K. M., Ed.; Am. Chem. Soc.; Washington, DC; **1982,** adv. Chem. Ser. No. 201, Chapter 4.

(17) C. Shi, W. Zhang, R. L. Birke, and J. R. Lombardi, J. Phys. Chem.; **1990,** 94, 4766.

(18) B. T. Freedman, F. S. Santillo, C. G. Zimba, L. A. Nafie, and J. C. Dabrowiak, J. Ramam Spectroscopy; **1983,** 14 (4), 266.

(19) E. Koglin, H. H. Lewinsky, and J. M. Sequaris, Surface Science; **1985,** 158, 370.

(20) F. R. Dollish, W. G. Fateley, and F. F. Bentley; 'Characteristic Raman Frequencies of Organic Compounds', 1974, John Wiley & Sons, Inc. New York.

(21) P. R. Carey, 'Biochemical Applications of Raman and Resonance Raman Spectroscopies'; Academic Press; **1982,** Chapter 4.

(22) M. Sekizaki, and K. Yamasaki, Spectrochim. Acta; **1968,** 25A, 475.

(23) S. J. Brown, S. E. Hudson, D. W. Stephan, and P. K. Mascharak, Inorg. Chem.; **1989,** 28, 468.

(24) R. J. Guajardo, S. E. Hudson, S. J. B rown, and P. K. Mascharak, J. Am. Chem. Soc.; **1993,** 115, 7971.

(25) P. R. Carey, 'Biochemical Applications of Raman and Resonance Raman Spectroscopies'; Academic Press; **1982,** Chapter 5.

(26) G. A. van der Marel and J. H. van Boom, J. Am. Chem. Soc. 1989, 111, p2722-2724.

Chapter 5

(1) J. B. Harborne, 'The Flavonoides: advances in research since 1986', Chapman and Hall, London, 1994.

(2) J. B. Harborne, T. J. Mabry, and H. Mabry, 'The Flavonoides', Chapman and Hall, London, 1975.

3) J. B. Harborne, and T. J. Mabry, 'The Flavonoides: Advances in Research', Chapman and Hall, London, 1982.

(4) J. W. McClure, in 'Plant Flavonoids in biology and Medicine: Biochemical, Pharmacological and Structure-Activity Relationships', (eds V. Cody, E. Middleton, and J. B. Harborne), Alan R. Liss, 1986, New York, pp. 77-85.

(5) T. A. Geissman, 'The Chemistry of Flavonoid Compounds', The Macmillan Company, 1962.

(6) D. A. Smith, and S. W. Banks, in 'PlantFlavonoids in biology and Medicine: Biochemical, Pharmacological and Structure-Activity Relationships', (eds V. Cody, E. Middleton and J. B. Harborne), Alan R. Liss, 1986, New York, pp. 113-124.

(7) M. Gabor, 'The Pharmacology of Benzopyrone Derivatives and Related Compounds', 1986, Akademiai Kiado, Budapest.

(8) F. M. Dean, 'Naturally Occurring Oxygen Ring Compounds', Butterworts, London, 1963, p. 280.

(9) T. J. Mabry, F. K. Markham, and M. B. Thomas, 'The Systematic Identification of Flavonoids', Springer, Berlin, 1970.

(10) P. K. Sengupta, and M. Kasha, Chem. Phys. Lett. **1979**, 68, 382.

(11) M. Itoh, Y. Fujiwara, M. Sumitani, and K. Yoshihara, J. Phys. Chem. **1986**, 90, 5672.

(12) W. E. Brewer, S. L. Studer, M. Standiford, and P. T. Chou, J. Phys. Chem. **1989**, 93, 6088.

(13) T. P. Dzugan, J. Schmidt, and T. J. Aartsma, Chem. Phys. lett. **1986**, 127(4), 336.

(14) J. H. Looker, and W. W. Hanneman; J. Org. Chem., **1962**, 27, 381.

(15) C. I. Jose, P. S. Phadke, and A.V. R. Rao, Spectrochem. Acta, **1974**, 30A, 1199.

(16) B. L. Shaw, and T. H. Simpson; J. Chem. Soc., **1955**, 655.

(17) H. L. Hergert, and E. F. Kurth; J. Amer. Chem. Soc.; 75, 1622, 1953.

(18) J. H. Looker, W. W. Hanneman, S. A. Kagal, J. I. Dappen, and J. R. Edman; J. Hetero-Cyclic Chem. 3, 55,1966.

(19) J. H. Looker, S. A. Kagal, J. I. Dappen, and J. R. Edman; J. Hetero-Cyclic Chem. 3, 61,1966.

(20) R. L. Birke, T. Lu and J. R. Lombardi; in 'Techniques for characterization of Electrodes and Electrochemical Processes', Chapter 5; Eds. R. Varma & J. R. Selam; John Wiley & Sons, Inc.; **1991.**

(21) A. Vivoni, J. R. Lombardi, and R. L. Birke, 1996, to be published.

(22) A. Barlow, and M. Diem, J. Chem Ed., **1991**, 68, 35.

(23) B. Dick, J. Phys. Chem., **1990**, 94, 5752.

(24) D. W. Scott, J. Molecular Spectroscopy, **1971**, 37, 77.

(25) D. W. Scott, J. Molecular Spectroscopy, **1969**, 31, 451.

(26) T. D. Bouman, M. A. Knobiloch, and S. Bohan; J. Phys. Chem., 1985, 89, 4460.

(27) M. Abe, and Y. Kyogoku; Spectrochim. Acta 43A, 1987, 1027.

(28) D. Lin-Vien, N. B. Colthup, W. G. Fateley, and J. G. Grasselli; 'The Handbook of Infrared and Raman Characteristic Frequencies of Organic Molecules'; Academic Press, Inc.

(29) S. Zou, J. Gao, C. Li, and Z. Tian; Acta Physico-Chimica Sinica (chinese), 1995, vol.11, No. 11, 1020.

(30) E. Koglin, H. H. Lewinsky, and J. M. Sequaris, Surface Science; 1985, 158, 370.

(31) O. S. Wolfbeis, A. Knierzinger, and R. Schipfer, J. Photochemistry 21 1983, 67-79.

Chapter 6

(1) H. Shizuka, S. Matsue, Y. Hirata, and I. Tanaka, J. Phys. Chem. **1977**,

81, 2243.

(2) K. K. Smith, and K. J. Kaufman, J. Phys. Chem. **1978**, 82, 2286.

(3) P. F. Barbara, L. E. Brus, and P. M. Rentzepis, J. Am. Chem. Soc. **1980**, 102, 5631.

(4) G. J. Woolfe, and P. J. Thistlethwaite, J. Am. Chem. Soc. **1980**, 102, 6917.

(5) P. Sengupta, and M. Dasha, Chem. Phys. Lett. **1979**, 68. 382.

(6) M. Itoh, and Y. Fujiwara; J. Phys. Chem. **1983**, 87, 4558.

(7) A. J. G. Strandjord, S. H. Courtney, D. M. Frienrich, and P. F. Barbara; J. Phys. Chem. **1983**, 87, 1125.

(8) D. A. Parthenopoulos, and M. Kasha; J. Chem. Phys. Lett. **1990**, 173, 4, 303.

(9) A. J. G. Strandjord, and P. F. Barbara; J. Phys. Chem. **1985**, 89, 2355.

(10) D. McMorrow, and M. Kasha; J. Phys. Chem. **1984**, 88, 2235.

(11) B. J. Schwartz, L. A. Peteanu, and C. B. Harris, J. Phys. Chem. **1992**, 96, 3591.

(12) G. A. Brucker, and D. F. Kelley, J. Phys. Chem. **1987**, 91, 2856.

(13) C. Rulliere, and A. Declemy, J. Chem. Phys. Lett. **1987**, 134, 64.

(14) M. Itoh, Y. Fujiwara, M.Sumitani, and K. Yoshihara, J. Phys. Chem. **1986**, 90, 5672.

(15) T. P. Dzugan, J. Schmidt, and T. J. Aartsma, Chem. Phys. Lett. **1986**, 127, 336.

(16) W. E. Brewer, S. L. Studer, M. Standiford, and P. T. Chou, J. Phys. Chem. **1989**, 93, 6088.

(17) Wei Zhang, "Time Resolved Surface Enhanced Raman Scatteing Studies of Surface Photochemistry and Electrochemistry", Ph. D. Thesis, 1995, City Univ. of New York.

(18) W. Zhang, A. Vivoni, J. R. Lombardi, and R. L. Birke: J. Phys. Chem. 99, 12846 (1995).

(19) M. Wang, J. R. Lombardi, and R. L. Birke, manuscripts, to be published, **1996.**

(20) R. L. Birke, T. Lu and J. R. Lombardi; in "Techniques for characterization of Electrodes and Electrochemical Processes", Chapter 5; Eds. R. Varma & J. R. Selam; John Wiley & Sons, Inc.; **1991.**

(21) R. L. Birke, and J. R. Lombardi; "Investigation of Radical Ions with Time-Resolved Surface Enhanced Raman Spectroscopy" in Molecular Engineering 4; pp277-310 Kluwer Academic Publishers, **1994.**

(22) G. A. Brucker and D. F. Kelley J. Phys. Chem. **1987**, 91, 2856.

(23) B. Dick; J. Phys. Chem., **1990**, 94, 5752.

(24) E. Maslowsky, Jr., Vibrational Spectra of Organometallic Compounds; John Wiley & Sons, Inc.; **1977.**

(25) F. R. Dollish; W. G. Fateley; F. F. Bentley; 'Characteristic Raman Frequencies of Organic Compounds'; John Wiley & Sons, Inc.; **1974.**